UNIVERSITÀ
CA' FOSCARI
DI VENEZIA

PhD Thesis in

SCIENCE AND MANAGEMENT OF CLIMATE CHANGE

Molecular tracers and untargeted characterization of water soluble organic compounds in polar ice for climate change studies.

PhD Candidate
Ornela Karroca

Supervisor
Prof. Andrea Gambaro

Co-Supervisor
Dr. Roberta Zangrando

GLOSSARY

1. ABSTRACT

The polar regions are an excellent archive of past atmospheric conditions rendering polar ice investigation extremely important for paleoclimate studies. The presence of organic compounds, such as amino acids and methoxyphenol compounds, could lead to important insights regarding the presence of past biological material and biomass burning information, respectively. Amino acids constitute an important fraction of organic matter, as well as a source of carbon, nitrogen and energy. Moreover, L-amino acids are the most common enantiomer present in nature and are indicative of phytoplanktonic material: on the other hand, D-amino acids are linked to the presence of bacteria. With the aim of detecting possible past bacterial presence, we investigated both D- and L-amino acid enantiomers in two ice cores: Talos Dome, East Antarctica, and Renland, Eastern Greenland. In selected Talos Dome ice core samples was performed a qualitative analysis to detect the chemical composition and to investigate the past and/or ongoing chemical transformations of the chemical species found.

Phenolic compounds are produced by lignin combustion and are specific molecular markers used to assess combustion sources. For this purpose, their presence was investigated in the Talos Dome ice core samples. For both, amino acids (D-/L- enantiomers) and methoxyphenols, were validated the respective analytical methods. Moreover, specific quality control assessments for each analyte were performed.

A part of this work was focused on the optimization of a preconcentration analytical method for several fatty acids and atmospheric markers. The preconcentration preliminary step was performed in order to be applicable to real ice and snow samples, with the purpose to ensure the detection of low concentrations with the disposable instruments. The presence of fatty acids provide important information since are mainly derived by phospholipids and triglycerides, which are accumulated during algal bloom, giving insights on the biological activity of the surrounding marine ecosystems.

2. INTRODUCTION

The polar ice is often used to extract paleoclimatic information since is considered to be a storage of past atmospheric composition. The snow deposition, in absence of snow melting, reflects the past atmospheric composition in polar regions allowing the deposition and conservation of important atmospheric markers. Moreover, the distance from anthropogenic sources makes the polar regions important for investigating the natural sources of atmospheric aerosol (Barbaro et al., 2017). Given the importance in terms of paleoclimate studies of polar ice matrices, as well as the low concentrations of atmospheric tracers archived in it, becomes fundamental the optimization of the analytical techniques used for the detection of atmospheric markers present in traces in order to achieve the highest sensitivity. The study of these markers is essential to detect specific environmental processes, such as biomass burning, investigating on the presence of levoglucosan and phenolic compounds, and primary production studying the presence of amino acid species. For this reason, during this thesis one of the main purposes was the development of a sensitive analytical method and the detection of amino acid and phenolic compounds in Antarctic and Arctic ice samples.

The amino acid compounds are studied widely in this thesis since represent a source of carbon, nitrogen and energy, and constitute a part of organic matter in marine and freshwater ecosystems. Amino acids are used by bacteria and phytoplankton species as a source of nitrogen and are released from soil organic matter, as well as by terrestrial plants, living phytoplankton and cellular lysis of senescent algae. They also play an important role in the carbon flux acting as intermediates, although they represent a small part of the total dissolved organic carbon due to the low concentrations (Berman and Bronk, 2003; Bronk et al., 1994). In past studies were performed analyses of amino acids in other environmental matrices, other than in polar ice as performed in this work, such as in seawater with early studies (Belser 1959; Tatsumoto et al., 1961; Palmark, 1963) followed by more recent works, and in atmospheric aerosols (Barbaro et al., 2015; Matos et al., 2016), since the amino acid compounds are an important component of organic nitrogen in

atmospheric aerosols (Chan et al. 2005). The aim of our work is to collect information as much as possible about the distribution of the markers in different matrices, trying to find out the processes involved in terms of air transport, chemical transformation, oxidation/reduction processes, deposition in remote areas, stability during a long-range transport, etc. Amino acids were found also to contribute to ice nucleating of atmospheric particles enhancing the process and to cloud condensation acting as nuclei (Kristensson et al., 2010; Szyrmer and Zawadzki, 1997). It was shown also that the presence of the amino acid compounds in the atmosphere is also influenced by sources such as biomass burning and volcanic emissions (Mace et al., 2003; Scalabrin et al., 2012). Nevertheless, one of the principle sources of amino acids in the atmosphere, especially in polar regions, is the emission from marine water through bubble bursting and wave breaking (O'Dowd et al., 2004). Moreover, in the work performed by Barbaro et al., 2015 were investigated and detected amino acids present in marine aerosols and in particles emitted from the oceans making crucial the investigation of the exchange processes between atmosphere and the ocean for better understanding the provenance of these compounds. In the same work were investigated particle size distributions in the Antarctic aerosols in which they suggest that the principal source of amino acids could be marine emissions. Such organic compounds emitted by marine water could be transported up to polar areas due to wind driven processes and be deposited. Furthermore, amino acids such as glycine and alanine, due to their presence detected over the Antarctic plateau and their greater stability, can be used as biogenic markers and to investigate the aerosol aging during the long-range transport. Other works performed on Arctic aerosol are in agreement with Antarctic studies. This fact states still further that the main source for amino acids in polar regions is marine water (Scalabrin et al., 2012; Barbaro et al., 2015).

In several works the methanesulfonic acid (MSA), an atmospheric oxidation product produced by marine biota, was used in ice core studies as a marker of past changes in marine productivity since it reflects in large-scale the changes in primary production (O'Dwyer et al. 2000). Nevertheless, it was shown in a couple of works (Curran et al., 2003; Isaksson et al. 2005) that the concentrations of MSA in ice sample can be influenced by several environmental parameters such as sea ice extension variations. Moreover, it was shown in the work (Abram et al. 2008) that MSA is able to spread inside solid ice cores. For this reason, become crucial to determine new compounds able to give a more reliable indication of past changes in primary production. Amino acids are linked to oceanic primary production and the fact that their presence was detected in Arctic and Antarctic aerosol suggests

that these compounds can be preserved in the ice, thus can be used as a marker to investigate past marine production changes (Barbaro et al., 2017). In fact, in the work Barbaro et al., 2017 we investigated the correlation between the amino acids in a shallow firn core from Holteldahlfonna glacier covering a period of 3 years (winter 2012 – spring 2015), and the oceanic phytoplankton abundance intended as Chlorophyll-a concentrations in the Barents sea, Greenland see and regions surrounding the Svalbard archipelago, in order to investigate whether such compounds are emitted or produced in the atmosphere during the period of phytoplankton bloom. The marked increase of the amino acid profiles in the period of maximum phytoplankton bloom confirms the significance of these compounds as markers of primary production, as well as gives further evidence about the source of the amino acids found in ice samples.

In this thesis was also investigated any eventual correlation between amino acids and sediments data collected in the areas surrounding the drilling site of the Renland ice core, being relatively coastal and most probably influenced by marine processes. In particular, we focused on IP_{25} index, a phytoplankton-derived biomarker, associated with sea ice diatoms and calcium carbonate ($CaCO_3$) intended as paleoproductivity proxy, being one of the main components of the whole biogenic fraction in sediment depositions, thus linked to phytoplankton and zooplankton which are the major source of organic carbon in seawater and sediments (Rühlemann et al., 1999).

An important feature of most amino acid compounds that attributes different biological properties is chirality due to the presence of an asymmetric center, classifying the amino acids in D- and L-enantiomers. The most common amino acid in nature is the L-enantiomer since during the protein and peptide biosynthesis L-amino acids are the only enantiomers used, leading to homochirality of life in Earth (Cronin and Pizzarello 1997). The occurrence of D-amino acids, on the other hand, is attributed to the presence of bacteria as generally are found in bacterial cell walls. Therefore, it results important to investigate about the presence either of amino acids in general and the specific enantiomers. For this reason, in this work the optimization of the enantiomeric separation of both D- an L- amino acids was performed, through reversed-phase liquid chromatography. Generally, the separation process requires a previous enantiomer diastereoisomerization through a chiral reagent (Buck and Krummen, 1987; Marfey, 1984). Although, due to the disadvantages that the procedure of the formation of diastereoisomers could lead, such as long preparation times, derivate instability or not an adequate reagent enantiopurity, this procedure in this thesis was omitted. There are

several other ways to separate two enantiomers, such as chiral ligand-exchange chromatography (Remelli et al., 1997), the use of α-cyclodextrin based chiral stationary phase (Armstrong et al., 1987), crown ether based (Gimenez et al., 1997) or teicoplanin based (Petritis et al., 2001) able to separate underivatized amino acids in reverse-phase mode. The most common detectors used generally (amperometric/electrochemical detectors) for the detection of amino acid enantiomers have a low specificity (Petritis et al., 2002). As the amino acids are thermolabile, ionizable and polar compounds, make the Electrospray Ionization (ESI) mass spectrometry used during this thesis suitable for the analyses of these compounds. Moreover, ESI-mass spectrometry is compatible with the reverse-phase separation through teicoplanin based stationary phase used during this work.

Another important argument largely studied is biomass burning, since is a significant source of aerosol particles (Crutzen and Andreae 1990). Biomass burning is one of the main sources of organic matter in the atmosphere (Gelencsér et al. 2007), intending for "biomass" the whole vegetal organisms that could be combusted in forest fires or used as a source of energy. The biomass is composed mainly by two fractions: lignin and carbohydrates. The carbohydrates, composed by monosaccharides and polysaccharides (cellulose and hemicellulose) represent the 70% of the whole mass (Faravelli et al., 2006). Lignin constitutes the other 30% and is composed principally by phenolic compounds (Iinuma et al. 2007; Simoneit 2002). In the ***Figure 1*** is reported the structure of lignin and the phenylpropanoid units, known as the lignin precursors linked with carbon-oxygen and carbon-carbon bonds (Christopher et al., 2014).

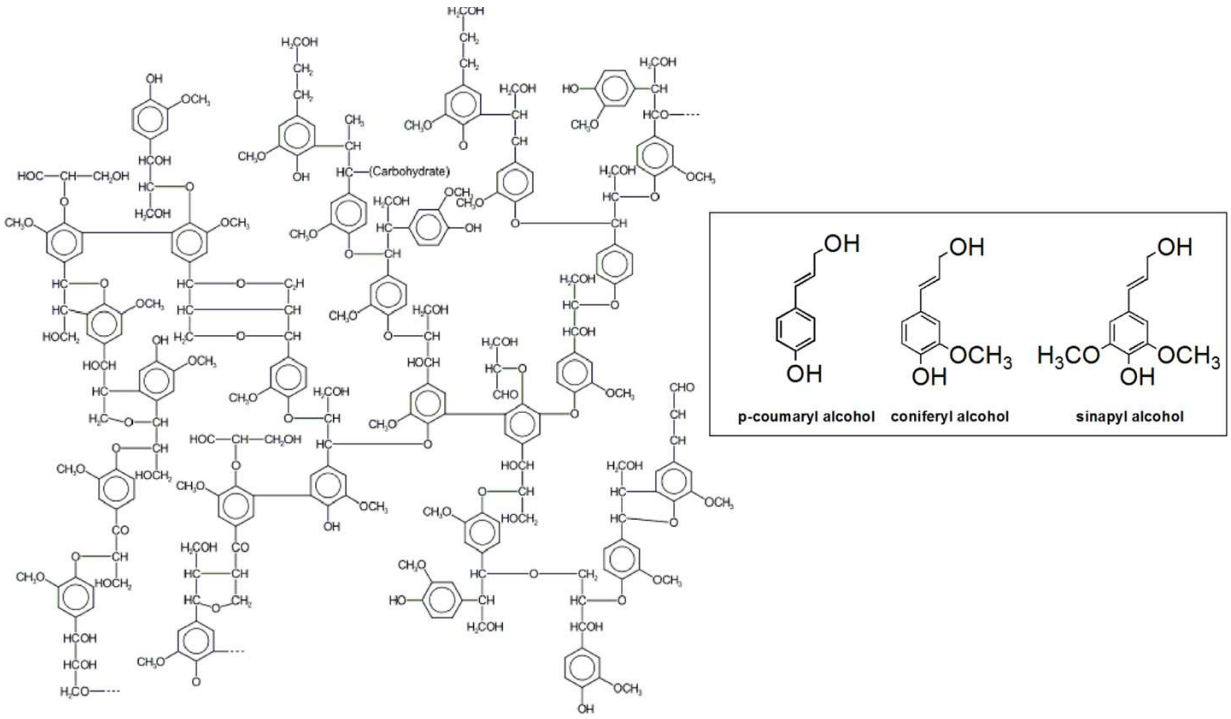

Figure 1 *– Structure of lignin (left) and lignin precursors (right).*

Since methoxyphenols are produced from lignin combustion, they are used for the assessment of combustion sources. The principal pyrolysis products are *coumaryl*, *vanillyl* and *syringil* compounds in the form of ketone, aldehyde, acid and alchyl derivates which are emitted during wood burning with a variability which depends on the plant classes. The main phenolic compounds emitted in tree smoke are vanillic acid, vanillin, syringic acid and homovanillyl alcohol. On the contrary, softwoods are characterized by a high proportion of coniferyl alcohols and a minor abundance of vanillyl compounds and sinapyl alcohol products. In the same way, p-coumaryl alcohol is the main component in grasses, producing during the burning acetosyringone, vanillin, syringic and vanillic acids (Oros et al., 2006a, Oros et al., 2006b). As a consequence, depending on the presence of these molecules it is possible to trace back to the type of combusted biomass (softwood, hardwood or grasses) considering that the concentrations and emissions of phenolic compounds are strongly related also to the atmospheric conditions (wind, humidity and temperature). The phenolic compound's concentrations are likely to be influenced by their stability in the atmosphere (Zangrando et al. 2013) depending on atmospheric conditions. In this work were chosen for the study the detection of phenolic compound molecules that better represent the main taxonomic classes mentioned above considering only the PCs having high emission factors calculated as the

amount of the emitted compound per mass unit of combusted wood (Oros et al., 2006a; Oros et al., 2006b; Simoneit, 2002).

Climate changes: past and future

The overall objective of our works is the study of climate change markers with the purpose of investigating the climate of the past and to better understand the anthropogenic forcing and the impact of human activities. In order to enrich our understanding on the composition of polar ice matrices and to investigate eventual chemical transformations over time, an untargeted characterization on Antarctic ice samples from glacial and interglacial periods was performed.

The human activities are altering the climate and the worlds atmosphere in many ways, increasing the concentrations of the global atmospheric CO_2 and contributing to rising global temperatures leading, as a consequence, to precipitation increases (IPCC, 3rd Assessment Report, 2001). The period when "Global effects of human activities have become clearly noticeable" was defined as Anthropocene by Crutzen and Stoermer (2000). In this work the authors state that the invention of the steam engine in 1784 and the beginning of the industrial revolution was the starting point of large emissions of CO_2 and methane such as to alter the natural composition of these two greenhouse gasses in the atmosphere. Nevertheless, is still unknown the exact period when human beings started influencing on the Earth climatic system. Several researchers suggest that the anthropogenic impacts on climate alteration began much earlier than what is known as Anthropocene, considering the deforestation, the agricultural practices, the fires of anthropogenic nature that occurred already thousands of years ago, dating back to the mid-Holocene (Ruddiman 2003). These hypotheses were suggested based on studies made on the natural cyclic variations of Earth's orbit which doesn't explain the abnormal concentrations of CO_2 and CH_4 during the Holocene period, showing an abnormal increase of CO_2 and CH_4 respectively 8000 and 5000 years ago not following the natural forcing. Moreover, palynologic studies as well as cultural, archeologic and historical evidences provide important information about the beginning of a strong agriculture expansion in Eurasia consisting in deforestation and rice cultivation, respectively 8000 and 5000 years ago which coincide with the increase of CO_2 and CH_4 as stated by analyses in ice core samples. Ruddiman (2007) suggests that the CO_2 and CH_4 emissions were likely to obstacle a new ice age predictable from the Earth's orbital variation studies. In the figures below are shown the CH_4 and CO_2 increases during the last 10000 years.

As can be seen from the graph extracted from Ruddiman, 2007 (***Figure 2***) the CO_2 concentrations reached a maximum value of 286 ppm before the preindustrial era. Further observations from the year 1958 performed by *NOAA (National Oceanic and Atmospheric Administration) Earth System Research Laboratory Global Monitoring Division* confirm the continuing increasing trend of carbon dioxide in the last 60 years with concentrations reaching values greater than 400 ppm and with a rising annual growth rate ***(Figure 3 b).*** The measurements are performed in the observatory situated in Mauna Loa (Hawaii).

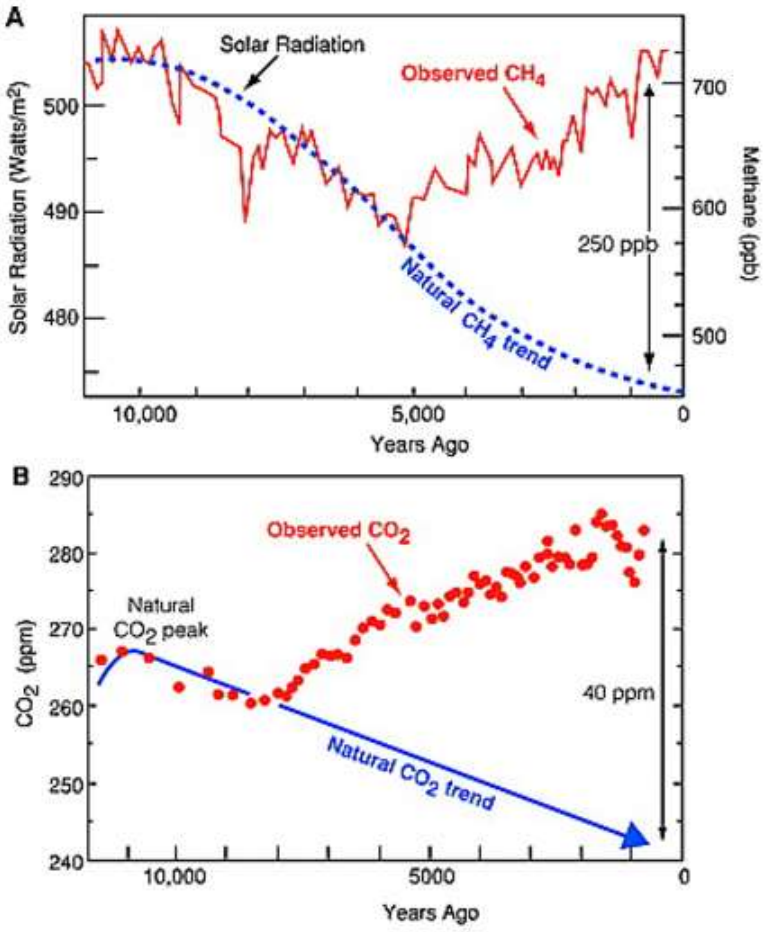

Figure 2 *– Increases of* ***A)*** *CH_4 and* ***B)*** *CO_2 due to human activities contrasting the downward trend (Ruddiman, 2007).*

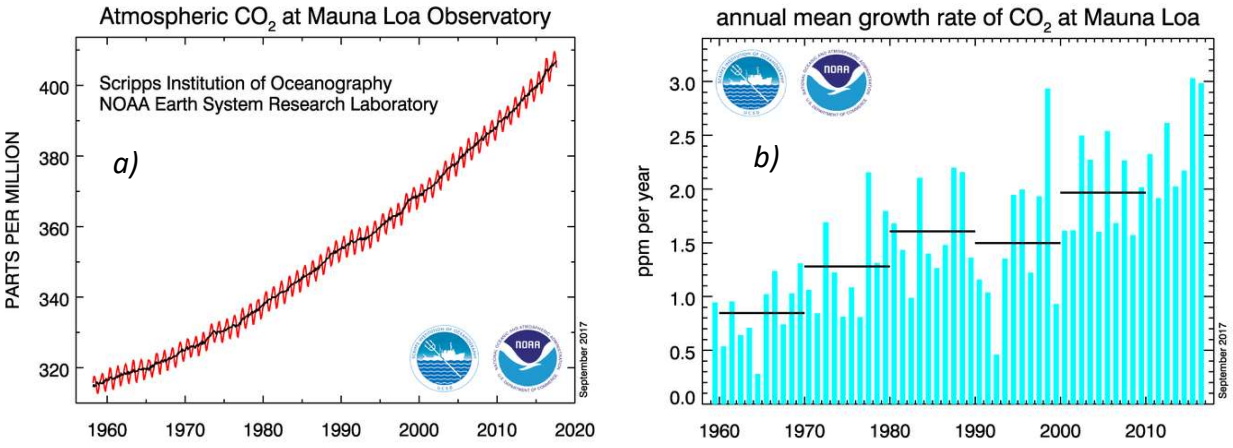

Figure 3 *– **a)** Atmospheric CO_2 (ppm) observed at Mauna Loa Observatory (Hawaii) and **b)** annual mean growth rate. (NOAA - National Oceanic and Atmospheric Administration)*

Thanks to scenarios performed using different carbon cycle models constructed making different socio-economic storyline assumptions is possible to join the past observed changes of CO_2 and the future projections. In the ***Figure 3 (a)*** are shown the CO_2 concentration variations observed in the ice cores EPICA and Vostok, determined analyzing the bubbles of air trapped inside the ice and the different projections indicated with the colored arrows. The variations observed in the distant past indicates the natural CO_2 changes ranging from 200ppm to 300ppm, conserving a constant trend for all about 600.000 years investigated. In the ***Figure 3 (b)*** are reported the observations of CO_2 atmospheric concentrations at Mauna Loa Observatory and the projections up to the year 2100. The scenario that predicts a higher level of CO_2 (A1FI) assumes a world with a very high future economic growth where people pursue personal wealth rather than an environmental quality, whereas the scenario that predicts a lower level of CO_2 (B1) assumes a future world with rapid economic growth which moves toward the introduction of clean and resource-efficient technologies. The scenarios that lie in-between are predictions obtained assuming intermediate storylines. As can be seen in the plot, all the scenarios predict CO_2 atmospheric concentrations ranging from nearly 480ppm to 1000ppm. The detailed carbon cycle models used as bases for climate model projections also in the Fourth Assessment Report, are reported in **IPCC 2001.**

a) *b)*

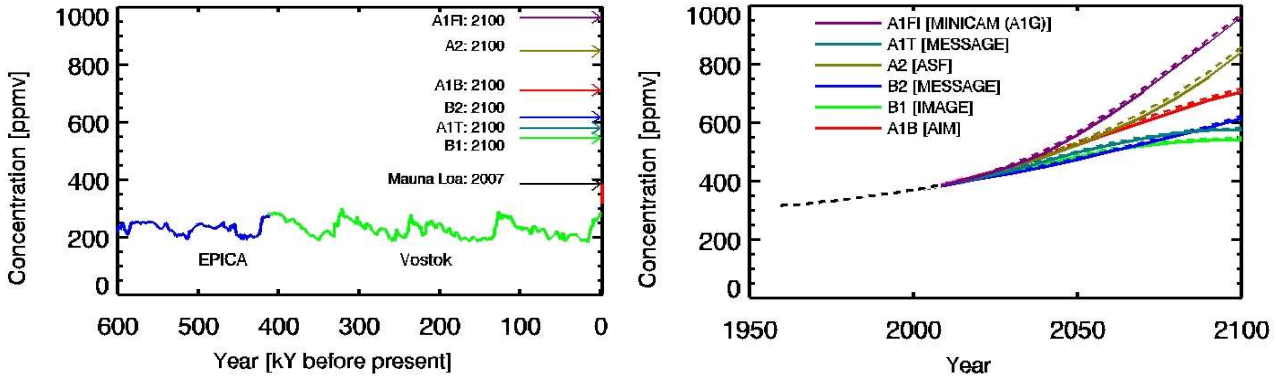

Figure 4 – a) *CO_2 concentrations derived from Vostok and EPICA ice cores. The red vertical line indicates the 50 years measurements in Mauna Loa site up to 2007. The colored arrows indicate the different scenarios up to year 2100 obtained with 6 different integrated assessment models and* ***b)*** *atmospheric observations indicated in dashed black line from 1958 to 2008 at Mauna Loa (Hawaii) and the same 6 different detailed scenarios indicated also in the figure* ***a)****.*

Ice cores and dating

The polar ice cores have been used widely for paleoclimatic reconstructions as multi-proxy archives in order to provide extremely important climatic and environmental records for hundreds of thousands of years (Legrand and Mayewski 1997). Several drillings have been performed in Antarctica and Greenland providing detailed paleoclimatic information of both hemispheres. The polar ice cores provide information in global scale for long time span (***EPICA Dome C*** Antarctic ice core reaches up to 800.000 years) whereas the mid-latitude ice cores are representative of regional climate and provide data for a shorter timescale. In order to ensure a good dating, the ice cores should derive from a permanent ice cap devoid of significant melting, characterized by positive snow accumulation. Moreover, the bedrock must be flat, the ice stratification must be horizontal and without mixed layers. These requirements restrict the drilling areas rendering adaptable for the drilling only polar ice and some mountain glaciers situated at high altitudes. The presence of air bubbles is an important evidence of past atmospheric greenhouse gas composition allowing a reconstruction back in time of the climate trend and an eventual assessment of the variations occurred due to anthropic activities.

Once the ice core is collected, the ice dating in relation to the depth is extremely important in order to assure a good interpretation of paleoclimatic and paleoenvironmental data. Therefore, the need for an accurate dating method applicable to all the ice cores becomes fundamental since an

intercomparison and a synchronization of the data deriving from different sites could help to understand the mechanisms involved (Schwander, 2006; Severi et al., 2012).
There have been used different ways to date the ice cores, as listed below:

- Layer counting

Each layer is representative to the snow accumulation occurred during the year: in wintertime the snow fall is more abundant and the surface melting during summer allows the distinction of each year. Nevertheless, this dating method becomes inaccurate when the stratification is not regular due to the mixing layers, which is common for deep ice cores where the weight of the overlying ice flattens the old layers (Fuhrer et al. 1993; Svensson et al. 2006; Schwander et al., 2006).

- Tephrachronology

This method uses tephra horizons which are volcano eruption dusts. The volcanoes during the eruption events release large quantities of H_2S and SO_2 which reaches the stratosphere and are oxidized into H_2SO_4. The sulfuric acid formed is solubilized in the water drops and reaches the soil with precipitation or through dry deposition. Therefore, the presence of high quantities of sulfate salts or a higher acidity detected with electric conductivity of the ice should be a unique evidence of volcanic eruptions which have been dated independently, rendering the tephra horizons time markers (Delmonte et al., 2013).

- Radiometric dating

The radiometric dating is performed analyzing the radioactive isotopes, such as 3^2Si, ^{210}Pb, ^{39}Ar, ^{81}Kr, ^{36}Cl, ^{10}Be and ^{14}C (Schwander, 2006).

- Ice isotopic composition

The isotopic composition of Oxygen-18 ($\delta^{18}O$) detected in the snowfall accumulated wintertime is lower than in the summertime snowfall, making possible the dating due to the seasonality profile. However, this method is accurate only when the snow accumulation is relatively high and if there are not significant snow melting/freezing during the year (Bradley 1999).

- Synchronization with other paleo-records

Generally, this dating method is used to improve the ice dating through synchronization with paleo-record deriving from more sites, reducing the uncertainty of paleoclimatic and paleoenvironmental reconstructions (Schwander, 2006; Severi et al., 2012).

- In-ice trapped gas dating

The air trapped inside the ice is enclosed inside the so-called "close-off" air bubbles where the air is blocked inside, hence representing the past atmospheric composition of the surrounding environment. Due to diffusive processes, the surrounding ice is older than the gasses trapped in the close-off. For this reason and because of the uncertainties regarding the quantification of the exact accumulation ratio, this dating method provides the ice dating with an error of nearly 10% (Schwander, 2006).

3. THESIS GOALS

The purpose of this thesis was the detection and assessment of D- and L- amino acids and phenolic compounds as climate change markers in polar ice. In this work were first performed the validation methods for D- and L- enantiomer amino acids and phenolic compounds followed by the quantitative analyses in Talos Dome and Renland ice samples. Moreover, with the purpose of detecting new climate change markers and to investigate eventual chemical transformations and oxidative processes, a qualitative analysis on glacial and interglacial period Talos Dome samples was performed.

A part of this thesis was dedicated to the optimization of the preconcentration method of several fatty acids and atmospheric markers through solid phase extraction and the applicability to snow samples from the Rendezvous ice core.

4. EXPERIMENTAL SECTION

4.1 REAGENTS AND STANDARD SOLUTIONS

The reagents and standard solutions employed during this thesis are listed below.

The ultra-grade methanol was purchased from Romil LTD (UK), formic acid used as an eluent additive for the HPLC system (≥98 %) was obtained from Fluka (Sigma Aldrich®, Switzerland), hydrochloric acid (HCl, 37%) was obtained from Carlo Erba. Ultrapure water (18,2 MΩ, 0.01 TOC) was produced by a Purelab Ultra System, supplied by Elga (UK). The amino acid solid standards (Sigma Aldrich®, purity ≥98 %) used for the preparation of each amino acid standard solution (D- and L-histidine, D- and L-alanine, D- and L-phenylalanine, D- and L-glutamic acid, D- and L-arginine, D- and L-asparagine, D- and L-aspartic acid, glycine, D- and L-glutamine, D- and L-isoleucine, D- and L-hydroxyproline, D- and L-leucine, D- and L-lysine, D- and L-methionine D- and L-ornithine, L-proline, D- and L-serine, D- and L- threonine, D- and L-tyrosine, D- and L- tryptophan, and D- and L-valine) were diluted in HCl 0.1M, whereas the methoxyphenol standard solutions (Sigma Aldrich®, purity ≥98 %) used for the preparation of each methoxyphenol standard (acetosyringone, vanillic acid, syringic acid, vanillin, isovanillic acid, sinapic acid, acetovanillone, ferulic acid, syringaldehyde and coniferaldehyde) were diluted in ultrapure water.

[^{13}C] labelled amino acids (purity 98 %) L-[1$^{3}C_3$] alanine, L-[$^{13}C_4$] aspartic acid, L-[$^{13}C_6$] arginine and

L-[$^{13}C_5$] glutamic acid) were purchased from Sigma Aldrich. L-[$^{13}C_1$] leucine, L-[$^{13}C_1$] proline, L-[$^{13}C_1$] phenylalanine, L-[$^{13}C_1$] valine and [^{13}C]-labelled methoxyphenols (valine and vanillic acid, purity ≥ 98 %) were supplied by Cambridge Isotope Laboratories Inc. (MA, USA).

The reagents and standard solutions used for the preconcentration analysis of atmospheric markers and fatty acids at the Department of Chemistry, University of Cambridge, were as follows.

The methanol, the water and the acetonitrile used as mobile phases are Optima® UHPLC-MS grade, purity > 99.9% (Fisher Scientific, Leicestershire, UK). The ammonium hydroxide and the formic acid were provided by Fluka (Sigma Aldrich®, Buchs, Switzerland), 1mL ampoules at 25% and 98%, respectively, LC-MS grade. The fatty acid and atmospheric marker standard solutions (BTCA, MBTCA, pimelic acid, terebic acid, salycilic acid, meso-erythritol, keto-pinic acid, methyl-tetrols, levoglucosan, cis-pinonic acid, pinolic acid, β-caryophillonic, β-nocaryophillonic, β-caryophillinic, lauric acid, myristic acid, arachidonic acid, palmitic acid, oleic acid, heptadecanoic acid, nonadecanoic acid, behenic acid, tricosanoic acid, heptacosanoic acid, octacosanoic, mellissic acid (Sigma Aldrich, purity > 99%), d3-malic acid*, d10-pimelic acid*, d4-salycilic acid*, d31-palmitic acid* (Cambridge Isotope Laboratories Inc. MA, USA) were diluted in UHPLC-MS grade water. The buffer solution was prepared with ammonium acetate (Sigma Aldrich, purity ≥ 99%) diluted in UHPLC-MS grade water.

4.2 QUANTITATIVE ANALYSES

The quantitative analyses executed during this work consisted in two steps: the validation of two analytical methods aimed to the quantification of phenolic compounds and D-/L- amino acids, and the subsequent application to quantitative analysis on Talos Dome and Renland ice core samples, as described below.

4.2.1 INSTRUMENTATION AND WORKING CONDITIONS

The instrument used to determine the analytes is an HPLC/ESI-MS/MS system that consists in Agilent 1100 Series HPLC Systems (Waldbronn, Germany) coupled with an API 4000 Triple Quadrupole Mass Spectrometer equipped with vacuum degasser and autosampler (Applied

Biosystem MSD SCIEX, Ontario, Canada) a binary pump, thermostated column compartment, operating with a TurboV electrospray source.

- D- and L- amino acid analysis

During the D- and L- amino acid analysis the electrospray source was set in positive mode. The optimization operation of the mass spectrometer Agilent 1100 Series HPLC System coupled with API 4000 Mass Spectrometer was performed selecting the best parameters such as to obtain a good selectivity. The optimization process led to the choice of the following parameters: temperature, 500 °C; ion spray voltage, 5.450 eV; entrance potential, 10 V; collision gas (*CAD*), 4 psi; curtain gas, 30 psi; GS1, 22 psi and GS2, 70 psi. An improvement of the sensitivity was possible optimizing parameters such as collision cell exit (*CXP*), collision energy (*CE*) and declustering potential (*DP*) through direct injection of 1 mg L^{-1} of each amino acid standard in source. The peak width of the first (*Q1*) and the third (*Q3*) quadrupole were set at 0.7± 0.1 amu at half peak height and at unit resolution. The first quadrupole selects the precursor ion and the third one selects the product ion. In the ***Table 1*** are summarized all the instrumental parameters for each D-/L- amino acid analyzed.

Amino acids		Elemental composition	Theoretical mass [M-H$^+$]	MRM transitions	DP	CE	CXP
Alanine	D-/L-Ala	$C_3H_7NO_2$	90.0550	90>44	32	17	7
Arginine	D-/L-Arg	$C_6H_{14}N_4O_2$	175.1190	175>70(116)	53(53)	33(21)	13(21)
Aspartic acid	D-/L-Asp	$C_4H_7NO_4$	134.0448	134>74(88)	34(34)	21(15)	13(13)
Glutammic acid	D-/L-Glu	$C_5H_9NO_4$	148.0604	148>84(130)	40(40)	24(14)	16(23)
Glycine	Gly	$C_2H_5NO_2$	76.0393	76>76(30)	33(33)	6(17)	11(4)
Hydroxyproline	D-/L-Hyp	$C_5H_9NO_3$	132.0655	132>68(86)	47(47)	31(21)	6(7)
Hystidine	D-/L-Hys	$C_6H_9N_3O_2$	156.0768	156>110(83)	46(46)	20(36)	20(15)
Leucine/Isoleucine	D-/L-Leu/Ile	$C_6H_{13}NO_2$	132.1019	132>86(69)	41(41)	15(26)	16(13)
Metionine	D-/L-Met	$C_5H_{11}NO_2S$	150.0583	150>104(133)	39(39)	15(15)	16(23)
Ornithine	D-/L-Orn	$C_5H_{12}N_2O_2$	133.0972	133>70(116)	45(45)	24(12)	11(15)
Phenylalanine	D-/L-Phe	$C_9H_{11}NO_2$	166.0863	166>120(103)	43(43)	18(38)	22(19)
Proline	L-Pro	$C_5H_9NO_2$	116.0706	116>70	42	24	13
Serine	D-/L-Ser	$C_3H_7NO_3$	106.0499	106>60(88)	34(34)	17(15)	10(16)
Thryptophan	D-/L-Trp	$C_{11}H_{12}N_2O_2$	205.0972	205>188(146)	53(53)	15(24)	17(13)
Tyrosine	D-/L-Tyr	$C_9H_{11}NO_3$	182.0812	182>165(136)	43(43)	15(21)	15(12)
Valine	D-/L-Val	$C_5H_{11}NO_2$	118.0863	118>72(55)	35(35)	17(30)	13(10)
Alanine*	L-[$^{13}C_3$]Ala	[$^{13}C_3$]H_7NO_2	93.0650	93(46)	37	19	8
Aspartic acid*	L-[$^{13}C_4$]Asp	[^{13}C4]H_7NO_4	138.0588	138>76(91)	42(42)	22(15)	7(10)
Arginine*	L-[$^{13}C_6$]Arg	[$^{13}C_6$]$H_{14}N_4O_2$	181.1391	181>74(121)	55(55)	21(21)	7(11)
Glutammic acid*	L-[$^{13}C_5$]Glu	[$^{13}C_5$]H_9NO_4	153.0772	153>135(106)	39(39)	13(19)	12(10)
Leucine*	L-[$^{13}C_1$]Leu	[$^{13}C_1$]$C_5H_{13}NO_2$	133.1052	133>86(44)	45(45)	16(31)	7(8)
Phenylalanine*	L-[13C1]Phe	[$^{13}C_1$]$C_8H_{11}NO_2$	167.0895	167>121(104)	51(51)	19(38)	11(10)
Proline*	L-[$^{13}C_1$]Pro	[$^{13}C_1$]$C_4H_9NO_2$	117.0739	117>70(68)	40(40)	24(41)	6(6)
Valine*	L-[$^{13}C_1$]Val	[$^{13}C_1$]$C_4H_{11}NO_2$	119.0895	119>72(55)	45(45)	18(29)	6(5)

Table 1 *– Summary of the theoretical masses, MRM transitions and the values of declustering potential (DP), collision energy (CE) and collision cell exit potential (CXP) for the analysis of D- and L-amino acids. In brackets are reported the values corresponding to the qualifier ion.*

A *CHIROBIOTIC TAG* column (2.1 x 250 mm, Advanced Separation Technologies Inc. USA) was used for the separation of the underivatized amino acids into D- and L- enantiomers. The operating conditions are as follows: flow rate was set at 200 µL min^{-1}, the column was maintained at 25 °C and the sample volume injected in the column was 10 µL. For the amino acid chromatographic separation, the mobile phase used consisted in the mobile phase A (0.1% formic acid) and in the mobile phase B (methanol containing 0.1% formic acid). In the amino acid determination procedure,

in order to elute most of the amino acids present, as a first step a mobile phase containing 30% of mobile phase B has been fluxed for 15 min. Subsequently, the composition of the mobile phase B was increased up to 100% and was maintained for over 5 min such as to clean the column from organic compounds and to elute some D- amino acids. This is an important step that lead to a greater stability and reproducibility in chromatographic separation. The equilibration step consisted in other 5 min of elution of 100% mobile phase B (Elena Barbaro et al. 2014). ***Table 1*** shows in detail the theoretical monoisotopic m/z value of each $[M + H]^+$ and $[M - H]^-$, the elemental composition, the mass accuracy and multi reaction monitoring (MRM) transitions for each amino acid in API 4000.

- Methoxyphenol compound analysis

For the methoxyphenol compound analysis the electrospray source was set in negative mode and the data was collected by multiple reaction monitoring (MRM) with a 50 ms dwell time. In order to evaluate the sensibility, a direct infusion of a standard solution of methoxyphenols of 1 ng μL^{-1} using a syringe pump (Model "11", Harvard Apparatus Inc., Holliston, MA, U.S.A) was performed. The instrumental conditions applied are as follows. The source temperature for the ESI source was 650°C; the pressure was 45.00 psi for the Nebulizer gas 60.00 psi for the auxiliary gas, 25 psi for the curtain gas and 6.00 psi for the collision gas; the ionization voltage was -4450 V. The collision energy (*CE*), the declustering potential (*DP*) and the collision cell exit potential (*CXP*) were optimized for the purpose of achieving the highest sensitivity possible. In the ***Table 2*** are summarized all the instrumental parameters for each methoxyphenol compound analyzed.

Methoxyphenols		Elemental composition	Theoretical mass [M-H$^+$]	MRM transitions	DP	CE	CXP
Vanillic acid	VA	$C_8H_8O_4$	167,0350	167>152(108)	-51(-51)	-19(-28)	-10(-9)
Vanillin	VAN	$C_8H_8O_3$	151,0401	151>136(92)	-54(-54)	-19(-27.5)	-11(-6)
Acetovanillone	VAC	$C_9H_{10}O_3$	165,0557	165>150(122)	-46(-46)	-19(-30)	-10.5(-9.5)
Homovanillic acid	HA	$C_9H_{10}O_4$	181,0506	181>151(122)	-48(-48)	-10.2(-23)	-11(-5)
Syringic acid	SyA	$C_9H_{10}O_5$	197,0455	197>182(121)	-47(-47)	-16(-22.7)	-15(-8.5)
Syringic aldehyde	SyAH	$C_9H_{10}O_4$	181,0506	181>166(151)	-42(-42)	-18(-25)	-12(-12)
p-Coumaric acid	PA	$C_9H_8O_3$	163,0401	163>119(93)	-52(-52)	-17(-42)	-8(-7)
Sinapic acid	SA	$C_{11}H_{12}O_5$	223,0612	223>164(149)	-52(-52)	-19(-27)	-15(-12)
Ferulic acid	FA	$C_{10}H_{10}O_4$	193,0506	193>178(134)	-42(-42)	-18(-21)	-11(-12)
Acetosyringone	SyAC	$C_{10}H_{12}O_4$	195,0663	195>180(165)	-53(-53)	-18(-27)	-13.5(-12)
[^{13}C]-Vanillin	[^{13}C]-VAN	[$^{13}C_6$]$C_2H_8O_3$	158,0674	157>142(97)	-54(-54)	-19(-28)	-8(-9)
[^{13}C]-Vanillic acid	[^{13}C]-VA	[^{13}C]$C_7H_8O_4$	169,0454	168>153(108)	-51(-51)	-19(-28)	-12(-9)

Table 2 *– Summary of the theoretical masses, MRM transitions and the values of declustering potential (DP), collision energy (CE) and collision cell exit potential (CXP) for phenolic compounds. In brackets are reported the values corresponding to the second transition.*

The column employed for methoxyphenol compound analysis is Synergi™ 4 µm Hydro-RP 80 Å, LC Column 3 x 2.1 mm supplied by Phenomenex®. The column was maintained at 25°C with a flow rate of 200 µL min^{-1}, the injection volume was 100 µL. The chromatographic run for methoxyphenol compound analysis was set in order to optimize the elution and the separation, paying particular attention to peak selectivity and resolution. Hence, the chromatographic run started with 20% of mobile phase B, increased up to 70% in the first minute and up to 100% in the following 5 min and maintained for further 2 minutes. Mobile phase B is decreased to 20% in 1 minute and has been fluxed for 7 min isocratically to wash the column from any remaining residuals of methoxyphenols. In the table below are shown in detail the instrumentation value of each [M + H]$^-$, the elemental composition, the mass accuracy and multi reaction monitoring (MRM) transitions for each phenolic compound analyzed in API 4000.

4.2.2 AMINO ACIDS AND PHENOLIC COMPOUNDS: Method validation

4.2.2.1 Chromatographic separation

An efficient enantiomeric separation is the mean issue of several works dealing with D- and L- amino acid separation. The separation method consists in the formation of diasteroisomers in conventional reversed-phase column with chiral reagents. Subsequently occurs the separation of the diastereoisomers formed in the column. In several works, efforts have been made to construct a stationary phase in order to achieve the best chromatographic performance in terms of enantiomeric selectivity and resolution. As a result of these efforts, a column with a stationary phase based on *teicoplanin aglycone* was made, which is the most selective column compared to other teicoplanin stationary phases and with higher resolution. This column, commercially known as *CHIROBIOTIC TAG*, based on covalently bonding macrocyclic glycoproteins to a high purity, (Sigma-Aldrich) is the most suitable column to employ in a HPLC-MS system which permits to separate chiral compounds without any previous derivatization because of the use of a volatile mobile phase with a high percentage of organic solvent (Berthod et al. 2000). As the chemical characteristics of amino acids differ, the required mobile phase composition must change for neutral, acid or basic compounds. A further improvement of enantiomeric separation is obtained using an alcoholic mobile phase

In order to exploit the highest performances of the instrument and to obtain the best enantioselectivity and peak resolution of amino acid chromatographic separation, were tested four different compositions the mobile phase using 10, 20, 30 and 40 % of eluent B. The test was performed considering retention time, peak width, enantioselectivity and resolution for each L- and D- amino acid, as shown in detail in Barbaro et al., 2014. The best enantioselectivity and the highest resolution for most of amino acids was achieved with a composition of 40% of eluent B. However, as in these conditions has occurred a peak enlargement of some D- amino acids such as D- arginine and D- lysine (Barbaro et al., 2014), for the chromatographic separation was preferred a starting composition of 30% of eluent B. It was not possible to separate leucine and isoleucine isomers using the teicoplanin aglycone stationary phase but it is possible using a CHIROBIOTIC T column (Petritis et al., 2001).

For the chromatographic separation of methoxyphenol compounds was used a C18-stationary phase column with polar endcapping recommended for the separation of weakly hydrophobic

compounds which was found to lead best chromatographic separation. Were tested other two types of chromatographic columns: Synergi™ 2.5 µm Fusion-RP 100 Å the stationary phase of which consists in a polar embedded C18 with TMS endcapping, recommended for separation of mixtures with polar or non-polar compounds, and Luna® 3µm C18(2) 100 Å provided with a C18 with TMS endcapping stationary phase. The chromatograms resulting from the chromatographic analysis employing the last two columns resulted less selective for the methoxyphenol compounds analyzed.

4.2.2.2 Quality control

The quality control was performed assessing parameters such as the sensitivity of the analysis, the reproducibility, the accuracy and the matrix effect (ME). One of the principal concerns of these analysis is the presence of matrix components that may affect the accuracy, as they may cause enhancement or suppression of ion intensity, consequently, enhancement or suppression of the signal (Kebarle & Tang, 1993; King et al., 2000). Mechanistic investigation of ionization suppression in electrospray). Matuszewski et al. suggest a method based on the internal standard to evaluate and to counteract the matrix effect. According to this method, the procedure of matrix effect (ME) assessment was performed calculating the matrix effect for each analyte as shown in ***Eq. 1***. In order to assess the method and the matrix effect, as reported in (Boyd, Basic, and Bethem 2011), two calibration curves for each analyte were constructed: one in ultrapure water and in one real matrix. A valuation of the matrix effects for the analysis in HPLC-MS system for amino acids and methoxyphenol compounds was performed.

$$\text{ME (\%)} = (\text{signal of standard in a matrix} / \text{signal of standard in ultrapure water}) \times 100 \quad \textbf{(Eq. 1)}$$

A value of 100% signifies that no matrix effect is observed, instead values less and greater than 100% indicates respectively a suppression and an enhancement of the ionization.

The consecutive step was the assessment of the matrix effect behavior using an internal standard, calculated as the ratio between the signal of the response of each amino acid and methoxyphenol compound with internal standard in the matrix and the signal of the response of the analyte with

internal standard in ultrapure water. Internal standards are ^{13}C-labelled isotopomers that were used to be compared with the analyte peak area. In the case of amino acid analysis, the isotopomers used were eight ^{13}C-labelled amino acids, whereas for methoxyphenols the internal standards used were labelled vanillic acid (VAH*) and labelled vanillin (VA*). For each analyte was chosen the isotopomer which led to better results in terms of error percentage (E%). The validation method was performed only for low concentrations, as in a previous work performed in Antarctic subglacial lake samples (Elena Barbaro et al. 2014) are reported relatively low concentrations of amino acids.

As shown in ***Table 3*** and ***Table 4***, we observed both suppression and enhancement of the matrix effect for several analytes, represented by ME% values. Using the analytical method that employs internal standards, indicated in the column IS, we observed that the matrix effect percentage in most cases was improved, in some cases slightly and in others more markedly. The successive phase executed in order to determine the accuracy of the method consisted in the determination of an error percentage (E%), determined, as follows, calculating how much the determined value (Q) deviate from the true one (T):

$$E(\%) = (Q-T)/T \times 100 \qquad (\textbf{Eq. 2})$$

As can be seen from the table below, a very high improvement is obtained in terms of error percentage (**E%**), leading to values much lower than the values obtained with external calibration curve. It was not possible to conduct an analysis of glutamine (Gln) and lysine (Lys) in the triple quadrupole instrument employed in this study because the chromatographic separation was not possible and their different exact masses didn't allow a quantification using the full scan HRMS method, as this method can separate the target compound that have the same nominal mass but a different exact mass from the background.

As seen in the tables below, the internal standard method enhances the accuracy of both analytical methods providing error percentages lower than the error provided by the quantification estimated without internal standard. Indeed, for most of the analytes considered in this study the error percentage of the quantification calculated with calibration curve constructed in ultrapure water and in real matrix is much higher than the error percentage resulting from the calibration curve with

internal standard. The higher values of error percentage calculated using the external calibration curve without internal standard are verified due to ionization suppression assessed through matrix effect quantification, which lead to a misleading quantification of the analytes. In our study, was observed a suppression of the ionization for some analytes during the determination of the matrix effect using the calibration curve obtained as described above.

Amino acids	IS	Calibration curve	ME% for AA	ME% for AA/IS	E% external synthetic calibration curve	E% method of standard additions	E% Internal standard method
L-Ala	Ala*	500 ppt	78	77	-8	89	-5
		1 ppb	98	98	2	25	-9
		5ppb	117	117	9	0	-10
D-Ala	Ala*	500 ppt	42	45	-57	-16	7
		1 ppb	41	42	-55	-8	5
		5ppb	43	45	-57	-9	-10
L-Asp	Asp*	500 ppt	108	112	151	-627	3
		1 ppb	106	113	107	-277	-2
		5ppb	106	110	65	-9	-10
D-Asp	Asp*	500 ppt	72	75	39	-209	-5
		1 ppb	100	109	9	-91	-8
		5ppb	103	112	14	-40	13
L-Arg	Arg*	500 ppt	99	83	-33	375	-2
		1 ppb	109	96	-44	153	-4
		5ppb	101	81	-34	0	-2
D-Arg	Arg*	500 ppt	129	109	-74	-5	-4
		1 ppb	165	135	-61	-32	-1
		5ppb	130	105	-31	-38	1
L-Leu	Arg*	500 ppt	111	93	1	-330	-10
		1 ppb	108	88	-1	-165	-7
		5ppb	101	63	78	30	13
D-Leu	Arg*	500 ppt	122	103	-18	-112	-10
		1 ppb	103	90	-30	-85	-9
		5ppb	76	62	2	-24	6
GLY	Ala*	500 ppt	50	50	33	-148	1
		1 ppb	90	90	18	-73	-6
		5ppb	56	56	46	10	-4
L-HYS	Arg*	500 ppt	119	84	-21	-233	-8
		1 ppb	129	82	-28	-132	-12
		5ppb	120	80	-22	-38	-9
L-PHE	Arg*	500 ppt	128	108	89	-472	-10
		1 ppb	112	98	65	-210	-9
		5ppb	109	106	52	5	-9
L-ORN	Arg*	500 ppt	87	73	8	206	9
		1 ppb	103	90	-24	68	-9
		5ppb	104	100	-26	-12	1
L-THR	Arg*	500 ppt	113	95	18	-55	-9
		1 ppb	102	89	6	-32	-6
		5ppb	101	98	3	-4	-1
L-TYR	Arg*	500 ppt	111	93	28	-126	-13
		1 ppb	100	88	13	-66	-6
		5ppb	100	97	13	-4	-5
L-GLU	Glu*	500 ppt	105	140	46	-338	-9
		1 ppb	102	131	24	-168	-3
		5ppb	94	114	9	-29	1
L-Val	Val*	500 ppt	100	100	62	-295	3
		1 ppb	100	100	50	-127	-1
		5ppb	102	102	29	-7	-7
L-PRO	Pro*	500 ppt	98	93	61	-398	-9
		1 ppb	99	96	61	-165	-9
		5ppb	111	106	50	7	-14
L-4-HYP	Pro*	500 ppt	114	108	160	-611	-8
		1 ppb	101	97	128	-259	-12
		5ppb	148	142	117	33	-8

Table 3 *– Matrix effect (ME%) and error percentage (E%) calculated with external synthetic calibration curve and with the internal standard method for amino acid compound analytical method.*

PCs	IS	Calibration curve	ME% for PCs	ME% for PCs/IS	E% external synthetic calibration curve	E% method of standard additions	E% Internal standard method
VA	VAN*	20 ppt	135	130	4	6	1
		1 ppb	103	103	5	8	2
		5ppb	98	103	5	7	3
VAN	VA*	20 ppt	147	147	-83	-83	-4
		1 ppb	99	100	-7	-7	-1
		5ppb	96	98	-2	-3	-2
VAC	VA*	20 ppt	119	119	-27	0	-6
		1 ppb	100	101	4	50	0
		5ppb	100	102	10	59	2
HA	VA*	50 ppt	109	106	13	17	6
		1 ppb	92	92	2	5	-8
		5ppb	99	101	5	8	1
SyA	VAN*	50 ppt	104	100	12	14	0
		1 ppb	97	97	1	2	-3
		5ppb	96	100	4	5	0
SyAH	VAN*	20 ppt	122	118	23	-18	1
		1 ppb	95	95	71	13	-6
		5ppb	97	100	69	12	-9
PA	VA*	50 ppt	105	102	-22	-21	-46
		1 ppb	101	102	12	14	-1
		5ppb	97	99	10	13	-1
SA	VA*	50 ppt	89	87	-32	-27	-40
		1 ppb	91	92	10	17	-10
		5ppb	94	96	13	20	-5
FA	VA*	50 ppt	109	107	-15	-14	-26
		1 ppb	98	99	22	24	-3
		5ppb	99	101	20	22	0
SyAC	VA*	50 ppt	105	103	22	24	3
		1 ppb	93	93	8	10	-7
		5ppb	101	103	10	12	3

Table 4 *- Matrix effect (ME%) and error percentage (E%) calculated with external synthetic calibration curve and with the internal standard method for methoxyphenol compound analytical method.*

The calibration curves were made using standard solutions of each analyte (amino acids and methoxyphenols) at concentrations ranging between 0.005 and 500 µg L^{-1} prepared in ultrapure water. Likewise, were prepared internal standard solutions at final constant concentration of 1 µg L^{-1}. Using these calibration curves, it was possible an assessment of the degree of closeness of the results obtained to the true value, in order to ensure the applicability of this analytical method to real samples. With the aim of performing this assessment, linearity range, slope, intercept and correlation coefficients were considered. In the ***Table 5*** and ***Table 6*** are shown the linearity range, the correlation coefficient (R^2), the limit of detection (*LOD*) and the limit of quantification (*LOQ*). *LOD* and *LOQ* values were obtained according to Bliesner (Bliesner 2006) who defines *LOD* as three times the signal-to-noise ratio of a known amount of a target compound present in a standard solution, and *LOQ* as ten times. The correlation coefficient, obtained plotting the ratio between the

concentrations of native and labelled analytes vs. the ratio between the relative peak areas, has a value of $R^2 \geq 0.97$, which states a good quality of the calibration curves.

Name	Sigle	IS	Slope	Intercept	R^2	Min ($\mu g\ L^{-1}$)	Max ($\mu g\ L^{-1}$)	LOD[1] ($\mu g\ L^{-1}$)	LOQ[1] ($\mu g\ L^{-1}$)
L-Alanine	L-Ala	Ala*	0,95	0,7	0,985	0,006	22,3	0,02	0,05
D-Alanine	D-Ala	Ala*	1,13	0,7	0,985	0,005	46,5	0,4	1,0
L-Arginine	L-Arg	Arg*	42,81	2,5	0,991	0,004	89,3	0,01	0,02
D-Arginine	D-Arg	Arg*	37,67	-25,1	0,996	0,005	101,5	0,1	0,3
L-Aspartic acid	L-Asp	Asp*	0,76	1,0	0,995	0,007	141,0	0,08	0,2
D-Aspartic acid	D-Asp	Asp*	0,27	-0,2	0,982	0,005	102,5	0,07	0,2
L-Glutamate	L-Glu	Glu*	1,54	0,2	0,993	0,007	132,5	0,004	0,01
D-Glutamate	D-Glu	Glu*	8,60	-6,3	0,992	0,005	98,0	0,05	0,2
Glycine	Gly	Ala*	1,78	2,7	0,962	0,005	16,9	0,08	0,3
L-Hydroxyproline	L-Hyp	Pro*	0,23	0,1	0,998	0,007	26,8	0,007	0,02
D-Hydroxyproline	D-Hyp	Pro*	0,72	0,0	0,998	0,005	21,8	0,08	0,2
L-Hystidine	L-Hys	Arg*	13,68	1,5	0,998	0,005	102,1	0,005	0,02
D-Hystidine	D-Hys	Arg*	10,47	2,8	0,996	0,006	118,5	0,01	0,04
L-Leucine/Isoleucine	L-Leu/Ile	Arg*	9,34	44,9	0,967	0,010	206,0	0,01	0,04
D-Leucine/Isoleucine	D-Leu/Ile	Arg*	15,09	46,9	0,983	0,011	211,0	0,006	0,02
L-Methionine	L-Met	Arg*	39,28	57,8	0,983	0,005	109,0	0,07	0,2
D-Methionine	D-Met	Arg*	36,96	16,7	0,992	0,005	107,5	0,8	2
L-Ornitine	L-Orn	Arg*	28,84	62,5	0,985	0,006	119,5	0,2	0,6
L-Phenilalanine	L-Phe	Arg*	93,64	355,3	0,970	0,009	173,5	0,01	0,03
D-Phenilalanine	D-Phe	Arg*	160,65	243,5	0,982	0,005	105,0	0,04	0,1
L-Proline	L-Pro	Pro*	0,69	0,6	0,965	0,005	21,0	0,008	0,02
L-Threonine	L-Thr	Arg*	17,85	42,8	0,988	0,009	182,5	0,005	0,02
D-Threonine	D-Thr	Arg*	25,32	23,9	0,992	0,006	126,0	0,009	0,03
L-Tyrosine	L-Tyr	Arg*	54,71	65,8	0,987	0,004	85,5	0,01	0,05
D-Tyrosine	D-Tyr	Arg*	57,64	71,0	0,989	0,006	112,5	0,01	0,4
L-Valine	L-Val	Val*	0,99	0,4	0,992	0,005	20,6	0,004	0,01
D-Valine	D-Val	Val*	11,04	2,0	0,994	0,005	20,4	0,06	0,2

(1) Barbaro et al., 2014

***Table 5** – Linear equation terms, linearity range, LOD and LOQ values of the calibrations curves for amino acids*

Name	Sigle	IS	Slope	Intercept	R^2	Min ($\mu g\ L^{-1}$)	Max ($\mu g\ L^{-1}$)	LOD ($\mu g\ L^{-1}$)	LOQ ($\mu g\ L^{-1}$)
Acetovanillone	VAC	VA*	1,2875	0,0332	0,999	0,006	1,2	0,003	0,010
Homovanillic acid	HA	VA*	40,434	302,64	0,999	0,03	21,8	0,003	0,01
Syringic acid	SyA	VA*	0,917	0,0023	0,999	0,006	1,1	0,001	0,005
Syringic aldehyde	SyAH	VAN*	0,9756	0,0568	0,997	0,006	11,4	0,002	0,006
p-Coumaric acid	PA	VA*	0,7358	0,0141	0,997	0,007	1,3	0,002	0,006
Sinapic acid	SA	VAN*	0,7135	0,0032	1,000	0,006	5,9	0,001	0,003
Ferulic acid	FA	VA*	3,1038	0,0356	0,999	0,006	1,1	0,001	0,003
Acetosyringone	SyAC	VA*	0,914	0,0065	0,998	0,006	1,2	0,003	0,009

***Table 6** - Linear equation terms, linearity range, LOD and LOQ values of the calibrations curves for methoxyphenol compounds.*

4.2.3 QUANTITATIVE ANALYSIS OF AMINO ACIDS AND PHENOLIC COMPOUNDS IN TALOS DOME

4.2.3.1 Talos Dome site

Antarctica is the biggest cold desert on Earth (Bargagli, 2005) with the presence of small ponds and lakes created from melting ice and snow during a few weeks in austral summer. The Talos Dome ice core has been subject to several analyses in our laboratories and other institutes such as the aeolian dust (Delmonte et al. 2010) investigating the variability and the provenance; the research of traces of volcanic activities in the late Quaternary period (Narcisi et al., 2010); analysis of nitrate, *MSA* (methanesulfonic acid), sodium, calcium and sulfate salts (Poluianov et al., 2014), analysis of $\delta^{18}O$ as a proxy of local temperature (Stenni et al., 2011); study of snow precipitation in the Talos Dome summit in terms of provenance and dynamic conditions (Scarchilli et al., 2011), etc.

Most of the work of this thesis was focused on the qualitative and quantitative analyses of Talos Dome ice core samples. This core is part of **TAL**os **D**ome **I**ce **C**or**E** (**TALDICE**), which is a European deep ice core research project led from Italy and involves other four European nations: France, Germany, Switzerland and United Kingdom. The purpose of this project is to drill a deep ice core in the Talos Dome (72°48'S; 159°06'E), a peripheral dome of East Antarctica with an altitude of 2318 m, in the Ross sea sector, in order to reach back the last two interglacial periods. The high resolution of the last 40 thousand years allows to have a good description of the climate during the Holocene, including the last interglacial period, and a description of the ***LGM*** (last glacial maximum, 26.50 thousand years BP), whereas the resolution of the older part of the ice core is lower (*www.taldice.org*). The drilling site is located about 250 km from the Ross Sea and about 290 km from the Southern Ocean, feature that attributes to the site a particular relevance, as its climate can be affected by these two marine areas. Furthermore, most of the North-West area of the Talos Dome lies below sea level, therefore the climate in this region is more sensitive to climate fluctuations compared to the rest of the East-Antarctic area (Frezzotti et al., 2004; Roland Warner, 1998). Another important feature of the Talos Dome site which increases the interest related to this region, is the snow accumulation; in the last 8 hundred years, it occurred an accumulation rate of ice equivalent per year of 80 kg m^{-2} y^{-1}. This value is higher than the rest of the East Antarctic Plateau due to the position of the site near coastal areas (Stenni et al., 2002; Urbini et al., 2006). Another characteristic reported in the work (Frezzotti et al., 2004) is the mean temperature of -41°C measured at 15 m deep; this temperature is expected to be even the annual mean surface temperature assuming that the temperature doesn't exceed 0°C during the summer. According to

the calculations performed by Frezzotti and others in (Frezzotti et al., 2004), the temperature of the ice near the bedrock is likely to be -20°C and no basal melting has ever occurred. In the same work is reported that the temperature is highly correlated to the height and the decrease in temperature shows a *super-adiabatic* gradient of 2.5°C (100 m)$^{-1}$. Instead, it has been shown a *sub-adiabatic* laps rate in the mountainous region in Victoria Land at 10 m of depth (0.5°C (100 m)$^{-1}$, Stenni et al., 2000) and in the traverses from Dumont d'Urville and Terra Nova to Dome C (1.0°C (100 m)$^{-1}$, Frezzotti and Flora, 2002; Magand et al., 2004). The quite different temperature gradient in the Talos Dome in comparison to the surrounding regions suggests the presence of calm atmospheric conditions with a high temperature inversion during wintertime. The snow accumulation in this region is due to the presence of katabatic winds in the whole Talos Dome area which blow mainly upwind in the South/South-Est direction before they change direction downwind, as shown in ***Figure 5***. Therefore, we can presume that the surface slope can control, in some sense, the wind direction and consequently even the wind-driven sublimation processes, having a huge impact on surface mass balance and on snow precipitation increasing or decreasing snow accumulation on short and medium spatial scales (from tens of meters to kilometers). This means that wind processes, consequently also the slope variations, have to be considered during the choice of a good drilling site (Frezzotti et al., 2004; Frezzotti et al., 2004b) even though it has been shown in the work (Urbini et al., 2008) that the distribution of snow accumulation in the Talos Dome region is not properly centered in the dome and that the accumulation gradient windward has decreased in the last centuries.

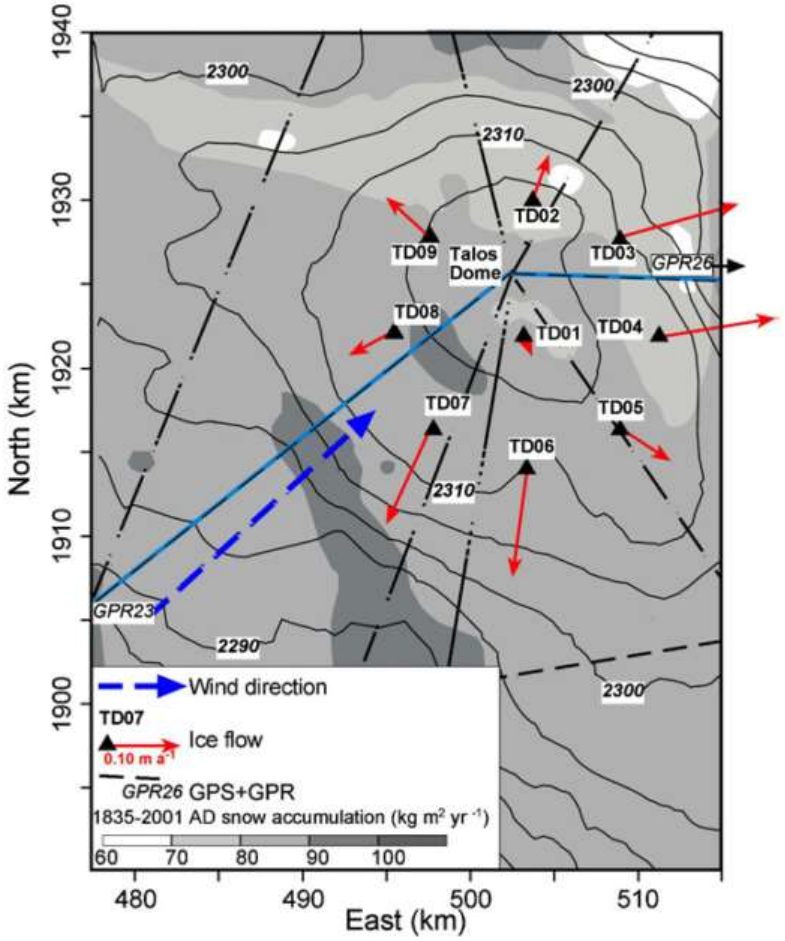

Figure 5 *– Snow accumulation (kg m^{-2} yr^{-1}) map in Talos Dome based on snow radar data. The dotted lines indicate the snow radar profiles, the red arrows represent the vector ice velocity and the blue arrows the prevalent wind direction. The lines representing the surface topography have a 5 m interval* (Urbini et al. 2008).

BEFORE TALDICE DRILLING PROCESS

The exact position of the drilling site was a decision made after several **R**adio **E**cho **S**ounding (**RES**) measurements performed during Antarctic expeditions in 1997, 1999, 2001 and 2003. ***RES*** is a method that uses electromagnetic waves and provides information about ice thickness, bedrock morphology and ice inhomogeneities. These measurements are crucial to determine the ice thickness of Talos Dome, as well as the sub glacial morphology, basal conditions, internal ice structure and internal dynamics. Another fundamental feature of the inner ice detected with RES is the disturbance from the ice flow. Is very important for ice-core drilling processes to perform the core drilling in an area where the ice core is not perturbed by significant ice flow, in order to provide a good quality ice core, able to give reliable results (Reeh, Johnsen, and Dahl-Jensen 1985). Therefore, it was necessary an exploration in terms of morphology of the Talos Dome site before

the ice core drilling. The first expeditions made in 1995, 1997 and 1999 were focused mainly in the morphology and the bottom surface of the whole glacier ice tongue of East Antarctic plateau. It has been found that many of the bottom surface in this region is not flat but irregular and slightly sloped. This kind of morphology is consistent with ablation processes occurred. In the same way, processes like the sea-water circulation and physical proprieties such as viscosity, temperature, etc., correlated to ablation processes can be involved in the formation of this kind of structure of the bottom (Bianchi et al., 2001). In 2001 and 2003 there have been other two expeditions in order to provide a better resolution of ice thickness of a more restricted area, as well as a better bottom morphology and internal layer profile. As mentioned above, the bedrock lying under the dome summit is slightly rippled, thus the last two expeditions were essential to select the best drilling site in Talos Dome, since a regular snow layering is an indication of a good time-depth core correlation. For the expedition made in 2003 there have been made further technical improvements as during the expedition in 2001 was not possible to detect continuously internal ice layers. During these measurements were not found evidences of the presence of basal melting or subglacial lakes. Thanks to this work and using an accurate elevation model, we know that the ice thickness in the Talos Dome region subjected to ***RES*** measurements varies from 800 m to 2900 m. The bedrock in the Talos Dome summit is a relatively low bedrock zone which has an altitude of about 440 m a.s.l and is covered by approximately 1900 m of ice.

The bottom of the summit being rippled and inhomogeneous, makes this site inappropriate for ice core drilling. For this reason, has been identified in the South-East direction at 5-6 km far a new site (**ID1**, 159°11'00"E; 72°49'40"S, ***Figure 6***) where the bedrock is relatively flat (Urbini et al., 2006). This was a very important work that provided extremely precious information about this site making possible a preliminary evaluation of Talos Dome topography and ice thickness. It suggested and also gave indications of a new drilling site that a few years later became one of the most important drilling sites for paleoclimatic studies which started with and belongs to the TALDICE project drilling campaign.

In the picture below are shown the aircraft legs, for a total of 20 legs, computed in 1999 (dotted line) and 1997 (continuous line) from Italian Antarctic expeditions during which the INGV-IT digital radar, developed from *Istituto Nazionale di Geofisica e Vulcanologia* (**INGV**) and University of Milan (Tabacco et al., 2002), was brought on board and linked to a global positioning system (GPS). In the aircraft wings were positioned two dipole antennas, one for the transmission of the signal and the other for back-signal reception of echo pulses (Bianchi et al., 2001; Tabacco et al., 1999).

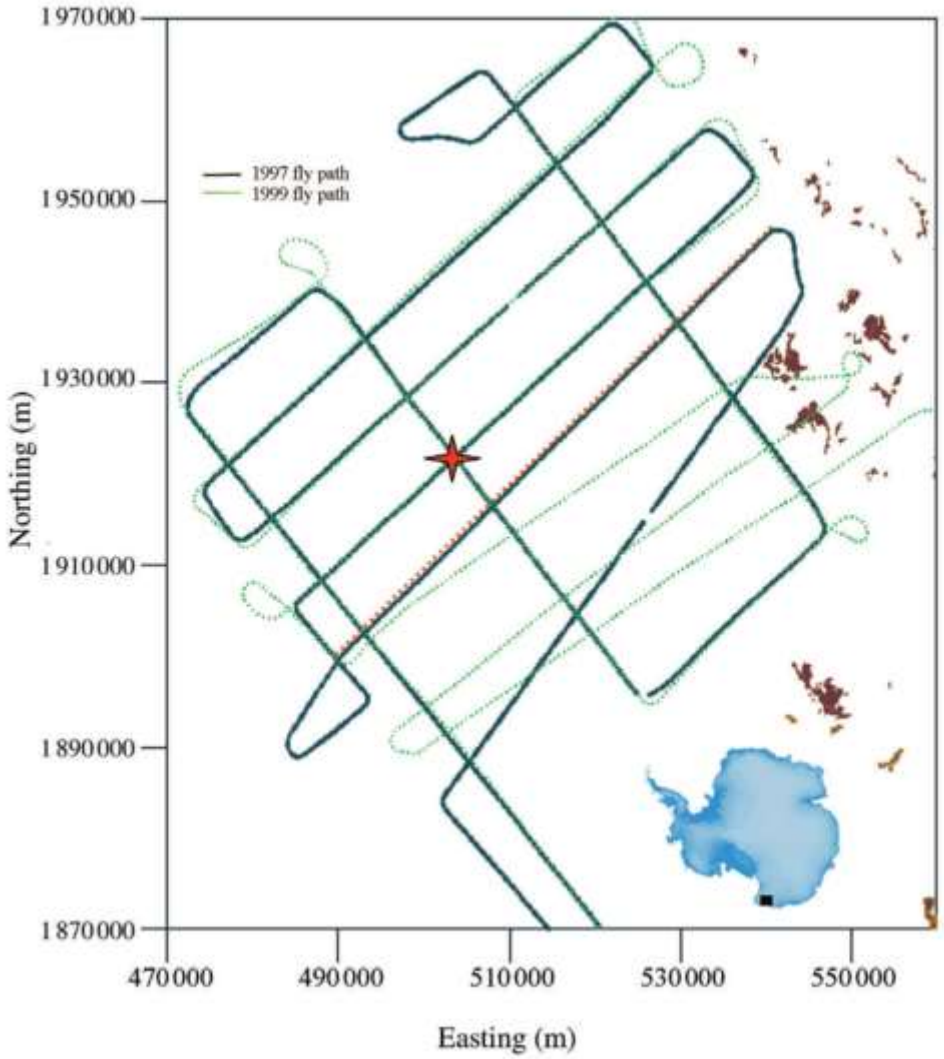

Figure 6 *– Flight paths on East Antarctica of the aircraft during the RES measurements referred to the 1997 Italian Antarctic expedition (dotted line) and 1999 (continuous line). The Talos Dome site is indicated with the red star, the mountains (on the right) are indicated with brown dots* (Bianchi et al., 2003).

In the **Figure 7** is shown an example of ice thickness measurement, made possible assuming that the electromagnetic wave propagation is a constant value. As a matter of fact, these values were carried out from pure ice laboratory measurements, the details of which are reported in the work of *Bianchi et al., 2003*. These assumptions made possible the conversion of time delay (μs) into ice thickness using the wave propagation velocity in the ice and in the air, considering that the distance of the aircraft from the surface of the Talos Dome was constantly 300 m. In the plot reported in the figure (*amplitude vs. time*) there are three main peaks indicated with A_0, A_1 and A_2: with A_0 is indicated the amplitude of the transmitted signal, with A_1 the amplitude of the reflected pulse from the surface of the ice and with A_2 the amplitude of the signal reflected from the bedrock.

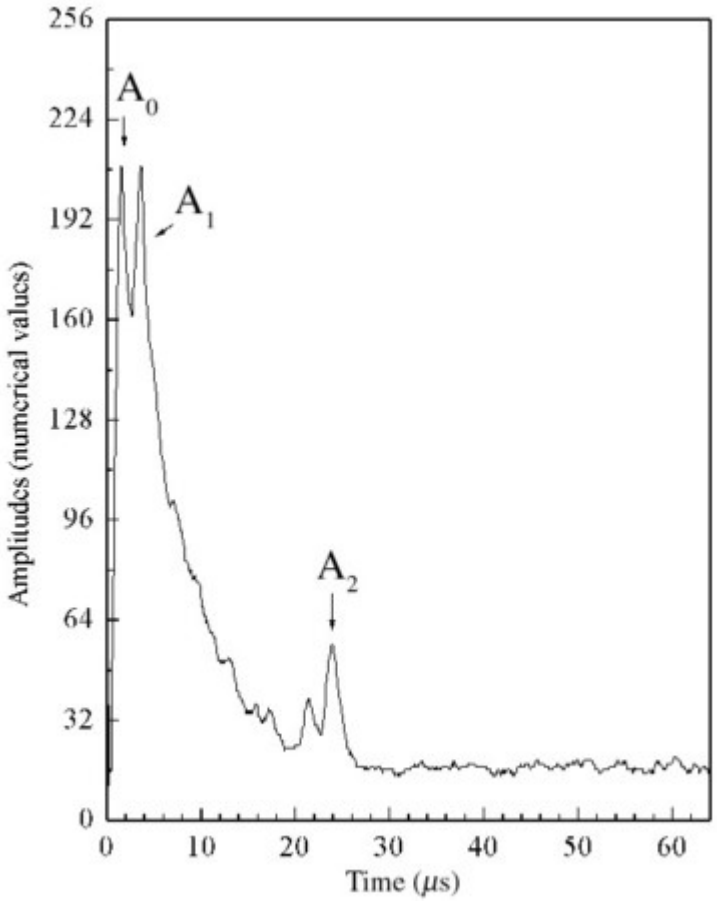

Figure 7 *– Measurements (time vs. amplitude) performed during the expedition at Talos Dome in 1999. The three main peaks A_0, A_1 and A_2 represent respectively the amplitude of the signal transmitted, the amplitude of the pulse reflected from the ice surface and the bedrock echo. The other small peaks are caused due to the density variations and the presence of layers in the internal ice* (Bianchi et al., 2003)*.*

In the following figure are reported the two aircraft legs of the Italian Antarctic Expeditions in 2001 and 2003. **ID1** indicated by the black square is the drilling site selected after the RES measurements and the site that became the main position for TALDICE project for ice coring.

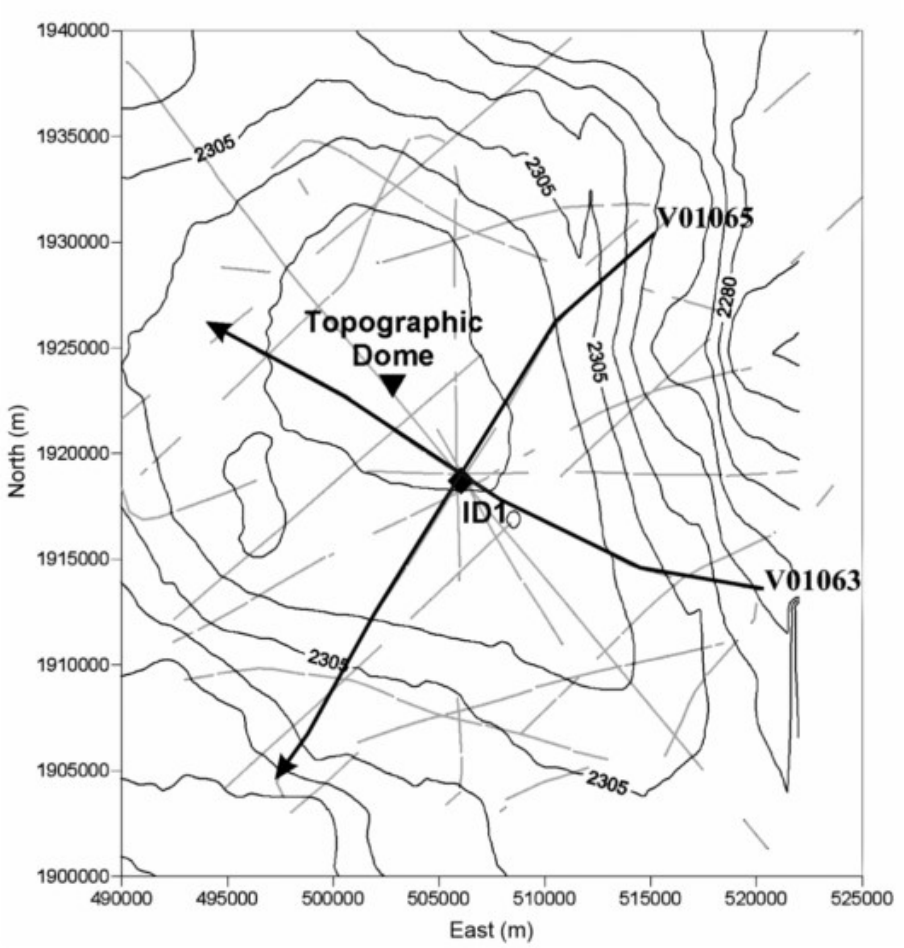

Figure 8 *– Flight paths on East Antarctica during Italian Antarctic RES expeditions during 2001 (black lines) and 2003 (light grey lines).* ***ID1*** *is the position of the drilling site selected. The geographic position of Talos Dome is indicated by a triangle.*

THE DRILLING PROCESS

Most of the Talos Dome ice core has been drilled during the austral summers of 2006 and 2007 and has been concluded at December 2007 for a total length of 1620.20m.

The TALDICE project started its activity the 14th of December in 2004, during the 20th Italian Antarctic Expedition. After setting up the working site and digging a groove 4m deep and 50m long used for the drilling process, the 5th of January 2005 started officially the drilling campaign of TALDICE. As a first step, the purpose of the project was to drill the upper 96 meters starting from 4.5m depth and to insert a tube in the ice in order to preserve the impermeability of the snow layer. Subsequently, it has been performed the bore with a diameter of 239 mm needed as a path for the drilling instruments. The first measurements made to the core were the dielectric properties (DEP) and the

density. The ice cores up to 480 m long were cut every 1 m length (bag). The core portions were sealed, signed and placed in proper boxes. During the drilling process made in 2006/2007 a depth of 1300.58 m has been reached. The ice core sections from 479 m to 667 m and from 1002 m to 1300 m has been cut in pieces of 1 m then sealed and signed. The remaining ice cores were stocked in the Talos Dome.

In 2007 the drilling process continued up to 1620.20 m of depth, reaching near the closeness of the bedrock and completing the mission of the project. In the same way, once the drilling operations were finished, the ice cores from 1300 m to 1600 m were cut in portions of 1 m. The last 20 m have been cut in portions of 50 cm and stocked. In the ***Figure 9*** is reported the progress of the ice coring during the drilling campaign in 2005-2007.

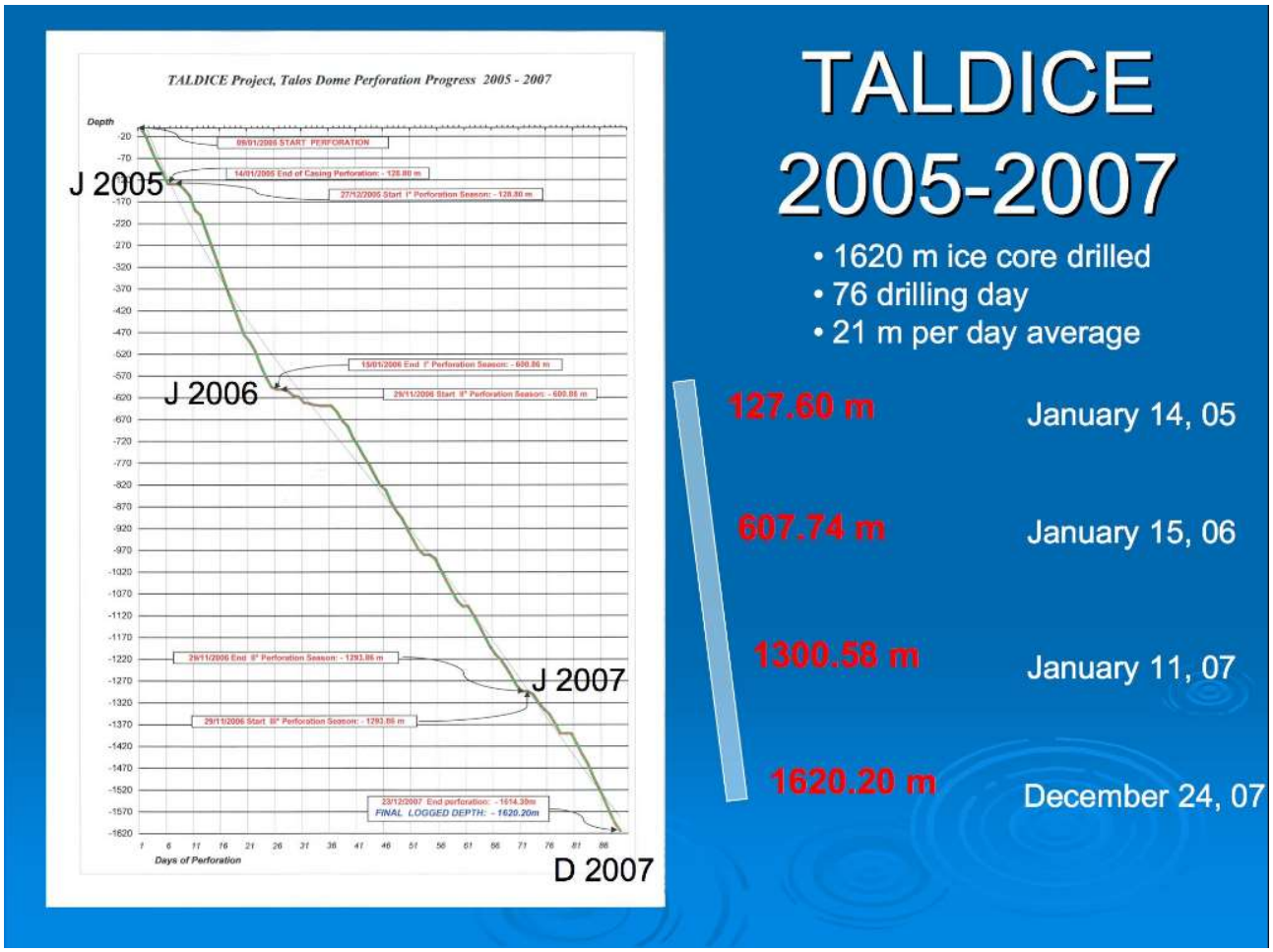

Figure 9 *– Progress of the drilling process of the Talos Dome ice core during the expeditions from 2005 to 2007 (www.taldice.org).*

The processing of Taldice ice core was performed in the cold room at *Alfred Wegener Institute* (AWI) *for Polar and Marine research* (Germany) after being transported in a freezer container first in Mario Zucchelli Station (**MZS**) and then by ship Italica to Europe. In the ***Figure 10*** is shown the transect ice core section divided in different parts, each of which is aimed for different analysis.

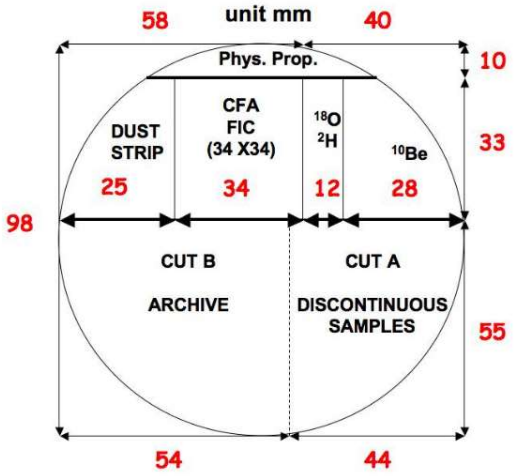

Figure 10 *– Scheme of the transect dissection of the Talos Dome ice core at the Alfred Wagner Institute performed from 2006 to 2008.*

(www.taldice.org/awi)

During the drilling process, it was required the use of an appropriate fluid in order to avoid eventual deformation or diminishing of the ice core diameter due to the surrounding ice hydrostatic pressure. The fluid used in the Talos Dome drilling consisted in a mixture of 68% Exxol D40 (chemical solvent) and 32% Solkane 141b (densifying agent). For the whole drilling process of Talos Dome ice core were used 25,920 liters (www.taldice.org/project/drilling/index).

4.2.3.2 Sample preparation

All the working process of the ice core was performed at a constant temperature of -22°C in the cold room of *Alfred-Wegener-Institute for Polar and Marine Research* in Bremerhaven, Germany. Here, the ice core has been sectioned in order to distribute the various sections to the laboratories responsible for the appropriate analysis. The ice samples were taken throughout the entire ice core (1620.20m). For the amino acid and methoxyphenol compounds analysis have been performed in samples collected in a range of 76 m-1450 m of depth of ice core that corresponds to a range in ice age of 692-157795 yrs BP. The total number of samples collected for amino acid and methoxyphenol compound analysis is 48. The pre-analytical procedures including washing, decontamination and

sample preparation were performed under a Class-100 laminar flow bench-hood located in a Class-1000 clean room in the Ca' Foscari University of Venice. For all washing operations was used ultrapure water, produced by the Chorus Ultra-Pure system (Elga Lab Water, High Wycombe, UK) composed of Chorus I, Chorus II and a Halodispenser.

Samples of Talos Dome ice core are kept at -20°C in the cold room of Ca' Foscari University of Venice and IDPA-CNR. The ice samples immediately after being brought out of the freezer, were individually decontaminated by washing with ultrapure water under Class-100 bench-hood. The washing technique ensures the elimination of any eventual traces of impurities present in the ice cores' surface or drilling fluid employed during the drilling process.

The preparation of the samples prior the analysis procedure was performed using 1.5 ml vials previously washed with ultrapure water and ultragrade methanol. Each sample was spiked with internal standard solution containing 7 labelled amino acids (L-Ala*, L-Arg*, L-Asp*, L-Glu*, L-Val*, L-Pro*, L-Leu*, L-Phe*) with a concentration ranging from 0.95 µg· L^{-1} to 1.18 µg· L^{-1} in vial and with internal standard solution containing two phenolic compounds (VA*, VAN*) with a concentration in vial respectively of 1.01 µg· L^{-1} and 1.02 µg· L^{-1}.

4.2.4 QUANTITATIVE ANALYSES OF AMINO ACIDS IN RENLAND SAMPLES

4.2.4.1 Renland site

The Renland ice core drilling was part of the *Renland Ice Cap Project* (***ReCAP***), a collaboration between Denmark, Germany and the United States. The climatic conditions of this site, situated in the Renland peninsula in the Eastern Greenland (***Figure 11***) were the main issue of the ReCAP project, since is considered to be strongly affected by Arctic sea ice export variation. The site is suitable to provide a continuous profile of the Holocene, as the characteristics of ice cap assure the absence of brittle ice through the ice core.

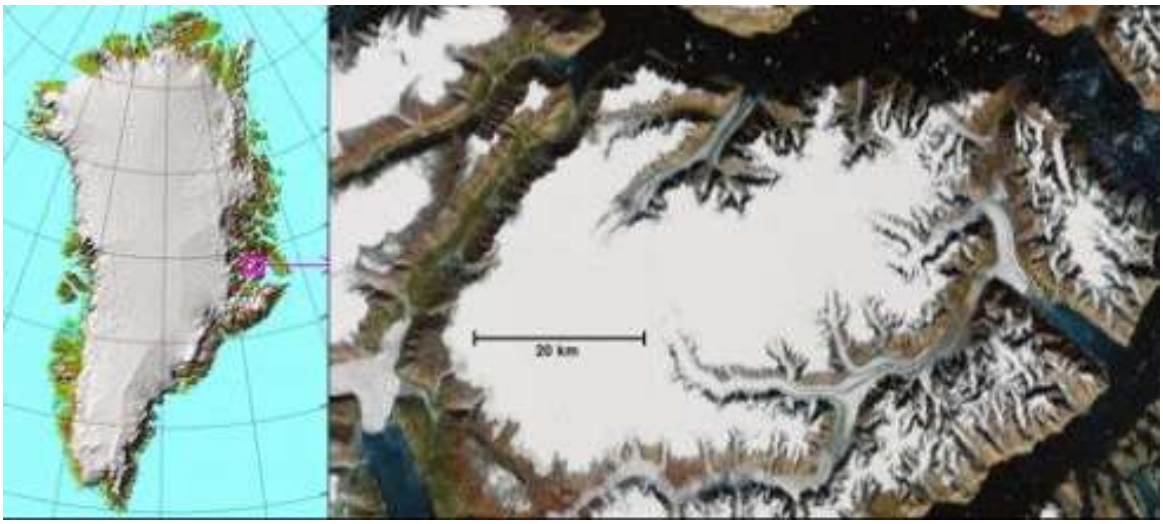

Figure 11 *– In the left is shown the map of Greenland and the Renland ice cap is highlighted by the purple square; in the right is shown a satellite image of the Renland ice cap.*

The topography of the of the eastern plateau has an elevation at the summit of 2340 m and the thickness of the ice in this point is almost 400m. The site is characterized by an accumulation rate of ice of 0.5 m per year.

The Renland ice core has been drilled in the summer of 2015 and the depth of the ice core was of 584 m. Since the length of the ice core was higher than 400 m, the deep drilling was performed. As in the case of the Talos Dome ice core it was necessary to use a drilling liquid in order to assure the same pressure approximately in the hole as in the surrounding ice, thus to avoid the inward movement of the ice and cause the closing of the hole due to the difference of pressure between the inner and the outer ice. The drilling fluid used is a combination of ESTISOL 240 and COASOL.

The measurement of the length of the ice core is performed fitting the top and the bottom of consecutive pieces of ice and then measuring the total length of the ice core. As for the Talos Dome ice core, the core was cut into bags (0.55 m sections) and three bags constitute a “run”. First, the core was cut in runs and each run was sectioned in five segments in parallel to the axis of the core, as shown in the figure below:

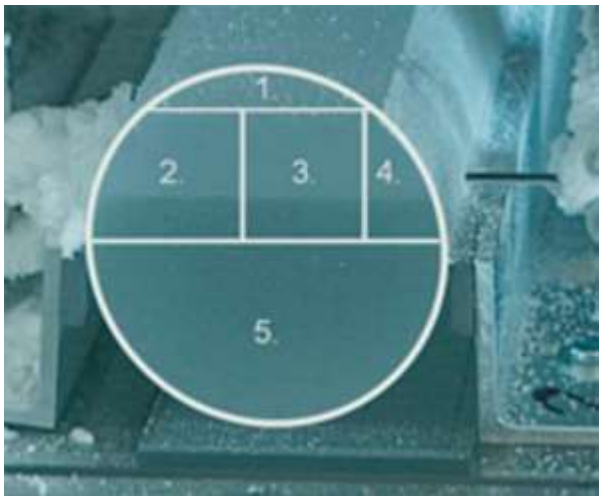

Figure 12 *– Cutting plan of the ice core.*

There are three horizontal cuts (***Figure 12***). The first cut (*section 1*) is collected for measurements of the physical properties. The second cut has been divided in three parts meant for different analysis: gas content measurements (*section 2*), chemical analysis of impurities (*section 3*) and stable isotopes (*section 4*). The *section 5* is cut into bags and stored at -25°C in a freezer in Copenhagen, after electrical conductivity measurements performed moving along the surface two electrodes with a 1000 V electrical potential difference. This measurement provides information about past volcanic eruptions due to the release of large amounts of SO_2 during these phenomena, since the acidity of the ice is measured.

Before the chemical analysis of impurities, the *section 3* is melted through *Continuous melting system*, consisting of controlled melting at a speed of 3 cm/min at -20°C in a cold lab on a gold coated plate. This melting process is necessary to remove the outer part of the ice in order to have only the part that was never in contact with the surrounding environment. The latter was carried subsequently in warm lab where occurs the melting. In order to remove the air bubbles, the uncontaminated ice was placed in a debubbler.

4.2.4.2 Sample preparation

The Renland samples analyzed during the thesis are 529 which correspond to a range in ice age in years of 2012 cal yr – 5090 b2k (Renland ice age: Bo Møllesøe Vinther, personal communication).
All the procedure of the sample preparation of Renland ice core samples was the same as for the

Talos Dome samples. Each sample was spiked with internal standard solution containing 8 labelled amino acids (L-Ala*, L-Arg*, L-Asp*, L-Glu*, L-Val*, L-Pro*, L-Leu*, L-Phe*) with a concentration in vial ranging from 0.85 µg· L^{-1} to 1.05 µg· L^{-1}. The samples were stock in freezer at -22°C until the analysis process.

4.3 PRECONCENTRATION OF FATTY ACIDS AND ATMOSPHERIC MARKERS: Method optimization

4.3.1 Rendezvous site

The Rendezvous ice core was drilled in the West Antarctic region, at S 74 26.941, W 078 09.937 and 1006 m elevation, between the Antarctic peninsula (*Palmer Land*) and Ellsworth Land on 15th and 16th of December 2012 using Twin Otter aircraft to access to the site. The drilling process of the Rendezvous ice core was part of the Palmer Land Drill campaign during which were drilled two other ice cores: *Palmer* and *Jurassic*. In the figure on the left are shown other ice cores drilled along the western coast belonging to previous campaigns (Thomas and Bracegirdle, 2014; Thomas et al., 2013).

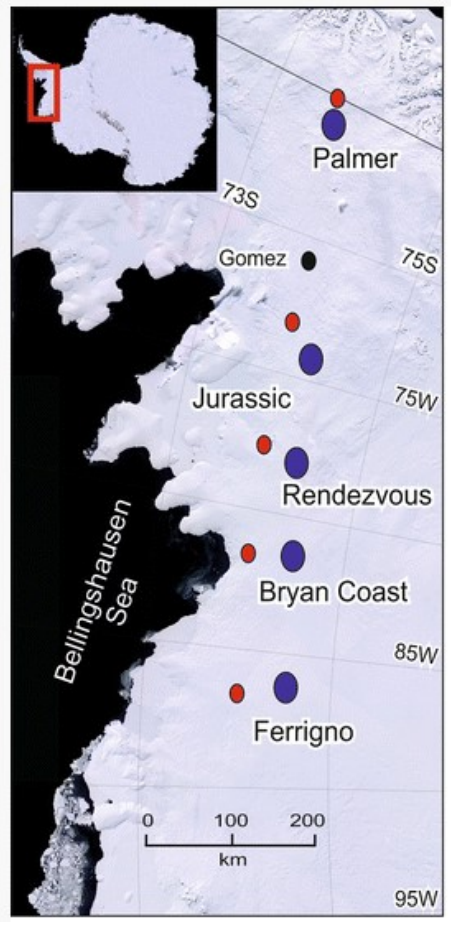

Figure 13 *– (blue dots) Ice core location and (red dots) closest ERA-Interim forecast sites (from the work of Thomas et al., 2014, aimed to study the precipitation pathways in the five ice cores reported in the figure.*

4.3.2 Instrumentation and working conditions

A liquid chromatography – ion trap tandem mass spectrometry *LC/(-)ESI-MS* was used for the chemical detection in preconcentrated samples of the atmospheric markers and the fatty acids analyzed. The analyses were performed in negative mode using an *Accela liquid chromatograph* (Thermo Scientific, San Jose, USA) and an *Orbitrap LTQ Velos* (Thermo Fisher, Bremen, Germany) with an ESI source.

The chromatographic separation was performed using a XBridge® C18 3.5µm 3.0 x 150mm column (Waters, Milford, USA). The mobile phases consisted of NH_4OH 0.5 mM in water, and methanol + 0.5 mM NH_4OH, respectively phase A and phase B. The chromatographic run applied was as follows: 0-1 min 100% A, 1-4 min from 100% to 70% A, 4-9 min 70% A (isocratic), 9-10 min from 70% to 0% A, 10-28 min 0% A (isocratic), 28-29 min from 0% to 100% A, 29-35 min 100% A (isocratic) for the equilibration of the column. The flow rate was 50 µL min^{-1} and, in order to enhance the ionization efficiency, a further flow of 5 mM NH_4OH in methanol in post-column injection was added.

In the table below are reported in detail the parameters of the autosampler:

Autosampler parameters	
Injection volume (µL)	20
Needle height (mm)	2
Syringe speed (µL/s)	8
Flush volume (µL)	400
Flush speed (µL/s)	100
Injection mode	Partial loop

Table 7 *– Autosampler parameters set for the analysis of the atmospheric markers and fatty acids.*

The mass spectra were performed in full scan with the following operation conditions: the resolution was set at 100 000 and the mass ranges at 80 – 600 *m/z* and 150 – 1000 *m/z* in data dependent mode, a multistage mass spectrometry composed, in this case, by 4 scan events (MS*n*, *n* = 1, 2, 3, 4), on the most intense precursor ion at the resolution of 30 000. The ESI source parameters are listed in the table below:

ESI source parameters	
Heater Temp. (°C)	400
Sheath gas (arb)	40
Aux. Gas flow rate (arb)	20
Sweep gas (arb)	0
Spray voltage (kV)	3,5
Capillary Temp. (°C)	350
S-Lens RF Level (%)	50

Table 8 *– ESI source parameters optimized for the analyses of the atmospheric markers and the fatty acids.*

The preconcentration performed in this work was carried out through Solid Phase Extraction (***SPE***) using *SPE-SAX* 1mL Hypersep^{TM} cartridges (Thermo Fisher Scientific, Bremen, Germany), a strong anionic exchange cartridge suitable to extract carboxylic and weak acids in aqueous and non-aqueous solutions (HyperSep^{TM} SAX Cartridges catalog). The purpose of this work is to extract the analytes in question present in 10 mL of sample and to elute them with 1 mL of a proper elution solution. Prior to the extracted compound elution, there are further steps to follow, aimed to optimize the extraction process, as well as to remove the rest of the compounds present as impurities. The choice of the solutions for the washing of the cartridges, the choice of the buffer and the elution solution for extracted compounds, as well as any eventual previous treatment of the samples, eventually changing slightly the pH with the purpose to enhance the extraction capacity, have been the main issue of this work and constitute the optimization step of the preconcentration method.

In order to test a 1:10 preconcentration of the analytes listed above, have been prepared 10 mL standard solutions at 50 µg L^{-1}. The steps of the preconcentration procedure are as follows: the *SPE* cartridges were positioned in the proper holder (***Figure 14 b***), a Visiprep vacuum manifold (Supelco, Sigma Aldrich), after inserting the disposable flow control valves, as shown in the **Figure 14** ***a)***.

a) *b)*

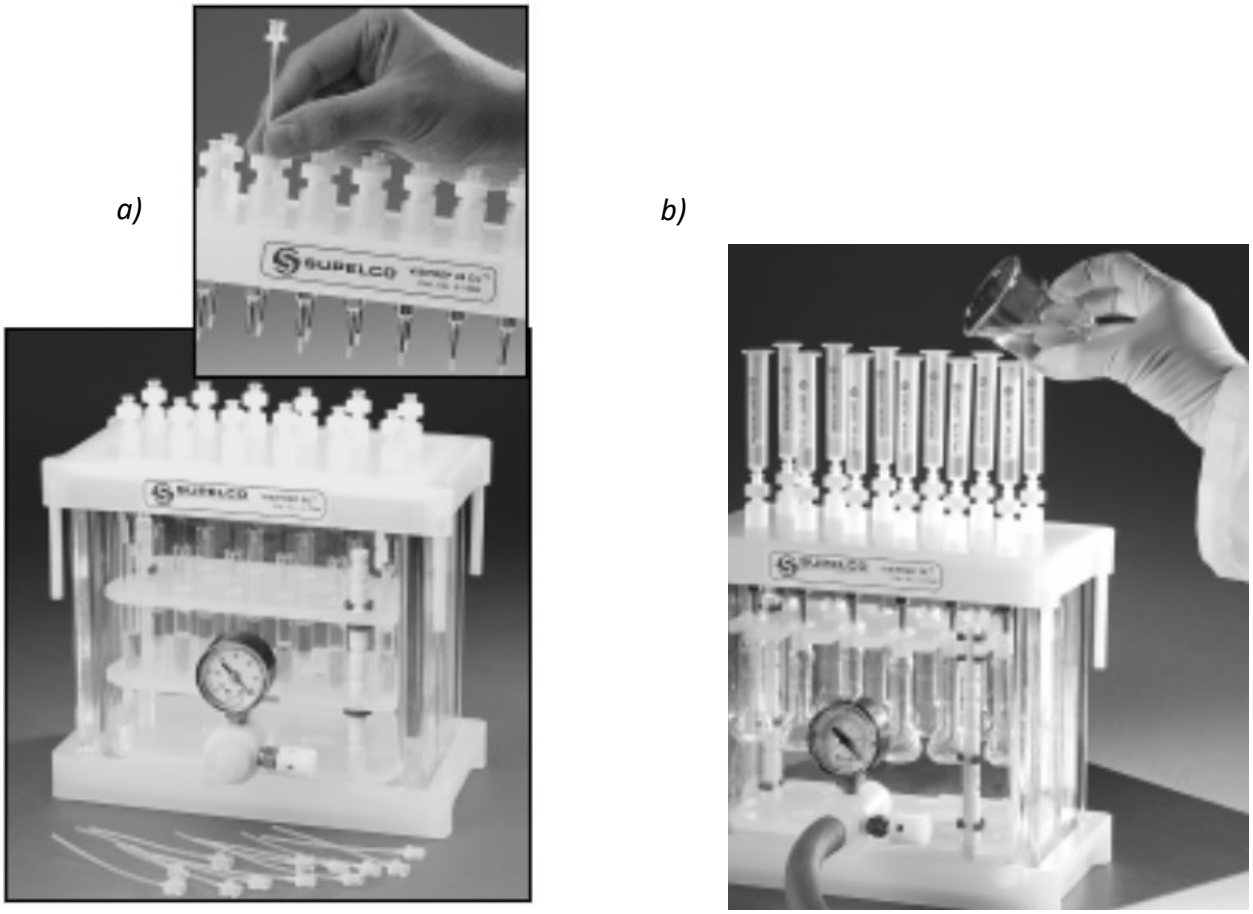

Figure 14 *– **a)** disposable flow control valve insertion and **b)** positioned SPE cartridges in the Visiprep vacuum manifold (Supelco, bulletin 190). In the underlying room are positioned the vials in which are collected the loading solutions*.

For each test, at least 2 replicates were performed and the blanks were made conducting the same steps as with the standard solutions, using ultra grade water instead of the test solutions. This procedure allows to have the same processing of the blank and standard cartridges with the aim of subtracting every eventual preconcentration of compounds present in the solutions as contaminants.

The first step was the conditioning of the cartridges with 1 mL of methanol and then with 1 mL of water. This phase was performed following the indications reported in the catalog of the user manual.

The second step was the loading of the sample or the loading of the standard in the case of the optimization test, in which it occurs the extraction of the analytes. The volume of the sample was

10 mL for each SPE cartridge. Several tests were made changing slightly the acidity of the samples by adding formic acid and changing the counterion of the solid phase in order to enhance the affinity. The exchange of the counterion was performed loading 5 x 1 mL of formic acid 2% in aqueous solution followed by 2 x 1 mL of water and 4 x 1 mL of NH_4OH solution at pH 7-8. We found out that this procedure enhances the extraction thus was used during the following tests.

The following step was the washing procedure, aimed to elute the residues of the previous steps. The choice of the washing solution was challenging, since in this phase the washing solution could elute a part or all the extracted analytes. For the type of cartridges that we used are planned two washing steps: a first wash with 1 mL of ammonium acetate buffer solution 25 mM followed by a second wash with 1 mL of methanol. We carried out that the methanol used as washing solution elutes a large part of the analytes. These conclusions were possible due to the analysis and the quantification of the analytes in all the washing solutions collected after the loading into the cartridge. In order to avoid the loss of analytes, the washing step with methanol was eliminated for all the successive tests. The buffers' role is the elution of the residues, as well as to restore a pH equilibration. Also, this step was modified basifying the buffer with ammonium hydroxide and assessing whether the loss of the analytes during this phase is minimal.

The most challenging step of this work was the choice of the elution solution, the role of which is to elute all the extracted analytes in the solid phase of the cartridge. Several tests were made changing even the solution or the pH, testing both acid and basic solutions. The better eluent in our case seemed to be a mix of methanol/water 1:1 basified with 5% of ammonium hydroxide.
This preconcentration method was not fully optimized and is still being improved. Nevertheless, we performed a preliminary preconcentration and analysis on a part of the Antarctic snow samples after reproducibility assessments made on the test that provided the best recovery factor. The results and all the considerations are reported in the section **Results and discussion.**

- **4.3.3 Sample preparation**

The Rendezvous snow samples were 2, dated 2010 and 2011 which were provided by the *British Antarctic Survey*. The sample preparation of the Rendezvous snow samples was performed at the laboratory at the Department of Chemistry of the University of Cambridge. The snow samples were

kept in the freezer at the *Chemistry of Atmospheric Science* laboratory until the preparation and the analysis procedure. The sample and standard preparation process was performed under a bench-hood. The washing procedure of the glassware and other material required for the preparation of samples and standards was performed first rinsing with ultrapure water and then with ultragrade methanol. The two snow samples were left melting at room temperature for 3 hours and have been collected 3 portions of 10 mL each. The preconcentration on *SPE* cartridges was performed immediately after the melting was complete.

Prior to the real sample preconcentration and analysis, several tests were performed using premade standard solutions at 50 μg L^{-1} of the following analytes: BTCA, MBTCA, pimelic acid, terebic acid, salycilic acid, meso-erythritol, keto-pinic acid, methyl-tetrols, levoglucosan, cis-pinonic acid, pinolic acid, β-caryophillonic, β-nocaryophillonic, β-caryophillinic, lauric acid, myristic acid, arachidonic acid, palmitic acid, oleic acid, heptadecanoic acid, nonadecanoic acid, behenic acid, tricosanoic acid, heptacosanoic acid, octacosanoic, mellissic acid, d3-malic acid*, d10-pimelic acid*, d4-salycilic acid*, d31-palmitic acid*. The labelled compounds were added with the purpose of using them as internal standards.

4.4 QUALITATIVE ANALYSES

4.4.1 INSTRUMENTATION

The instrument used to perform the qualitative analysis in Talos Dome ice core samples is an UHPLC/ESI-HRMS and *nano*UHPLC/*nano*ESI-HRMS system that consists in UltiMate 3000 (Thermo Fisher Scientific™, Germany) coupled with an LTQ Orbitrap® XL (Thermo Fisher Scientific™, Germany). The qualitative analyses have been performed using two different analytical approaches: a conventional analytical method using HPLC-ESI source and subsequently a *nano*System-*nano*ESI source in order to obtain more information about the organic species present in the samples. The column used for the preliminary analysis in UHPLC-ESI/HRMS was ZORBAX SB-Aq C18 (150 mm x 2.1 mm, 3.5 μm), (Agilent, Waldbronn, Germany) whereas the column used for the analysis with the nanoUHPLC-nanoESI/HRMS was HYPERSIL Gold IntegraFrit AQ C18 (150 mm x 75 μm, 1.9 μm), (New Objective, Massachusetts, US). Other material used for the nano-system were the online filters (M525 0.5μm) (IDEX Corporation), 0.5mL Hamilton syringe for the post-column injection and Picotip

needle (ED 360µm x ID 50µm, needle tip 15µm ± 1µm) (New Objective, Massachusetts, US)

4.4.2 A PRELIMINARY QUALITATIVE ANALYSIS: UHPLC-ESI-MS METHOD

4.4.2.1 Sample preparation

All the sample preparation procedure was performed in our clean room under a Class-100 laminar-flow bench hood. Each sample was spiked with a mix solution of labelled compounds used as internal standard, that consists in six labelled amino acids (L-Ala*, L-Glu*, L-Leu*, L-Phe*, L-Pro* and L-Val*) and two labelled phenolic compounds (VAH*, VAN*). The concentration in vial (2 mL Amber Vials, Agilent, Waldbronn, Germany), previously washed accurately with Ultragrade methanol under laminar flow bench-hood) of the internal standard was 200 µg L^{-1}. In order to reduce the dilution of the sample due to the addiction of internal standard solution, the samples were prepared using a minimum amount of internal standard of 25 µL in a total volume of 700 µL. The concentration of the internal standard was established after a previous assessment of the signal, operating with the chromatographic and mass spectrometer working conditions chosen in order to have the best response in terms of sensitivity and chromatographic separation. The list of the samples of Taldice ice core selected for the qualitative analysis, the depth and the ice age *AICC2012* (years BP 1950) is shown in the ***Table 9***. The total number of the samples analyzed in full scan with UHPLC-ESI/HRMS is 37.

Sample name	Depth (m)	Ice age [(1)]
TD27	26	103
TD52	51	319
TD103	102	887
TD151	150	1483
TD176	175	1822
TD202	201	2188
TD227	226	2541
TD251	250	2906
TD277	276	3315
TD302	301	3726
TD327	326	4155
TD352	351	4587
TD377	376	5076
TD403	402	5594
TD427	426	6069
TD451	450	6553
TD478	477	7113
TD502	501	7625
TD527	526	8208
TD554	553	8864
TD575	574	9369
TD606	605	10102
TD627	626	10586
TD651	650	11149
TD726	725	13308
TD751	750	14248
TD775	774	15186
TD800	799	16368
TD826	825	17871
TD850	849	19625
TD868	867	21255
TD896	895	24206
TD926	925	27495
TD963	962	31034
TD1001	1000	34607
TD1027	1026	36810
TD1077	1076	40294

[(1)] AICC2012 (years BP 1950)

Table 9 *– Talos Dome ice core samples analyzed in full scan with UHPLC-ESI/HRMS Orbitrap LTQ XL*

4.4.2.2 Working conditions

The results of this preliminary qualitative analysis in negative mode provided a relatively small number of ions. Therefore, we decided to select the most significant samples which provided a greater number of frames and which are representative of different periods.

The full scan spectra were acquired in a restricted mass range of 100 *m/z* – 600 *m/z* in order to enhance the sensitivity and to obtain as much frames as possible from the analysis. The optimization of the parameters of the Orbitrap mass spectrometer was performed with the aim of improving as much as possible the signal intensity. The parameters that were optimized were:

- AGC Target Value

The AGC target value (Automatic Gain Control) is a parameter that controls the ion population in the ion trap, providing a different sensitivity depending on the number of ions present in the trap. The range of AGC values in order to have a good accuracy are $5 \cdot 10^5 – 1 \cdot 10^6$. Greater values lead to a signal decrease or mass accuracy deviation due to space charge effects (Kalli et al., 2014; BenDaniel & Duke, 1966). After several tests in which an assessment of the *total ion current* (TIC) was performed, The AGC value used in these analyses was $3 \cdot 10^5$.

- Maximum ion injection time

The maximum injection time is the maximum time in seconds ions are allowed to accumulate in the ion trap before being injected in the Orbitrap. The range of maximum ion injection time values suggested for a good identification is 50-150 ms. In our case, after testing different values, we set a maximum time of 500 ms since the analytes that we analyze are present in ultra-traces. As can be noticed, this parameter is in some sense dependent from the AGC parameter, as they cooperate depending on the amount of ions reaching the trap.

- Microscan number

The microscan number is a parameter correlated to the acquisition time. A good microscan number is a compromise between the acquisition time and the signal/noise ratio. The assessment of the best value was performed testing the total ion current for different microscan number values. As a result of these evaluations, the microscan number was set at 3.
A more intuitive image for a better understanding of the distribution of the selected samples in time is shown in the figure below (***Figure 15***) where is reported the plot of the $\delta^{18}O$ values in the period of interest obtained from the work of Stenni and others (Stenni et al., 2011) performed in the Talos Dome ice core. The green squares represent the Taldice samples analyzed with UHPLC-ESI/HRMS whereas the blue triangles represent the samples analyzed subsequently with nanoUHPLC-nanoESI/HRMS, as shown in the next section.

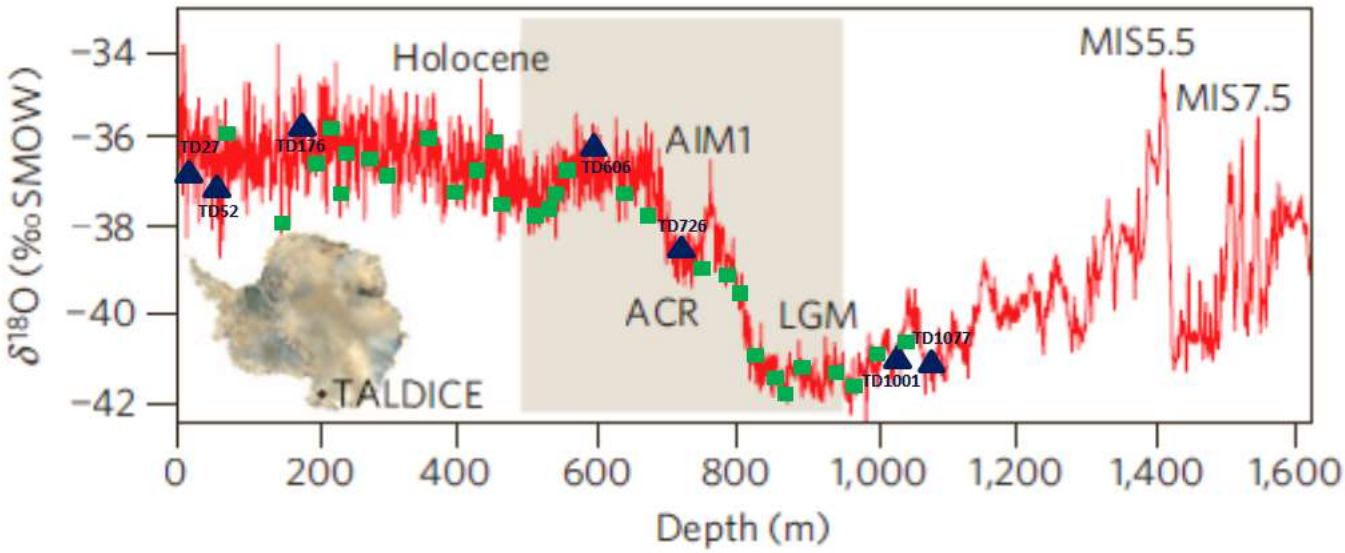

Figure 15 *– Plot of $\delta^{18}O$ values in Talos Dome ice core samples versus depth profile indicating the Antarctic Cold Reverse (ACR), the Antarctic Isotopic Maximum (AIM1), the Last Glacial Maximum (LGM) and the Marine Isotope Stages 5.5 and 7.5 (MIS5.5 and MIS7.5). The green rectangles indicate the samples analyzed preliminarily with ESI-UHPLC/MS whereas the blue triangles indicate the samples analyzed with nanoUHPLC -nanoESI/MS after the preliminary analysis* (Stenni et al., 2011).

As mentioned above, the qualitative analysis of the Talos Dome ice core samples was performed first with UHPLC-ESI-MS and then with *nano*UHPLC-*nano*ESI-MS method. The purpose of this decision was the need to provide a preliminary composition of the samples, considering that a following and more exhaustive analysis will be performed using a more sensitive (and challenging) method such as the *nano* technique.

In this work was used the reverse phase chromatography, thus a C_{18} chromatographic column, due to its adaptability to a wide range of organic compounds, included hydrophilic molecules. For the UHPLC-ESI-MS analysis was used a *ZORBAX SB-Aq C_{18} 150 x 2.1 mm, 3.5 µm* (Agilent) column. The mobile phases in both UHPLC-ESI-MS and *nano*UHPLC-*nano*ESI-MS methods are ultra-pure water containing 0.01% formic acid (HCOOH, mobile phase A) and acetonitrile (CH_3CN, mobile phase B) containing 0.01% formic acid.

The operation conditions were set after several optimization tests performed in order to obtain the best chromatographic separation and the highest sensitivity in terms of detection of most of the organic compounds. The tests made to obtain these results were performed with a mix solution of

methoxyphenol compounds, amino acids, glucose and levoglucosan, since can be considered to represent most of the organic family compounds due to the variety of the functional groups. In the table below are shown in detail the autosampler and injection parameters:

Autosampler parameters: UHPLC	
Draw speed (nL/s)	1000
Draw delay (ms)	5000
Dispense speed (nL/s)	10000
Dispense delay (ms)	2000
Dispense to wait speed (nL/s)	20000
Sample height (mm)	3
Puncture depth (mm)	5
Wash volume (µL)	400
Wash speed (nL/s)	20000
Loop wash factor	3
Flush volume (µL)	15
Flush volume 2 (µL)	2
Injection volume (µL)	19

Table 10 *– List of the autosampler and injection parameters in the UHPLC-ESI-HRMS analysis*

The best chromatographic run obtained after several tests aimed to ensure the best elution of the analytes was set as follows. The length of the analysis was 50 min during which the first 5 min the composition of the mobile was set at 97% of mobile phase A and was let flowing isocratically. At 5 min started a linear gradient reaching 1% of mobile phase B in the following 10 min. At 15 minutes from the beginning of the analysis, a 99 % of eluent B was maintained constant for 20 min and then, at 35 min the composition of the elution solution was set again at 97% of mobile phase A and was maintained for 15 min. This step is required to elute the last non-eluted compounds and to equilibrate the column. The flow during the entire analyses was 150 µL min^{-1}.

The subsequent step was the optimization of the mass spectrometer. In the table below are reported the parameters set for the source and the mass spectrometer:

Mass spectrometer	
AGC	$3 \cdot 10^5$
Maximum Ion Injection Time (ms)	500
Microscan	3
Resolution	60000
Mass range (m/z)	100 - 600

ESI-Source	
Temp. (°C)	200
Sheath gas (arb)	39
Auxiliary gas (arb)	5
Sweep gas (arb)	0
Capillary Temp (°C)	225
Voltage (kV)	3.5

Table 11 *– Mass spectrometer and ESI-source parameters*

The mass calibration and the tuning are the first steps before acquiring an analysis. The mass calibration is a procedure that must be completed every 48 hours in order to have accurate results from the Orbitrap analyzer in terms mass accuracy. As a matter of fact, the Orbitrap mass spectrometer when accurately calibrated provides exact masses of *m/z* ions with an accuracy even lower than 5 ppm.

The mass calibration is executed through direct injection of a standard solution in acetonitrile (50%), methanol (25%) and acetic acid (1%) commercially available provided by Thermo Fisher company. There are two calibrating solutions provided for the calibration in positive and negative mode. The flux for the two polarities is 10 µL min^{-1} for the positive mode and 5 µL min^{-1} for the negative mode. Another important step that leads to a higher accuracy of an error within 2 ppm, is the introducing of a lock mass that the instrument uses to monitor constantly the mass accuracy through an internal calibration. The lock masses used generally are impurities present in the surrounding environment, in the solvents or in the inner instrument that are constantly present and can be spotted during the acquisition of a mass spectrum.

The tuning is an essential procedure that allows an optimization of the instrument parameters in order to obtain the highest response in terms of intensity from the mass spectrometer. This process is done adjusting a set of parameters depending on the type and the *m/z* value of compounds that are meant to be analyzed.

4.4.3 QUALITATIVE ANALYSIS: *nano*UHPLC-*nano*ESI-HRMS METHOD

The *nano*ESI source provide a better ionization efficiency, therefore as a consequence a better sensitivity, since the lower flow rate compared to a normal ESI technique produces smaller charged droplets during the spraying process (Schmidt et al., 2003). As a consequence, the instrumentation *nano*UHPLC suitable to low flows need a further optimization.

The optimization of the analytical method was achieved similarly to the previous one, performing several tests with the aim of obtaining the highest performances in terms of chromatographic separation and signal quality. The nanoHPLC chromatography's instrument employs a fluidic system made by glass capillaries with tight internal diameters which renders challenging the injection and ionization parameter optimization, the choice of the best flow rate, the injection volume and source parameters as well as the reproducibility. Further problems arose during the analysis due to the low flexibility of the *nano*-system to the variation of mobile phase in terms of volume and composition, leading to dropping during the spray formation. The needle employed in the *nano*ESI sources, due to the small internal diameter, are often subjected to clogging, therefore online filters were used with the purpose of filtering eventual impurities present in the mobile phases or in the samples. The choice of a good spray voltage was fundamental to obtain a good ionization and less dropping phenomena and was selected after several tests assessing the total ion current behavior.

4.4.3.1 Operating conditions

The chromatographic separation was performed with reversed phase chromatography using a C18 HYPERSIL Gold Integrafrit AQ column with *nano*UHPLC instrument. The mobile phases employed are ultra-pure water containing 0.01% formic acid (HCOOH, mobile phase A) and acetonitrile (CH_3CN, mobile phase B) containing 0.01% formic acid with a flow rate of 0.250µL min^{-1}. The length of the analysis was 50 min during which the first 5 min the composition of the mobile was set at 99% of mobile phase A and was let flowing isocratically. At 5 min started a linear gradient reaching 1% of mobile phase B in the following 20 min. At 15 minutes from the beginning of the analysis, a 99% of eluent B was maintained constant for 20 min and then, at 35 min the composition of the elution solution was set again at 99% of mobile phase A and was maintained for 15 min.

In the table below are shown the parameters set for the autosampler during the qualitative analyses in *nano*UHPLC-*nano*ESI/HRMS method.

Autosampler parameters: nanoUHPLC	
Draw speed (nL/s)	50
Draw delay (ms)	5000
Dispense speed (nL/s)	2000
Dispense delay (ms)	2000
Dispense to wait speed (nL/s)	4000
Sample height (mm)	3
Puncture depth (mm)	5
Wash volume (µL)	400
Wash speed (nL/s)	4000
Loop wash factor	3
Flush volume (µL)	20
Flush volume 2 (µL)	5
Injection volume (µL)	4

Table 12 *– List of the autosampler and injection parameters in the nanoUHPLC-nanoESI-HRMS analysis*

In order to optimize the ionization efficiency and to improve the spray formation, it was necessary the use of a post-column injection performed injecting through a T-junction a further quantity of a different solvent solution for positive and negative mode. Since the *nano*ESI source works in atmospheric conditions and temperature, sometimes the declustering is more difficult compared to a normal ESI source, especially when the mobile phase is composed by a high percentage of water. Assessment of the total ion current employing different mixtures of organic solvent were performed, leading to the choice of a composition of methanol/acetonitrile at 95:5 acidified at 1% with acetic acid for the positive mode and pure methanol for the positive mode. In both cases the flow rate was set at 100µL min^{-1}. In the following tables are shown the mass spectrometer parameters for the analyses carried out with *nano*UHPLC-*nano*ESI method. The voltage applied to the *nano*ESI source was +2.00 kV for the positive mode and -2.00 kV for the negative mode.

Mass spectrometer	
AGC	$3 \cdot 10^5$
Maximum Ion Injection Time (ms)	500
Microscan	3
Resolution	60000
Mass range (m/z)	100 - 600

Table 13 *– Mass spectrometer and nanoESI-source parameters.*

4.5 DATA ELABORATION

4.5.1 Quantitative analysis

The amino acid and phenolic compound quantitative analysis in the Antarctic and Arctic samples were performed after the method validation and the assessment of the appropriate parameters in order to evaluate the quality of the analysis.

The data elaboration for the quantitative analysis of methoxyphenols and amino acids in Talos Dome ice core and for the amino acids in Renland ice core in API 4000 was performed with Analyst Software 1.5.2 (Applied Biosystems, MDS SCIEX Instruments) as follows: for each analyte two transitions were considered and for the quantification was chosen the most intense one. Extracting a small range (±10 ppm) in the ion chromatograms centered on the exact *m/z* of each amino acid, are achieved the extracted ion chromatograms (*XIC*s) making possible the peak integration, therefore the quantification of the target compounds. The peak areas of the analytes and labeled internal standards of the calibration curves and the samples have been exported in Excel worksheet and elaborated further. For each analyte have been determined *LOD* and *LOQ* values, matrix effect, error percentage and linearity range. The quantification has been performed correcting with the relative instrumental response factor.

The quantification relative to the fatty acid and atmospheric marker preconcentration tests, as well as the snow sample quantification, were performed with Quanbrowser, Xcalibur Software 2.1.0 (Thermo Fisher Scientific, USA) after the peak integration and the construction of the calibration curves for each analyte. The concentrations were calculated using the linear regression coefficients.

4.5.2 Qualitative analysis

The data elaboration of qualitative analysis in Talos Dome ice core was performed using the SIEVE 2.0 (Thermo Fischer Scientific), a software able to make differential analysis, therefore to provide statistical differences between the frames present in the samples and in the blanks. This software, after the alignment step if necessary during which the chromatograms are aligned making possible a better comparison, allows different types of data analyses, depending on the different requirements, as well as on the number of samples. In the beginning of the experiment in SIEVE, it's possible to choose the type of molecules that it is going to search (the alternatives in SIEVE 2.0 are Proteomics or Small molecules, in our case this setting was set in Small molecules), the algorithm and the type of the experiment. The algorithm chosen in our case was Chromatographic Alignment and Framing whereas for the experimental type we used both Two sample differential Analysis, for an intercomparison between two groups of data (for example in our case between the replicates of a sample and the replicates of the blank), and Control Compare Trend (for a greater number of data groups) so as to ensure that a given frame is significantly present in the sample.

During the creation of a new experiment in Sieve is required to set a certain number of parameter such as the range of *m/z* in which we are focused, the retention time range of interest and the mass accuracy of the *m/z* value. According to the positive or the negative mode of the analysis that is going to run is required to set the charge of the ion $[M+H]^+$ or $[M-H]^-$, the threshold and the peak width. In our case, we performed analysis both in positive and negative mode hence we ran one at a time, first the negative mode and then the positive mode analysis. In both cases we set a threshold at 8000 for the standard HPLC analysis and 5000 for the Nano analysis. These values were carried out as a result of preliminary tests performed with the purpose of assessing the background role in the analyzed samples.

The result of the SIEVE experiment gives a table with information regarding all the frames resulting from the background subtraction, such as *m/z* value, retention time, signal intensity, standard deviation, ratio, P-value, etc. For each frame is possible to see the peak, therefore to establish the significance from the reproducibility of the replicates. The subsequent step consisted on the identification of each frame. The software provides an automatic identification through incorporated databases such as PubChem and Spider. Nevertheless, it has been preferred to identify manually the frames in order to verify each of them with the isotopic patterns obtained from

Xcalibur Software (Xcalibur 2.0, Thermo Fischer Scientific), Metlin database, Chemspider and Pubchem.

Xcalibur is a software that provides the chromatograms of the analysis performed from the Orbitrap instrument. From the whole chromatogram is possible to filter one frame at the time: in this way is possible to see the retention time and the peak shape that, as will be explained better below, it turned out to be fundamental for the identification not only for the single frames but even for homologous and family compounds. For each *m/z* value the software generates the molecular formula using the atoms previously set in the list. The maximum number of each atom employed for the generation of molecular formulas from the software can be set manually. We applied constraints regarding the number of atoms setting the following values according to the work (Kind and Fiehn 2007) in which is stated that the limit of the number of atoms can be calculated dividing the mass range of the spectra by the mass of the atom. The results are reported in the table below, with a further restriction after a heuristic decision made taking into account molecular formulas present in NIST, Wiley and DNP libraries.

Mass Range [Da]	Library	C max	H max	N max	O max	P max	S max	F max	Cl max	Br max	Si max
< 500	DNP	29	72	10	18	4	7	15	8	5	
	Wiley	39	72	20	20	9	10	16	10	4	8
< 1000	DNP	66	126	25	27	6	8	16	11	8	
	Wiley	78	126	20	27	9	14	34	12	8	14
< 2000	DNP	115	236	32	63	6	8	16	11	8	
	Wiley	156	180	20	40	9	14	48	12	10	15
< 3000	DNP	162	208	48	78	6	9	16	11	8	

Table 14 – *Constraints for number of atoms during the formula generation for different ranges of masses after an examination of Miley and DNP databases (Kind and Fiehn, 2007).*

Once we put the *m/z* value with the aim to generate all the possible molecular formulas, the mass tolerance is required. In our case, we set a mass tolerance of 5 ppm and the masses of the molecules generated will be in a range of ±5ppm of the given mass. Depending on the mode the analyses were acquired, before the running it is required to set the charge (-1 if the analysis were acquired in negative mode ore +1 if they were acquired in positive mode).

After running the calculation, the software provides a list of molecular sorted according to the mass accuracy. In the list of the molecule formulas generated providing a given m/z value it compares, beside the mass tolerance, another value called RDB (Ring Double Bond equivalent) which indicates the degree of unsaturation (Laws, 1963). The next step is to find out which of the formulas proposed from Xcalibur is the real molecule present in the sample. In order to do so, shall be performed a comparison between the simulated isotopic pattern and the real one carried out selecting the peak which corresponds to the *m/z* considered. During the comparison between the theoretical and the real isotopic pattern, the isotopic cluster ratios of each isotope were verified paying attention to the mass accuracy to be less than 5 ppm.

Metlin, Chemspider and Pubchem databases were used to verify first if the molecule formula generated from the software exists and then to check the structure and the characteristics of the molecule. Metlin is a database trademark of the *Scripps Research Institute* designed for metabolomic analysis that allows the research of organic compounds setting the *m/z* value of the frame, the mass accuracy, the charge and the type of adducts. Chemspider and Pubchem are databases of chemicals which provide other than the molecular structures and main characteristics, even the mass spectrum for most of the molecules present in the database. This procedure, even more if there is the possibility of a MS/MS spectrum compared to those in the libraries, provides a good likelihood identification.

KENDRICK MASS ANALYSIS

The identification of the molecules starting only from a *m/z* value and a chromatogram is a procedure that turned out to be a challenging work and that could lead easily to misleading interpretations. With the purpose of ensuring a more reliable possible identification, we applied some mathematical instruments used previously in several works regarding molecular identification in direct infusion analysis. The *Kendrick Mass Analysis* is a technique developed from Edward Kendrick in 1963 with the aim of identifying compounds that differ by one or more -CH_2- groups. According to this work, all the frames that differ by one or more CH_2 have the same mass defect. As a consequence, putting in a diagram the *Kendrick Mass Defect* (KMD) in the y-axis versus the *Kendrick Mass* (KM) in the x-axis, calculated as shown in the equations below, all the frames that belong to a homologous series arrange in a horizontal line.

$$KM = m/z\ \ observed\ frame\ \cdot \frac{14.000}{14.0156} \qquad \text{(Eq. 3)}$$

$$KMD = |KMD - nominal\ mass\ of\ the\ frame| \qquad \text{(Eq. 4)}$$

The vertical distribution of the frames in the diagram indicates the presence of molecules with different composition, hence belonging to different family compounds. As can be intuited, the same procedure can be applied even for other repetitive units, making the identification simpler and narrowing down the list of the possible molecules.

THE VAN KREVELEN DIAGRAMS

The *Van Krevelen diagrams* were developed for the first time in 1950 from Dirk Willem van Krevelen, a coal and polymer scientist, with the aim of studying the physiochemical changes in the coal (Krevelen, 1950), recently rediscovered and used in analytical chemistry. In these diagrams are plotted the atomic ratios **O/C** on the x-axis and **H/C** on the y-axis which means that the shift across the diagram indicates a change in elemental composition as well as reaction processes, such as oxidation, reduction, dehydration or decarboxylation, as shown in the figure below:

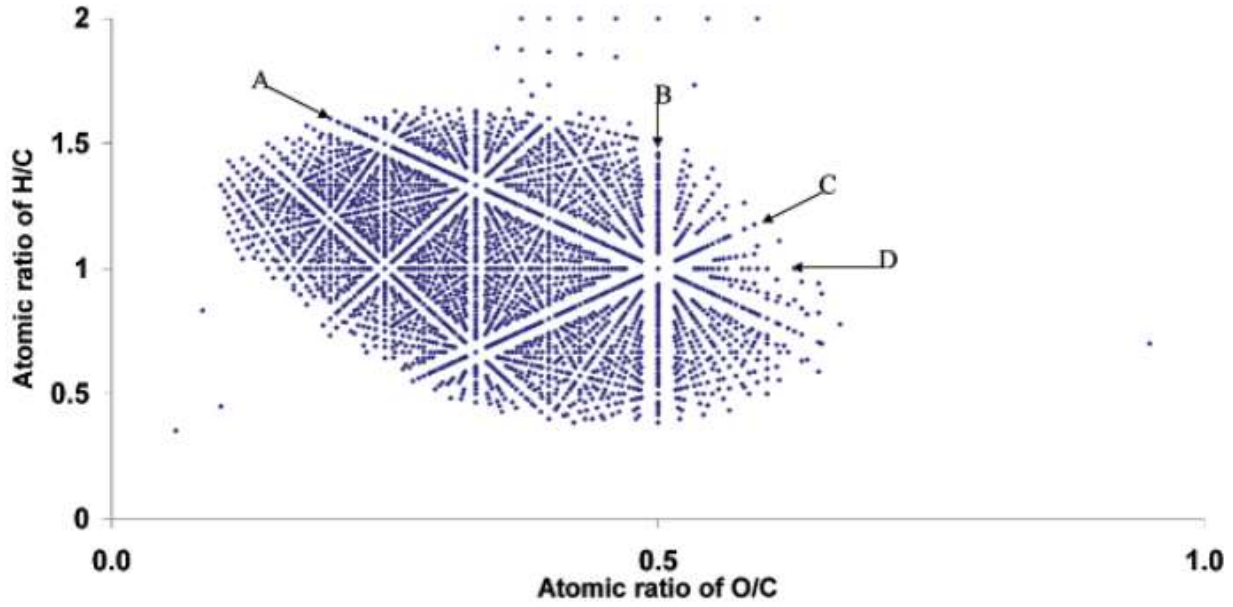

Figure 16 *– Van Krevelen diagram (Kim et al., 2003) for the elaboration of ultra-high resolution mass spectrum data. The line A in the plot represents metilation (downwards/right) or demetilation (upwards/left); The line B indicates dehydrogenation (downwards) or hydrogenation (upwards); line C indicates hydration (downwards/left) or condensation (upwards/right); line D indicates oxidation (right) or reduction (left).*

The distinctive lines in the diagram indicate different chemical reactions, as well as different eventual past or ongoing biologic activities (Krevelen, 1950). In fact, as the equation of the lines in the diagram is:

$$\frac{H}{C} = a \cdot \frac{O}{C} + b \qquad \text{(Eq. 5)}$$

then the different chemical reaction depending on the values of the slope *(a)* and the intercept *(b)* are:

Metilation/demetilation	b = 2
Oxidation/riduction	b = 0
Hydration/condansation	a = -2
Decarbocylation	a = 0, b = 2
Hydrogenation/dehydrogenation	Vertical lines

Another important feature of the Van Krevelen diagrams is that, as the different organic family compounds, both natural and anthropogenic, locate in given regions of the diagram (Kim et al., 2003), it could be helpful to provide information about the source or even the chemical processes occurred. In the figure below is shown a van Krevelen diagram reproduced from studies performed in previous works highlighting the regions in which are located some of the major biomolecular compounds.

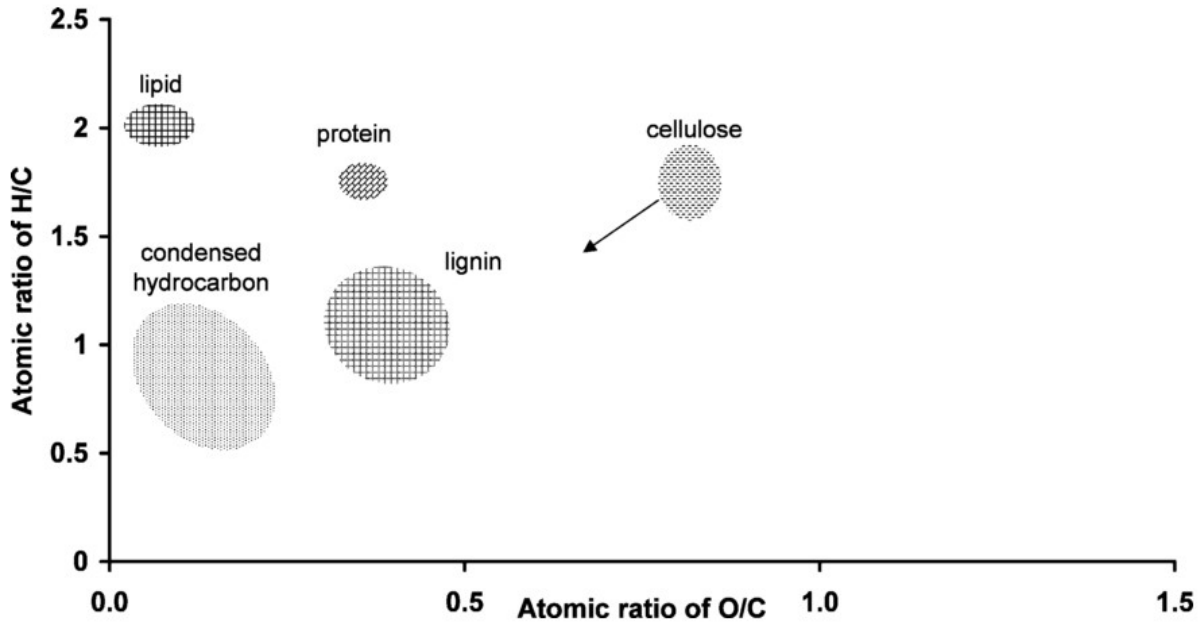

Figure 17 – *Van Krevelen diagram (previous works from Krevelen, 1950; Perdue et al., 1990; Visser, 1983) and the location of some main organic biomolecular compounds.*

AVERAGE OXYDATION STATE OF CARBON (**OSc**)

The oxidation state of the carbon is another important feature to be investigated in order to assess the oxidation state of the chemical species present in the samples. The oxidation is intended as an environmental process and provides precious information in terms of description and understanding of the transformation of organic species in the environment, as oxidizing environments tends to foster oxidation processes.

The definition of the oxidation state of carbon is the charge that the carbon would have if all the electrons involved in bonds with atoms with higher electronegativity are lost and all the electrons of the less electronegative atoms involved in bonds with the carbon are gained. The $\overline{OSc}$ value of a given organic compound is linked to the O/C and H/C ratios and can be calculated as follows:

$$\overline{OSc} = 2 \cdot \frac{O}{C} - \frac{H}{C} \qquad \textbf{(Eq. 6)}$$

This equation is generally used for molecules containing only C, O and H. The presence of other heteroatoms in the molecule such as P, N and S are excluded from the calculus and only C, H and O are considered, causing a deviation in the **OSc** plot. This is a consideration made taking into account that the presence of these atoms contributes less to the average **OSc** value.

In the figure below is represented a diagram built plotting the number of carbon atoms (x-axis) versus the average carbon oxidation state (y-axis) of data resulted from a work of aerosol samples. As can be intuited, The **OSc** value increases with the increase of carbon-oxygen bonds; in the contrary, the **OSc** value decreases with the increase of Carbon-hydrogen bonds. As a consequence, in the upper side (**OSc** > 0) of the diagram we can find oxidized chemical species, whereas in the bottom part (**OSc** < 0) we can find the reduced ones. In the diagram can be noticed vectors that indicates different types of reactions: the frames located in the vertical lines are indicate oxidation/reduction reactions, attributable to functionalization with polar functional groups; the horizontal lines indicate oligomerization and the diagonal lines fragmentation reactions. Oftentimes, there is a conjunction of different reaction types, rendering the displacement in the OSc-n°C space more complex (Kroll et al. 2011).

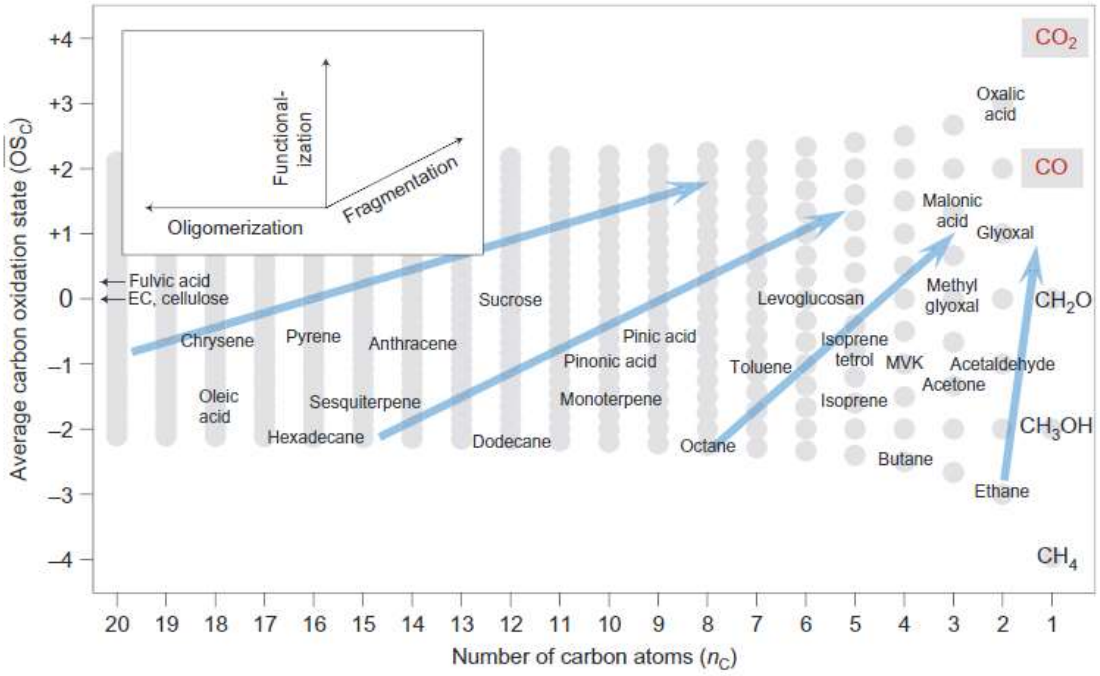

Figure 18 *– Diagram of the average carbon oxidation state (OSc) in relation to the number of carbons (n_C) of atmospheric aerosol data analysis* (Kroll et al. 2011).

DOUBLE BOND EQUIVALENT (DBE)

The concept of *double bond equivalent* (DBE) and *degree of unsaturation* for the organic compounds was introduced for the first time in 1950's (Pontet, 1951; Soffer, 1958).

The DBE value is parameter used for the assessment of the degree of unsaturation, as well as the aromaticity index and the presence of the number of hydrogen atoms, as a decreasing number of hydrogen atoms leads to increasing unsaturation, therefore to higher DBE values. There has been used several equations to calculate DBE, including phosphorus, halogens and sulfur in addition to carbon, hydrogen and nitrogen (Stubbins et al. 2010). According to (Koch and Dittmar 2006) DBE parameter depends only on the number of atoms of carbon, hydrogen and nitrogen, whereas the presence of oxygen and sulfur doesn't affect the DBE value. However for this work, as the most common compounds found in positive mode in the samples are composed by C, H, N, O, S and P, according to most recent works in which have been considered even the phosphorus atoms, we decided to use the following equation, considering a generic molecule $C_cH_hN_nO_oS_sP_p$ (Wozniak et al., 2008):

$$DBE = n_C + 1 - \left(\frac{n_H}{2} - \frac{n_n}{2} - \frac{n_p}{2}\right) \qquad \textbf{(Eq. 7)}$$

5. RESULTS AND DISCUSSION

5.1 PHENOLIC COMPOUNDS AND AMINO ACIDS IN TALDICE SAMPLES

After the method validation and determination of the linearity ranges and *LOD* values, the amino acid and *PC*s analysis and quantification on the ice samples were performed. The concentrations of amino acids and methoxyphenols in Talos Dome samples resulting above *LOD* values range from 0.002 µg L^{-1} to 8.2 µg L^{-1} for amino acids, and from 0.005 µg L^{-1} to 66.2 µg L^{-1} for methoxyphenols. Have been subtracted the LOD values and multiplied for the accumulation rates for each analyte and consequently were considered for a further assessment only the analytes with concentrations above the LOD values in more than 50% of all the total processed samples of Talos Dome. The analytes present in more than 50% of the samples are the amino acids L-Ala, L-Asp, L-Arg, L-Leu/Ile, Gly, L-Hys, L-Phe, L-Thr, L-Glu, L-Val, L-Pro, L-4-Hyp and the methoxyphenols VA, VAH and VAC. In the ***Table 15*** and ***Table 16*** are shown in detail the amino acids and phenolic compounds, respectively, found in the Talos Dome samples. The values, expressed in 10^{-2} mg/m^2/y, are referred to the results obtained after the considerations described above.

The ice core is referred to the Antarctic Ice Core Chronology (*AICC2012*, Veres et al., 2013).

Sample name	Ice age (yrs BP)	L-ALA	L-ASP	L-ARG	L-LEU	GLY	L-HYS	L-PHE	L-ORN	L-THR	L-GLU	L-VAL	L-PRO	L-4-HYP
TD_77	647	0,0013	0,0036	0,0012	0,0023	0,0151	0,0018	0,0004	0,0143	0,0003	0,0047	0,0022	0,0112	0,0015
TD_103A	965	0,0249	0,0274	0,0080	0,0043	0,0453	0,0150	0,0030	0,0390	0,0044	0,0050	0,0119	0,0089	0,0073
TD_127A	1273	0,0982	0,1083	0,0480	0,0014	0,1648	0,0612	0,0176	0,0951	0,0180	0,0177	0,0542	0,0788	0,0580
TD_151A	1595	0,0153	0,0223	0,0051	0,0021	0,0400	0,0071	0,0020	0,0182	0,0013	0,0030	0,0048	0,0033	0,0031
TD_176A	1924	0,1109	0,0741	0,0220	0,0472	0,1145	0,0396	0,0233	0,1540	0,0214	0,0179	0,0463	0,6207	0,1029
TD_202A	2286	0,0048	0,0117	0,0048	0,0012	0,0234	0,0060	0,0010	0,0114	0,0009	0,0091	0,0043	0,0028	0,0013
TD_227A	2638	0,0078	0,0254	0,0122	0,0024	0,0313	0,0174	0,0013	0,0455	0,0009	0,0053	0,0044	0,0053	0,0021
TD_251A	2996	0,0049	0,0145	0,0079	0,0004	0,0224	0,0082	0,0007	0,0357	0,0002	0,0042	0,0022	0,0061	0,0027
TD_302A	3806	0,0302	0,0265	0,0101	0,0112	0,0472	0,0089	0,0051	0,0247	0,0035	0,0094	0,0096	0,0037	0,0098
TD_327A	4221	0,0023	0,0074	0,0020	0,0004	0,0209	0,0024	0,0001	0,0120	0,0001	0,0072	0,0028	0,0018	0,0008
TD_352A	4660	0,0143	0,0196	0,0060	0,0019	0,0234	0,0051	0,0031	0,0338	0,0024	0,0056	0,0058	0,0018	0,0045
TD_377_378	5128	0,0170	0,0348	0,0197	0,0036	0,0263	0,0157	0,0038	0,0137	0,0038	0,0086	0,0066	0,0040	0,0030
TD_403A	5624	0,0043	0,0022	0,0018	0,0013	0,0112	0,0049	0,0002	0,0082	0,0001	0,0027	0,0011	0,0115	0,0019
TD_427A	6101	0,0127	0,0146	0,0071	0,0040	0,0240	0,0066	0,0032	0,0263	0,0026	0,0086	0,0050	0,0147	0,0099
TD_451_452	6602	0,0132	0,0175	0,0038	0,0027	0,0267	0,0080	0,0020	0,0169	0,0011	0,0070	0,0063	0,0083	0,0031
TD_478A	7212	0,0029	0,0082	0,0034	0,0010	0,0112	0,0042	0,0004	0,0166	0,0002	0,0051	0,0025	0,0047	0,0015
TD_502	7765	0,0019	0,0053	0,0027	0,0003	0,0175	0,0031	0,0002	0,0136	0,0007	0,0061	0,0019	0,0019	0,0005
TD_527A	8367	0,0230	0,0276	0,0094	0,0081	0,0425	0,0181	0,0048	0,0437	0,0055	0,0050	0,0098	0,0247	0,0099
TD_554A	9018	0,0063	0,0101	0,0051	0,0013	0,0307	0,0041	0,0007	0,0112	0,0008	0,0054	0,0035	0,0034	0,0015
TD_575	9480	0,0032	0,0061	0,0037	0,0012	0,0155	0,0032	0,0006	0,0106	0,0007	0,0045	0,0019	0,0023	0,0009
TD_627A	10686	0,0054	0,0138	0,0037	0,0027	0,0267	0,0059	0,0007	0,0164	0,0008	0,0073	0,0051	0,0025	0,0017
TD_651A	11255	0,0143	0,0192	0,0075	0,0051	0,0346	0,0114	0,0034	0,0209	0,0039	0,0015	0,0078	0,0051	0,0036
TD_726A	13384	0,1022	0,0111	0,0026	0,0014	0,0088	0,0030	0,0004	0,0135	0,0002	0,0033	0,0036	0,0251	0,0025
TD_751A	14342	0,0089	0,0135	0,0067	0,0016	0,0175	0,0002	0,0013	0,0149	0,0016	0,0052	0,0049	0,0021	0,0031
TD_775A	15288	0,0042	0,0083	0,0061	0,0011	0,0270	0,0025	0,0002	0,0087	0,0003	0,0088	0,0022	0,0019	0,0006
TD_800A	16462	0,0177	0,0189	0,0169	0,0066	0,0401	0,0128	0,0024	0,0304	0,0022	0,0032	0,0092	0,0136	0,0063
TD_826A	18080	0,0059	0,0120	0,0075	0,0010	0,0211	0,0059	0,0007	0,0226	0,0004	0,0025	0,0030	0,0022	0,0011
TD_850A	19876	0,0021	0,0015	0,0016	0,0005	0,0103	0,0016	0,0005	0,0145	0,0001	0,0013	0,0008	0,0007	0,0003
TD_868A	21644	0,0090	0,0104	0,0021	0,0020	0,0086	0,0043	0,0007	0,0122	0,0008	0,0022	0,0038	0,0097	0,0021
TD_896A	24742	0,0101	0,0115	0,0017	0,0030	0,0166	0,0039	0,0014	0,0119	0,0014	0,0016	0,0024	0,0197	0,0070
TD_926A	28128	0,0115	0,0127	0,0106	0,0058	0,0136	0,0013	0,0046	0,0029	0,0058	0,0158	0,0116	0,0019	0,0122
TD_963_965	31337	0,0092	0,0092	0,0024	0,0012	0,0094	0,0044	0,0010	0,0180	0,0008	0,0024	0,0038	0,0153	0,0026
TD_1001A	34940	0,0035	0,0048	0,0024	0,0003	0,0115	0,0024	0,0004	0,0065	0,0006	0,0028	0,0013	0,0014	0,0003
TD_1027A	36932	0,0193	0,0207	0,0107	0,0050	0,0389	0,0102	0,0041	0,0313	0,0034	0,0066	0,0068	0,0131	0,0108
TD_1077	40803	0,0037	0,0028	0,0021	0,0010	0,0171	0,0027	0,0004	0,0054	0,0001	0,0022	0,0010	0,0012	0,0002
TD_1151A	46669	0,0070	0,0111	0,0032	0,0025	0,0202	0,0049	0,0003	0,0237	0,0007	0,0052	0,0048	0,0019	0,0014
TD_1179A	48956	0,0173	0,0186	0,0023	0,0038	0,0175	0,0100	0,0032	0,0313	0,0029	0,0058	0,0079	0,0088	0,0035
TD_1202A	51332	0,0444	0,0577	0,0095	0,0100	0,0731	0,0342	0,0064	0,0657	0,0068	0,0071	0,0175	0,0156	0,0121
TD_1251A	57754	0,0075	0,0103	0,0038	0,0022	0,0195	0,0037	0,0011	0,0123	0,0017	0,0058	0,0023	0,0141	0,0043
TD_1277A	62455	0,0047	0,0030	0,0023	0,0017	0,0129	0,0034	0,0012	0,0123	0,0013	0,0028	0,0022	0,0026	0,0017
TD_1301A	71002	0,0167	0,0257	0,0077	0,0051	0,0204	0,0037	0,0046	0,0122	0,0052	0,0491	0,0080	0,0587	0,0111
TD_1327A	80943	0,0074	0,0098	0,0028	0,0029	0,0216	0,0039	0,0010	0,0141	0,0002	0,0033	0,0028	0,0043	0,0036
TD_1351A	92749	0,0047	0,0146	0,0050	0,0018	0,0202	0,0049	0,0015	0,0100	0,0009	0,0074	0,0045	0,0082	0,0039
TD_1378A	108845	0,0162	0,0251	0,0051	0,0039	0,0282	0,0171	0,0012	0,0864	0,0023	0,0066	0,0066	0,0347	0,0033
TD_1401A	125917	0,0078	0,0095	0,0050	0,0014	0,0191	0,0090	0,0005	0,0303	0,0004	0,0067	0,0044	0,0088	0,0021
TD_1427BA	138223	0,0041	0,0073	0,0104	0,0006	0,0104	0,0042	0,0005	0,0646	0,0008	0,0016	0,0007	0,0018	0,0007
TD_1451A	159568	0,0015	0,0030	0,0015	0,0006	0,0126	0,0010	0,0002	0,0046	0,0003	0,0038	0,0010	0,0002	0,0003

Table 15 *– Amino acid concentrations (*10^{-2} mg/m^2/y*) in Talos Dome ice samples.*

Sample name	Ice age (yrs BP)	VAH	VA	VAC
TD077	**647**	0,119	0,015	0,022
TD103	**965**	0,097	0,036	0,028
TD127	**1273**	0,129	0,520	0,107
TD151	**1595**	0,034	0,015	0,019
TD 176	**1924**	0,165	0,034	0,026
TD_202	**2286**	1,668	0,036	0,095
TD_227	**2638**	0,048	0,024	0,020
TD_251	**2996**	0,100	0,082	0,037
TD_302	**3806**	0,069	0,027	0,021
TD_327	**4221**	0,046	0,037	0,027
TD_352	**4660**	0,036	0,016	0,017
TD_377_378	**5128**	0,043	0,017	0,015
TD_403	**5624**	0,194	0,035	0,031
TD_427	**6101**	0,130	0,085	0,041
TD_451_452	**6602**	0,090	0,038	0,021
TD_478	**7212**	0,068	0,032	0,023
TD_502	**7765**	0,103	0,011	0,020
TD_527	**8367**	0,639	0,058	0,042
TD_554	**9018**	0,061	0,052	0,026
TD_575	**9480**	0,131	0,017	0,028
TD_606	**10187**	0,083	0,019	0,021
TD_627	**10686**	0,121	0,018	0,019
TD_651	**11255**	0,041	0,065	0,015
TD_726	**13384**	0,041	0,027	0,013
TD_751	**14342**	0,064	0,019	0,019
TD_775	**15288**	0,139	0,045	0,034
TD_800	**16462**	0,336	0,492	0,136
TD_826	**18080**	0,197	0,021	0,030
TD_850	**19876**	0,039	0,015	0,019
TD_868	**21644**	0,156	0,452	0,096
TD_896	**24742**	0,096	0,026	0,017
TD_926	**28128**	0,136	0,044	0,036
TD_963_965	**31337**	0,089	0,377	0,077
TD_1001	**34940**	0,068	0,041	0,022
TD_1027	**36932**	0,075	0,019	0,016
TD_1077	**40803**	0,124	0,016	0,026
TD_1151	**46669**	0,235	0,020	0,038
TD_1179	**48956**	0,092	0,022	0,020
TD_1202	**51332**	0,283	0,042	0,024
TD_1251	**57754**	0,039	0,166	0,021
TD_1277	**62455**	0,171	0,023	0,027
TD_1301	**71002**	0,083	0,042	0,022
TD_1327	**80943**	0,079	0,025	0,017
TD_1351	**92749**	4,943	0,021	0,259
TD_1378	**108845**	0,059	0,023	0,020
TD_1401	**125917**	0,048	0,032	0,017
TD_1427	**138223**	0,049	0,039	0,020
TD_1451	**159568**	0,076	0,073	0,032

Table 16 *– Phenolic compound concentrations (*10^{-2} mg/m^2/y*) in Talos Dome ice samples.*

An examination of an eventual trend of amino acids in the ice core should lead to a hypothesis of past biological activity, as primary productivity could have influence the abundance and the composition of amino acids, being the amino acids a part of the organic matter present in marine ecosystems, as well as in freshwater, and used as a source of nitrogen by several phytoplankton species and bacteria (Berman and Bronk 2003). D-amino acids are a proof of the presence of bacteria as they derive from the biodegradation of peptide-glycan membranes (Wedyan and Preston 2008); although were not found significant quantities in this work, except for D-aspartic acid, which leads to the hypothesis of the presence of bacteria. The phenolic compounds present in significant quantities in the Taldice samples resulted to be the vanillic acid, vanillin and acetovanillone. It was noticed that the trend of the vanillic acid, recognized as a tracer of the conifer combustion (Simoneit, 2002) and present in higher quantities in the Taldice samples compared to vanillin and acetovanillone, differs from the other two in certain periods, suggesting possible different sources. The amino acid found to be present in higher quantities in the Antarctic samples in this work is glycine with an average percentage on the total amino acids detected in this work of 28.6% (***Figure 19***), which is consistent with the results found in the Holtedahlfonna glacier in the Svalbard island (Barbaro et al. 2017) in which was observed that Glycine was the most abundant amino acid found due to a greater stability in time.

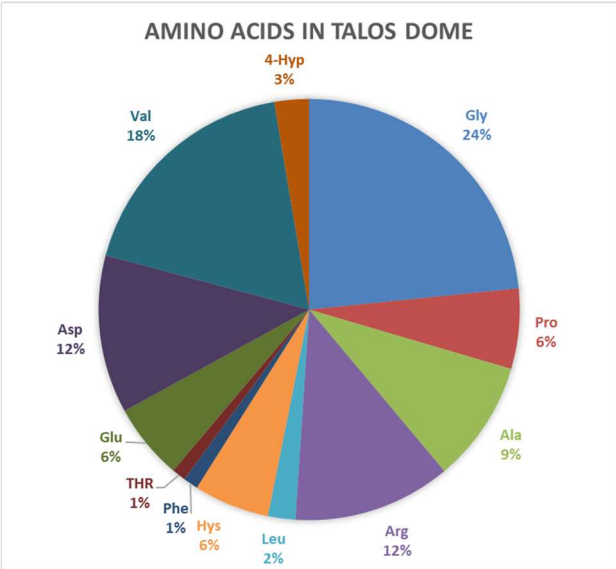

Figure 19 *– Pie diagram expressed in abundance percentage of amino acids detected in the samples.*

In order to evaluate a possible correlation between the amino acid trend and the temperature, a plotting of the obtained concentrations of the amino acid and phenolic compounds versus the values of $\delta^{18}O$ was performed. The low resolution of these analyses on grounds of the low number of samples available, doesn't allow an accurate evaluation in terms of trend and comparison with other data, nevertheless an approximate trend can be assessed. The resolution of the upper part of the core representing the earliest samples is higher compared to the rest but still were not found evidences of a possible meaningful correlation with other records from Taldice or regional ice cores.

However, in both cases is noticed especially in the late period a barely similar trend with the temperature which should be likely to follow the same pattern, especially in the case of the amino acids, since the biologic activity is correlated to the temperature. In the same way, phenolic compounds are produced from lignin combustion (Simoneit, 2002) and higher temperatures, as well as higher CO_2 concentrations, increase the plant productivity, hence the probability to have fire activities (Daniau et al., 2010; Marlon et al., 2008).

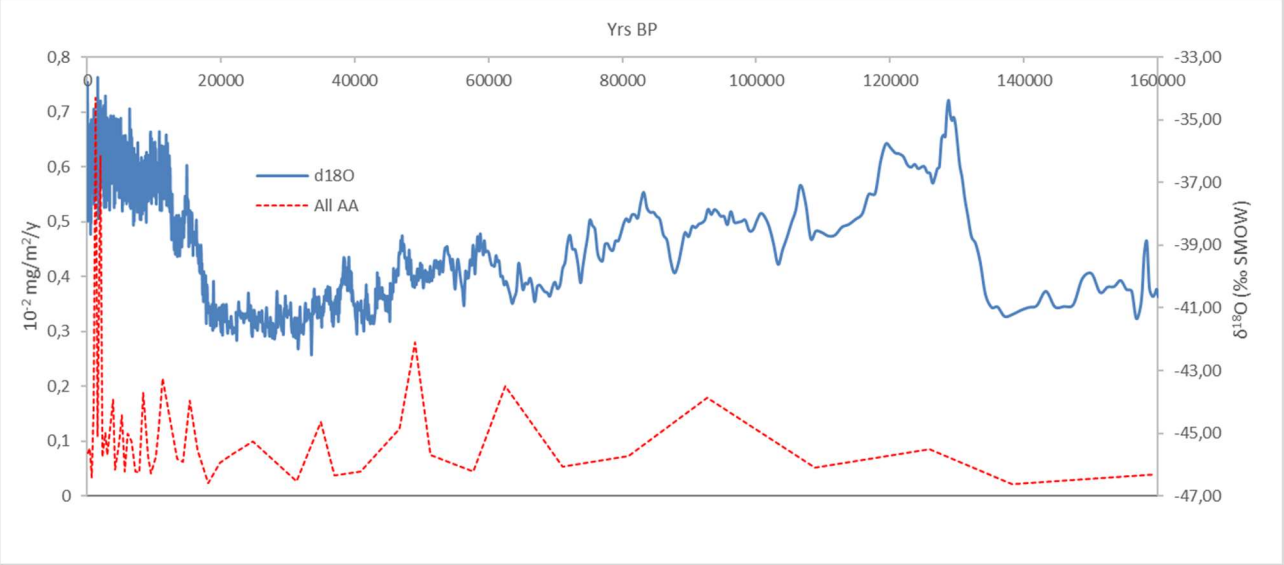

Figure 20 *– Plot representing the trend of the total amino acids present in the Talos Dome samples (red line). The blue line represents the trend of the $\delta^{18}O$ values in the core.*

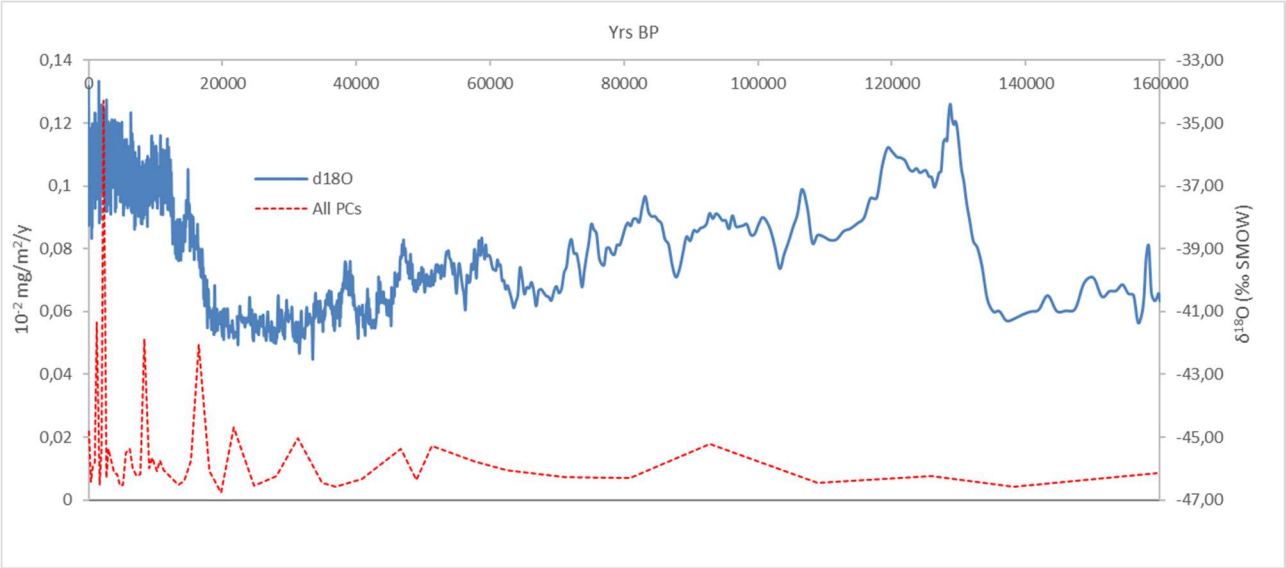

Figure 21 *– Plot representing the trend of the total PCs reported in present in the Talos Dome samples (red line). The blue line represents the trend of the $\delta^{18}O$ values in the core.*

In the figures below are shown the amino acids (***Figure 23***) and methoxyphenols (***Figure 24***) found in the Taldice samples analyzed in this work. As can be noticed, all the amino acids have approximately the same trend except for proline and glutamic acid which show a different behavior in certain points of the plot.

The phenolic compounds detected in the Taldice samples are vanillin, vanillic acid and acetovanillone. The abundance of the vanillin (VAH) far exceeds vanillic acid (VA) and acetovanillone (VAC), as shown in the figure below, in accordance with other works regarding the study of phenolic compounds in environmental matrices. In the work *Free phenolic compounds in waters of the Ross Sea* (Zangrando et al., 2017) submitted for publication, was studied the ratio VA/VAH as an indicator of the oxidation process of vanillin into vanillic acid (Net et al., 2011). This work suggests that VA/VAH ratio in seawater in comparison to the atmospheric aerosols is lower probably due to a newly emission of phenolic compounds, hence the airborne oxidation process have not started.

In the work Zangrando et al., 2016, are reported the values of phenolic compounds in Antarctic aerosols. It has been noticed that the VA/VAH ratio at the coastal sites are lower than the plateau regions, which states the oxidation in aerosols of vanillin to vanillic acid. The values of VA/VAH ratio turned out from the analyses in seawater and aerosols in Zangrando et al., 2016 are respectively 0.04±0.02 and 0.13±0.06. The average ratio VA/VAH in the 48 samples in the Taldice core turned

out to be 0.76, that is higher than the ratio found out in aerosols and seawater, probably due to the airborne oxidation progress during the air transport and the atmospheric deposition, confirming furthermore the assumption made in the work mentioned above.

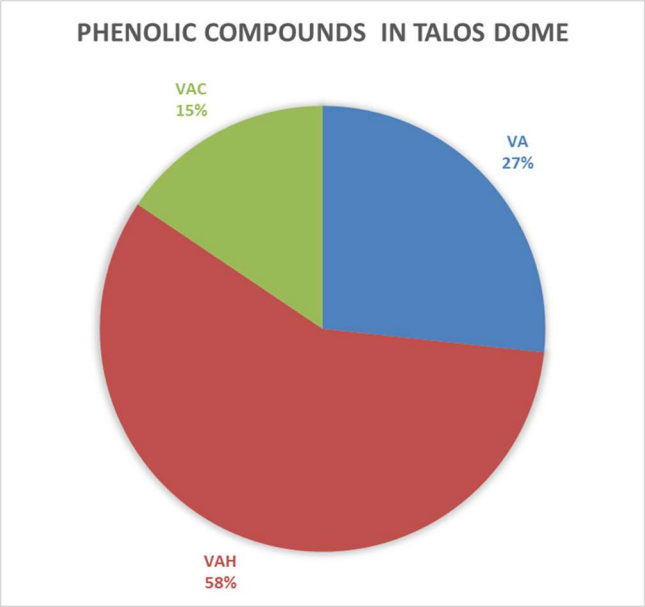

Figure 22 *– Pie diagram expressed in abundance percentage of the phenolic compounds detected in the samples.*

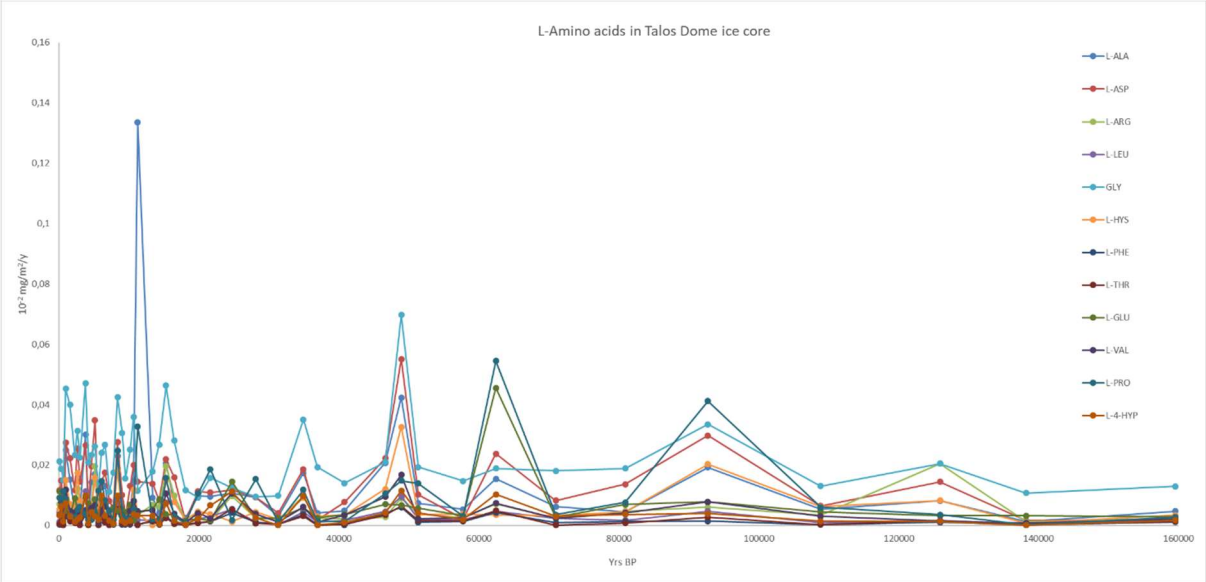

Figure 23 *– Amino acids detected in the Talos Dome ice core reported in 10^{-2} mg/m^2/yr.*

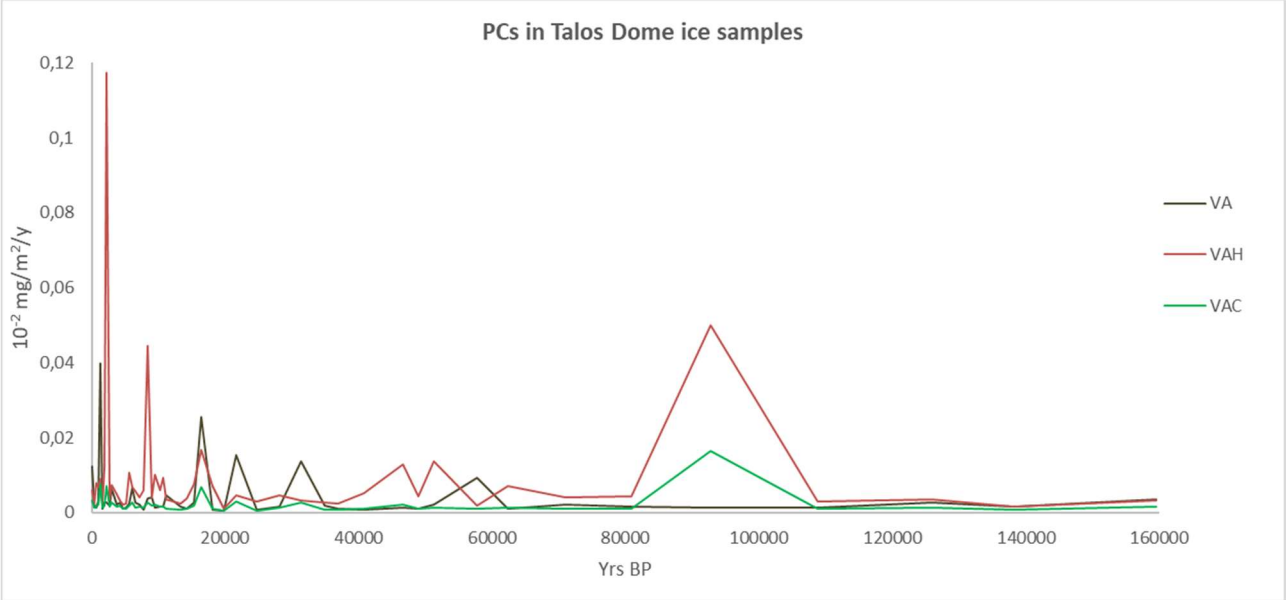

Figure 24 *– Phenolic compounds detected in the Talos Dome ice core reported in 10^{-2} mg/m^2/yr.*

In both amino acid and phenolic compound data elaboration was performed an assessment of the relative abundance of the analytes in the glacial and interglacial period showing a similar abundance in the hole temporal extent of the samples, thus the quite absence of significant differences.

5.2 AMINO ACIDS IN RENLAND SAMPLES

The Renland ice core samples analyzed in this work were 529 for a time range of 5000 year, a resolution much higher than the Taldice samples, which allows a better evaluation in terms of time extent of the analytes detected in this core.

In this work, in Renland ice core samples were performed analyses of D- and L- amino acids applying the same operating conditions used for the amino acid analyses in Taldice core and the analytical method validated during this work. The quantification was performed correcting the results with the instrumental response factor for each analyte, obtained through tests performed in the meanwhile the analyses were in process, with solutions in ultrapure water containing labelled (concentrations ranging from 0.85 µg L^{-1} to 1.05 µg L^{-1}) and native (concentrations ranging from 0.95 µg L^{-1} to 1.15 µg L^{-1}) amino acids. The results are expressed in concentrations (µg L^{-1}) since until now

we don't have data regarding the flux and deposition information for the Renland ice core. Nevertheless, since the time range of the samples is about 5000 years belonging to the Holocene, we neglected significant flux differences: however, this further consideration will be conducted in the future as soon as the information regarding the local temperature and fluxes will be available.

The amino acids detected in the Renland samples are L-Ala, L-Pro, L-Val, L-Arg, L-Ser, Gly and L-Orn in concentrations that range from 0.001 µg L^{-1} to 5.46 µg L^{-1}. The concentration values, reported in table X in the supplementary section, were obtained subtracting 1/2LOD for each amino acid. The LOD values used are the same as for the Taldice amino acid analysis. There were not found significant quantities of D-amino acids. In accordance to other works, as mentioned above, Gly and Ala are the most abundant amino acids found with respectively a mean percentage of 25.0% and 27.5% on the total amino acids quantified followed by L-Ser (16.1%), L-Orn (13.5%), L-Arg (7.0%), L-Val (5.4%) and L-Pro (5.2%).

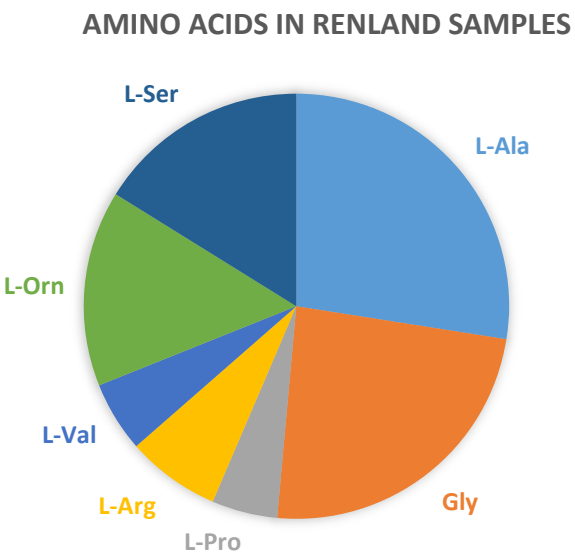

Figure 25 *– Pie diagram expressed in abundance percentage of the amino acid compounds detected in the Renland ice core samples.*

In the major part of the samples, all the amino acids follow the same trend, as can be noticed in the figure below where is reported a part of the results obtained. There were not observed significant different behaviors of any amino acid in particular.

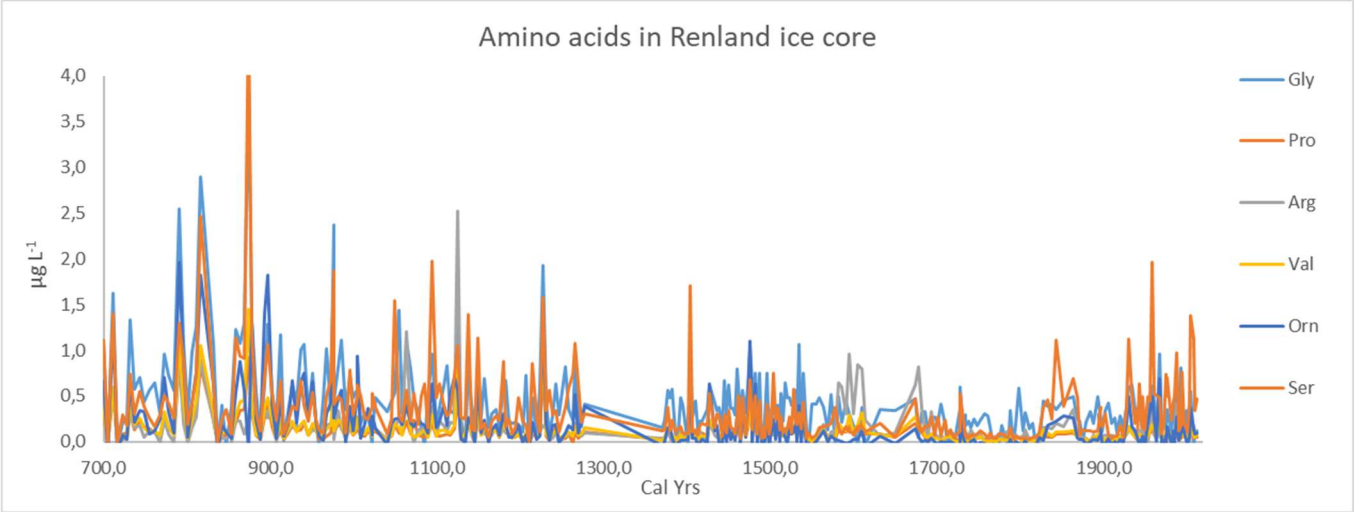

Figure 26 *– Amino acid concentrations in the time range 2012 – 700 cal yrs.*

There was performed a comparison between the alanine concentration, since was found to be the most abundant amino acid present in the samples, with other records from regional ice cores and marine sediment in order to evaluate a possible correlation and to understand the origin. The sites considered for this purpose and which provided interesting information are the *GRISP2* ice core ammonium data (Mayewski, 1999) and the $CaCO_3$ paleoproductivity records of two marine sediments collected in the Fram Strait (Muller et al., 2012). In the figure below are shown the site locations.

Figure 27 *– Location of the ice cores (Renland and GRISP2) and marine cores (MSM05/5_712_2 and MSM05/5_723_2) in the study area.*

It was found a similar trend in ammonium records in *GRISP2* ice core comparing with alanine the first 600 years, as can be noticed in the figure below. The time range used for the comparison was selected because of the good resolution of the Renland data in this period. The correlation is observed intermittently, depending also on the inhomogeneous resolution of the amino acid data, making the quantification of the correlation between the two datasets misleading. The similar trend found in the two ice cores may be interesting in understanding the source of the amino acids detected, providing insights also on the atmospheric transport and on the regional climate, since ammonium was found to be one of the major components of the low-latitude air mass in *GISP2* study area, together with biogenic nitrate ions (Mayewski et al., 1997). Another important feature is the source of NH_4^+, found to be both anthropogenic and natural. Furthermore, the presence of ammonium in polar ice was found to be linked to the temperature variations and biogenic emissions (Fuhrer et al., 1993; Fuhrer et al., 1996) as well as to NH_3 which in turn is linked to bacterial decomposition and biomass burning (Legrand et al., 1992).

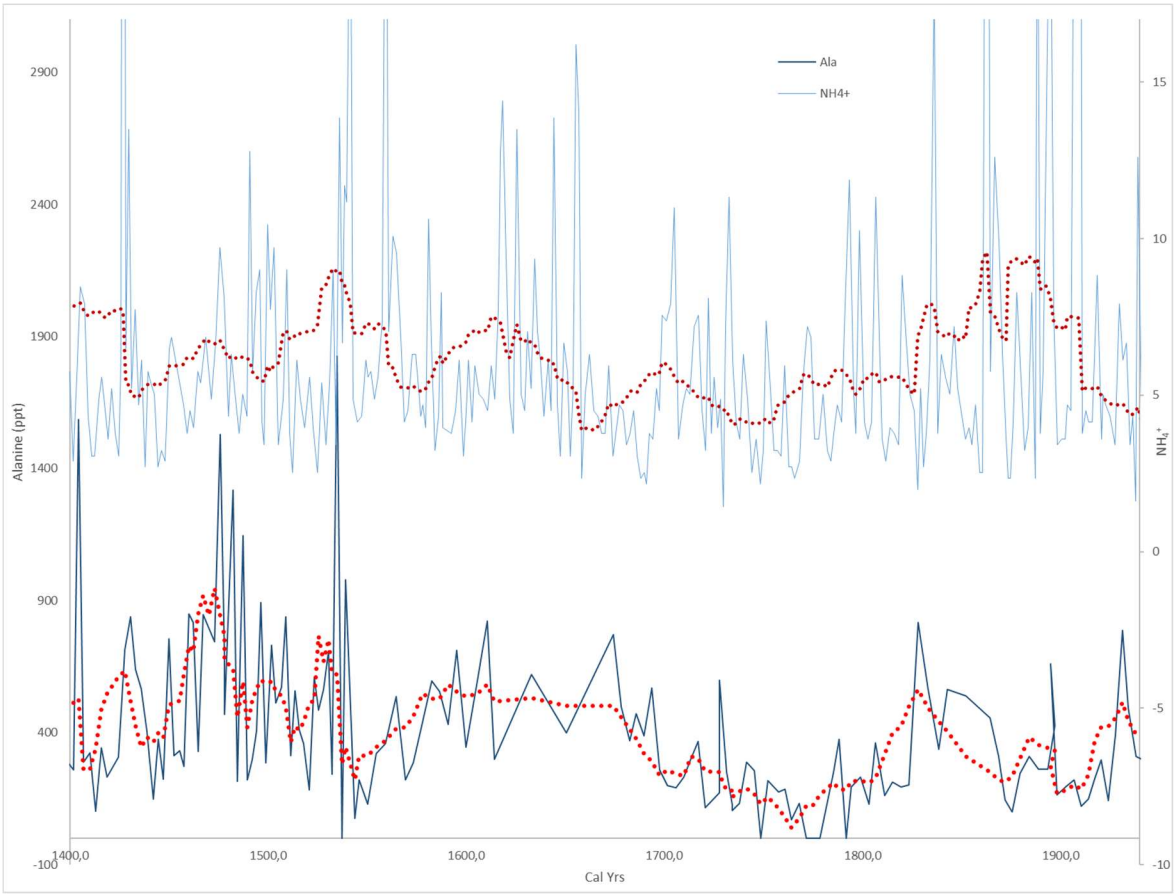

Figure 28 *–NH_4^+ (µg Kg^{-1}) and Ala concentration profiles in GRISP2 and Renland, respectively***.** *The red dotted line represents the mobile average.*

A further assessment was made comparing paleoproductivity expressed as calcium carbonate ($CaCO_3$) records from sediment cores collected in the Fram Strait region, as described above. $CaCO_3$ is one of the main components of the whole biogenic fraction in sediment depositions, hence linked to phytoplankton and zooplankton which are the major source of organic carbon in seawater and sediments (Rühlemann et al., 1999). The Renland ice cap is a site located in a coastal area suggesting that it would be plausible a similar trend of the amino acids found in the ice core and $CaCO_3$, intended as paleoproductivity, detected in sediment cores near the study site. We didn't expect a perfect correlation given the different type of matrices and the different transport dynamics involved: nevertheless, being the site in a coastal area we assume that the marine circulations could affect the East Greenland ice shelf environmental conditions. In fact, it can be noticed from the figure below an increasing trend toward the earliest part of the time range followed by a rapid decrease, as observed in the alanine trend.

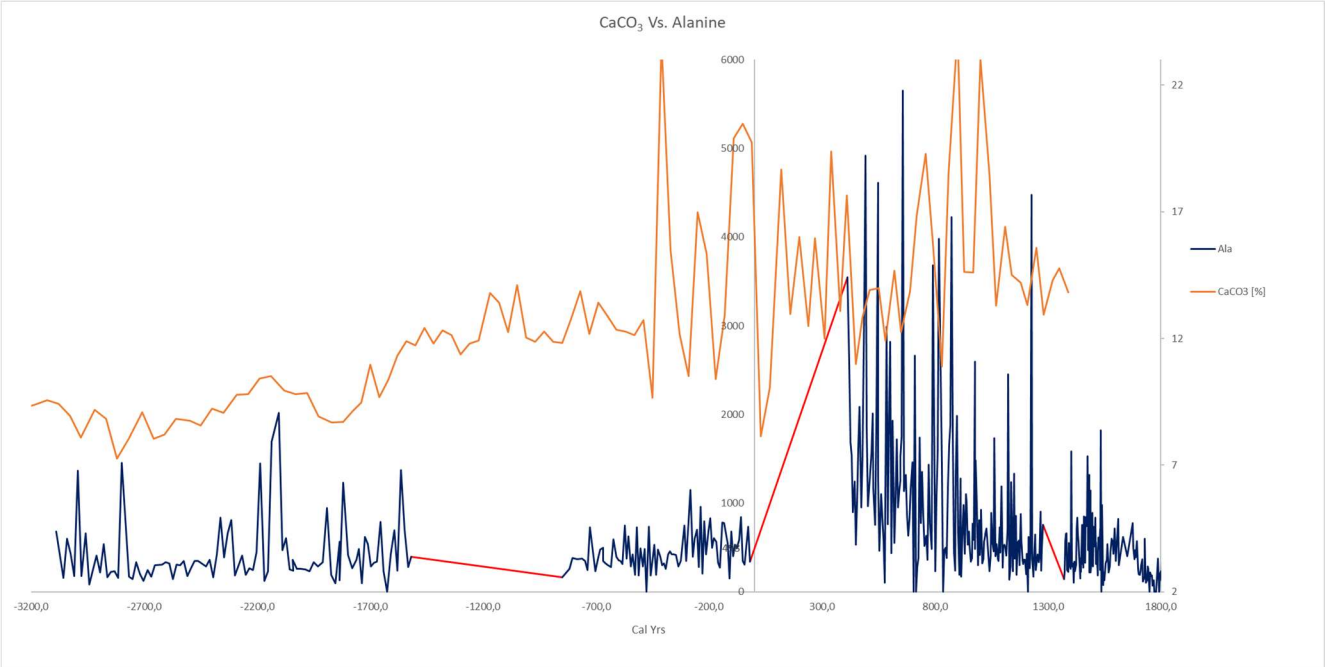

Figure 29 *– $CaCO_3$ [%] paleoproductivity observed in marine sediment MSM05/5_723_2 and Ala concentration profile. The red lines indicate the lack of data.*

In the same work (Muller et al., 2012) were made measurments on the marine sediment MSM05/5_712_2 of IP_{25}, a monounsaturated hydrocarbon considered a sea-ice biomarker, since is produced exclusively by sea-ice diatoms (Belt et al., 2007), as well as measurements of brassicasterol and dinosterol accumulation, phytoplankton-derived biomarkers (Boon et al., 1979; Volkmann et al., 1998) expressed as P_BIP_{25} and P_DIP_{25} index, respectively. In the figure below are shown the concentration profile of Ala and P_BIP_{25} index, wich turns out to follow roughly the trend of $CaCO_3$ with a maximum at 800 – 1400 cal yrs followed by an abrupt decrease, as observed also in the amino acid trend.

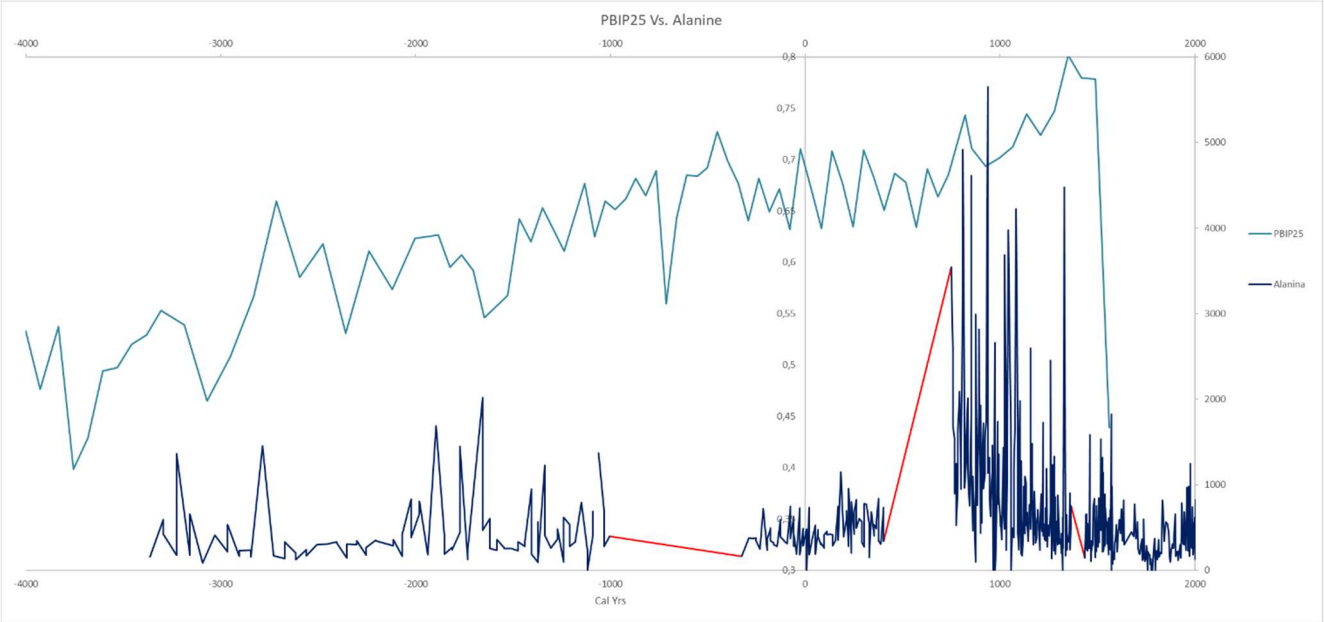

Figure 30 *– Concentration profile of Ala and P_BIP_{25} index in MSM05/5_712_2 marine sediment (Muller et al., 2012).*

5.3 QUALITATIVE ANALYSIS IN TALDICE

The first step was the assessment of two analytical methods: UHPLC-ESI/HRMS and *nano*UHPLC-*nano*ESI/HRMS with the aim to examine the sensitivity and to determine whether the *nano*-technique is more sensitive. In a first analysis, it turned out that in the *nano*-technique it was necessary to increase the threshold in comparison to the UHPLC-ESI/HRMS method due to the high background noise observed. In the table below are shown the parameters set in SIEVE software.

Method	Threshold	Ratio sample/blank	Frames
NanoHPLC-nanoESI/HRMS	50000	>5	580
HPLC-ESI/HRMS	8000	>2	215

Table 17 *– Parameters set in Sieve software for the statistical evaluation of the analysis performed in UHPLC-ESI/HRMS and nanoUHPLC-nanoESI/HRMS.*

The number of data was filtered so that to include only the frames that are significantly present in the samples, selecting only the frames with a given ratio sample/blank value. For the *nano*-technique it was required a greater value of ratio to avoid including background frames. As can be noticed from the number of frames obtained from the two methods, the *nano*-technique is much more sensitive. For this purpose, was compared also the signal intensity which turned out to be up to 10000 times higher in the case of the *nano*-technique; however, also the background signal was found to be higher. For this reason, the comparison was made between the ratio signal to noise resulting 100 times higher, except for the sample TD52 for which was observed a strong signal suppression in positive mode, probably due to the high matrix effect. The quantification of the sensitivity in the two cases was evaluated furthermore considering the signal of the internal standard, confirming the values reported above.

Given the importance that the exact mass of the ion has during the identification of the molecule, a further evaluation was made with the mass accuracy of the instrument, performed checking the exact mass given by the instrument of the internal standards and comparing it to the real one. This step was a further check performed other than the external mass calibration made every 48h with a calibrating solution and the internal mass calibration set with the introducing of a lock mass (or lock masses). In our case was considered the labelled vanillin, since resulted to have the best peak quality and a higher signal, giving a mass accuracy within a range of ±2ppm.

The Taldice samples analyzed in *nano*UHPLC-*nano*ESI/HRMS in positive mode are TD27, TD176, TD606, TD726, TD1001 and TD1077 and in negative mode are TD27, TD52, TD606, TD726, TD1001 and TD1077. At first, were performed the analyses in negative mode and subsequently in positive mode, using the working conditions described above. The samples selected for both the analyses were decided after a preliminary evaluation in UHPLC-ESI/HRMS that was made in order to choose the most significant ones for the analysis with the *nano*-technique. It was excluded from the elaboration the analysis in positive mode of the sample TD52 due to the high signal suppression observed, as mentioned above, and was replaced by TD176 resulted to be the most interesting from the list of the samples excluded from the analysis in *nano*ESI.

The total molecules identified in this work are 157 in positive mode and 214 in negative mode. The different ionization led to the identification of different family compounds in the two cases, as shown in the table below.

	Negative mode	Positive mode
Family compounds		
	CHO	CHON
	CHON	CHOS
	CHOS	CHOP
	CHONS	CHO
		CHONP
		CHN
		CHONS
		CHNS

Table 18 *– Family compounds identified in positive and negative mode.*

In negative mode were identified less family compounds with a large dominance of CHO compounds, followed by CHON, CHOS and CHONS. On the contrary, the data elaboration of the positive mode analyses led to the identification of a higher number of family compounds with e prevalence of CHON, CHOS and CHOP compounds. The organic nitrogen-oxygen compounds (CHON) can be attributed to reactions that involve the presence of NO*x* gasses (Mazzoleni et al., 2010) as well as to the presence of amino acids. As mentioned in the section ***Data elaboration***, the Kendrick diagram was crucial for the identification of homologous series standing in horizontal lines in the *Kendrick diagram* and differing by -CH_2- units, and it turned out to be extremely helpful in case of uncertain identification. Another way to assure a good identification was made possible by the comparison of the chromatograms since the retention time and the peak shape of the homologous species are similar. Below is shown an example of homologous species chromatograms obtained in the sample TD726, corresponding, from the top to the bottom, to $C_6H_6O_2N_2$, $C_8H_{10}O_2N_2$, $C_7H_8O_2N_2$ and $C_6H_6ON_2$.

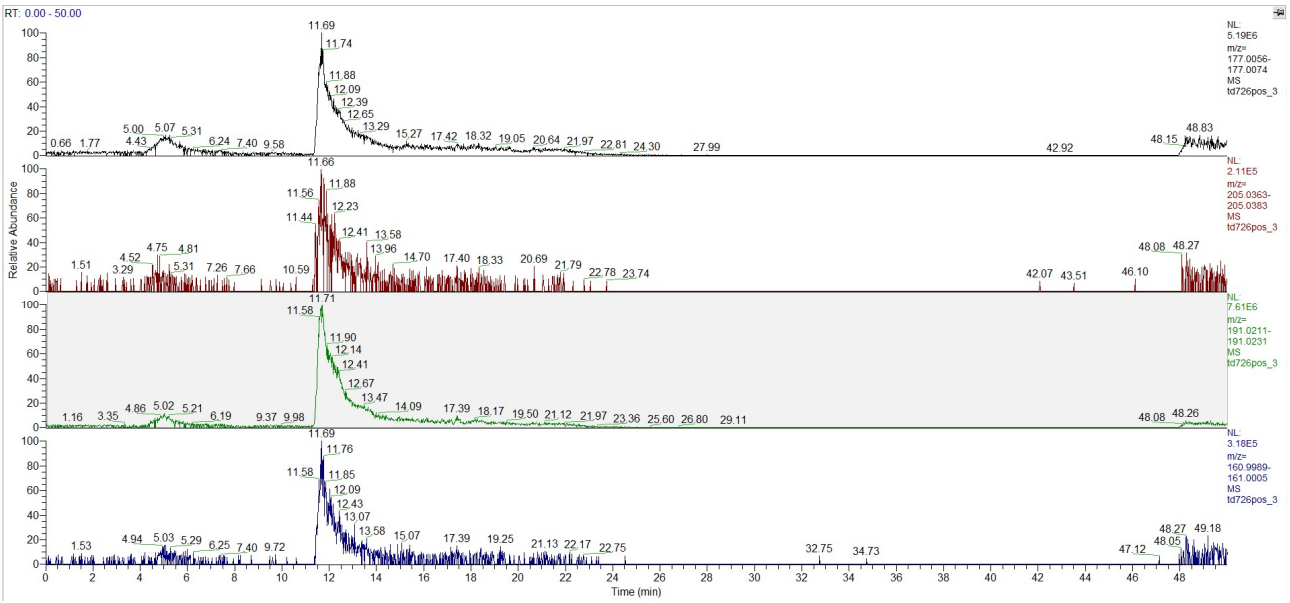

Figure 31 *– Chromatograms of the homologous species to $C_6H_6O_2N_2$, $C_8H_{10}O_2N_2$, $C_7H_8O_2N_2$ and $C_6H_6ON_2$ observed in the sample TD726.*

In the ***Figure 32*** is reported as an example the Kendrick diagram reporting in the X-axis the *Kendrick mass* and in the Y-axis the *Kendrick mass defect*, for the analyses in positive (red triangles) and negative (blue squares) mode of sample TD27. The same was made for every sample analyzed. In the diagram is observed an increase in the mass defect with the molecular mass due to the increase of oxidation and/or unsaturation number with higher molecular masses (Smith et al., 2009).

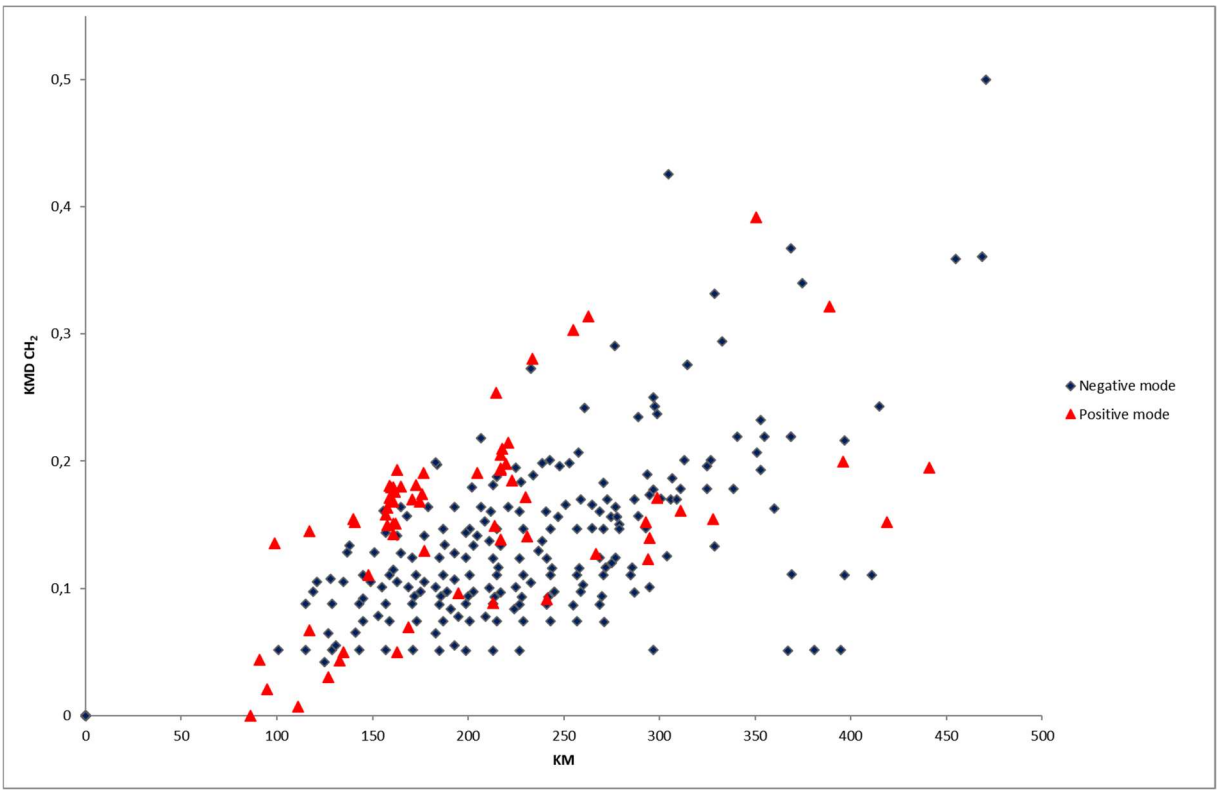

Figure 32 *– Kendrick diagram of sample TD27 performed with the frames obtained and identified in positive (red triangles) and negative (blue squares) mode.*

VAN KREEVELEN DIAGRAMS

The Van Krevelen diagrams are obtained plotting the ratio hydrogen/carbon versus the ratio heteroatoms/carbon with the aim of describing the evolution of the organic matter present in the matrices in terms of saturation/unsaturation and oxidation/reduction. In this work, the *Van Krevelen diagrams* constructed were H/C vs. O/C given the high number of compounds containing oxygen. In the ***Figure 33*** is reported the Van Krevelen diagram of sample TD27.

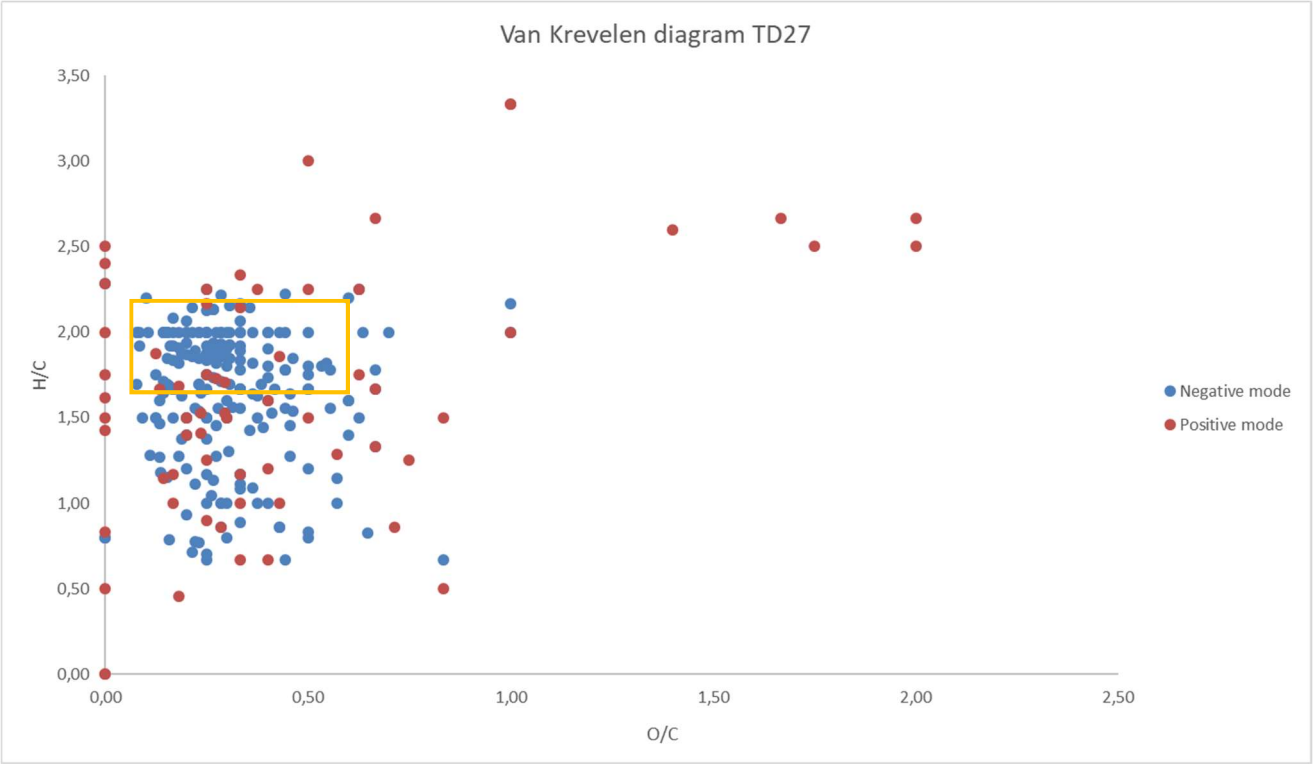

Figure 33 *– Van Krevelen diagram of the sample TD27 performed with the frames obtained in negative (blue circles) and positive (red circles) mode.*

As can be noticed, especially in positive mode are observed compounds with O/C ratio equal to zero indicating the presence of compounds not containing oxygen, such as CHN (the major part), CHS and CHNS, observed in positive mode in this work. The region highlighted by the yellow square in the diagram (H/C>1.5 and O/C <0.5) is characterized by a large number of frames, indicating a significant oxidation process. Comparing the *Van Krevelen diagrams* obtained in this work with the diagram obtained from past studies performed first in (Krevelen, 1950) and then in (Visser et al, 1986) in which are collocated the possible biologic family compounds (***Figure 17***) we can suggest that the compounds found in the samples derive from lipids, lignins, proteins (the most populated area) and condensated hydrocarbons. The molecules with higher values of H/C and lower values of O/C (more specifically H/C>1.5 and O/C <0.5) are likely to be aliphatic, whereas the compounds having lower values of H/C (more specifically H/C<1 and O/C<0.5) are likely to be aromatic (Kourtchev et al., 2013).

In the figure below are highlighted some of the principle lines observed in the *Van Krevelen diagram*

that indicate the chemical transformations. The horizontal lines (in the figure lines *d* and *h*) indicate oxidation (to the right, toward greater O/C values) or reduction reactions (to the left, toward lower O/C values). The diagonal lines (in the figure lines *e*, *f* and *g*) indicate metilation reactions, whereas the vertical lines (in the figure lines *a*, *b* and *c*) indicate hydrogenation (upward, higher H/C values) or dehydrogenation (downward, lower H/C values) reactions. The horizontal lines (in the figure lines *d* and *h*) indicate decarboxylation reactions whereas the line *i* passing for the origin of the axis indicate hydration or dehydration reactions (Kim et al., 2003).

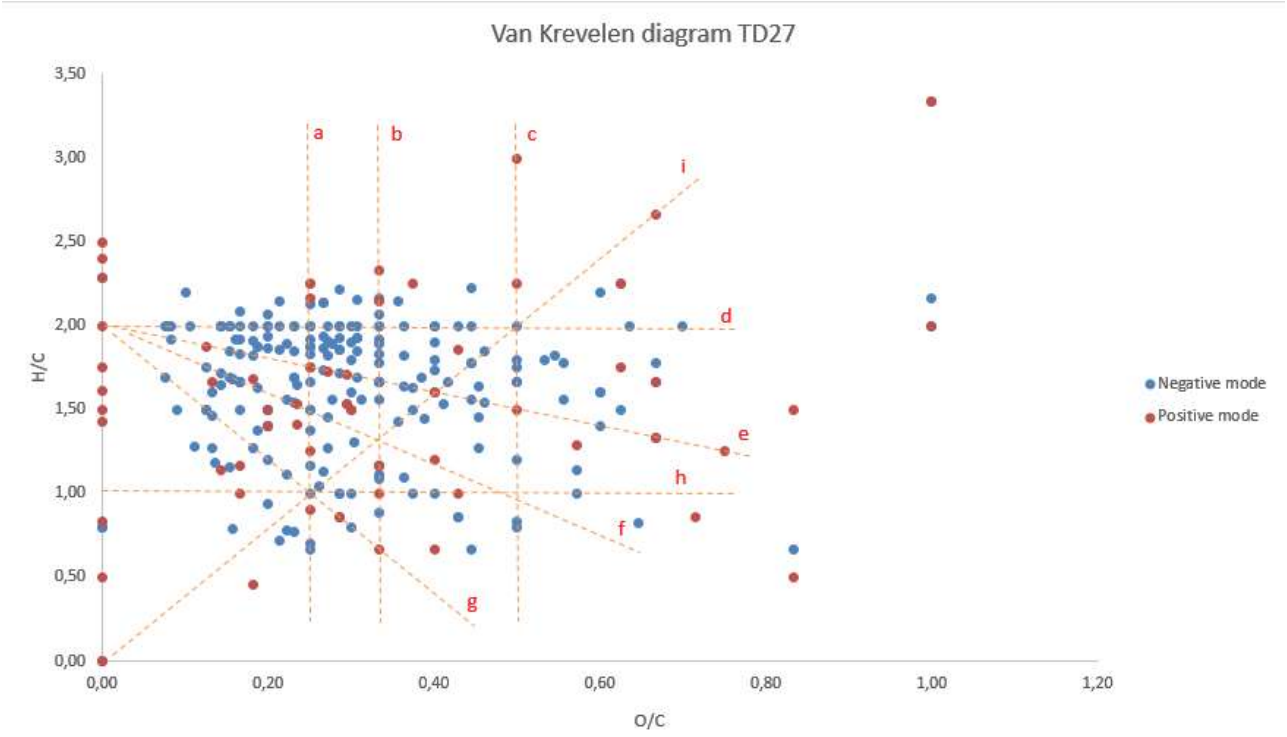

Figure 34 *– Van Krevelen diagram of the sample TD27 performed with the frames obtained in negative (blue circles) and positive (red circles) mode. The dotted lines indicate the chemical transformations.*

DOUBLE BOND EQUIVALENT (DBE)

The *Double Bond Equivalent* value, calculated as shown in ***Eq. 7*** (Wozniak et al., 2008) gives insights on the presence of double bonds and rings in the molecule (Smith et al., 2009). In the figures below are shown the plots of DBE values versus the carbon number. Were considered only the molecules with integer DBE number.

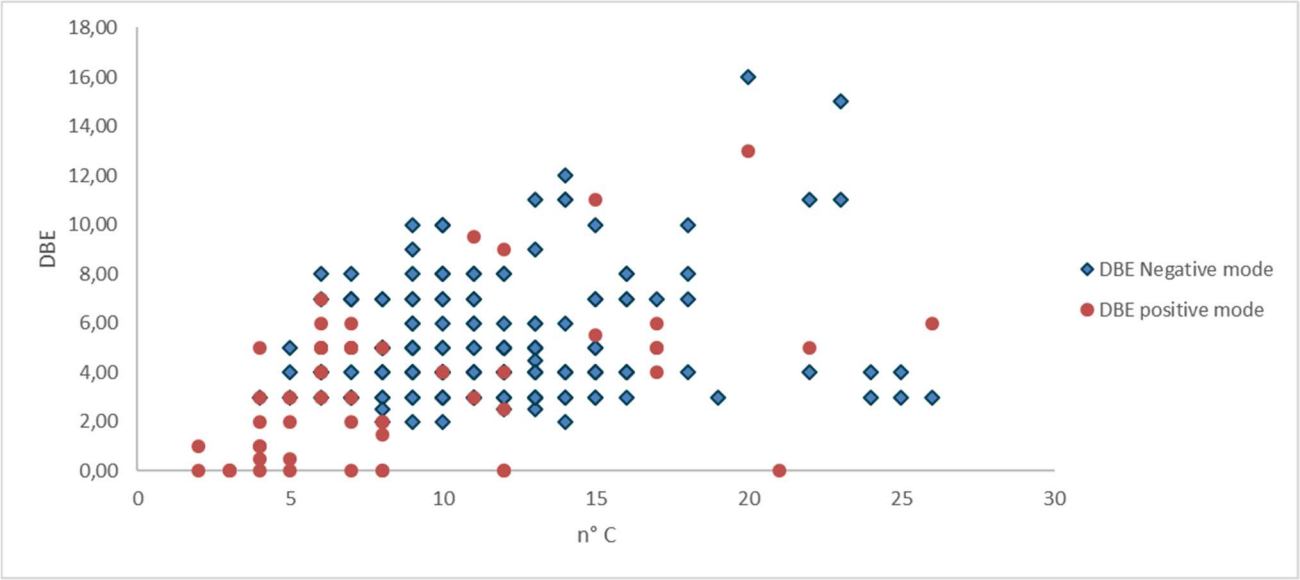

Figure 33 *– DBE diagram of the sample TD27 performed with the frames obtained in negative (blue squares) and positive (red circles) mode.*

In the diagram above can be noticed the difference between the molecules identified in the two cases. In fact, the compounds identified in positive mode are characterized mainly by small DBE values, therefore by small carbon numbers. On the contrary, compounds found in negative mode are compounds with higher number of carbons and DBE values.

OXYDATION STATE OF CARBON (OSc)

The OSc diagrams are an important instrument for assessing the oxidation state of organic compounds in environmental matrices. The OSc values were calculated using the equation Eq. 6 described in the section **Data elaboration**. In the figure below is shown the OSc diagram of the compounds found in the sample TD27. The negative values of OSc indicate reduced molecules, on the contrary positive values indicate oxidized compounds. Since the variety of family compounds identified is higher in positive mode, this is reflected even in the high variability of the OSc values varying from +3 to -3. The diagram reported in ***Figure 18*** (Kroll et al., 2011) which attributes stable organic molecules to different OSc values, gives further insights on the understanding the molecular structure and reactions involved. According to the diagram (Kroll et al., 2011) moving in the horizontal in the OSc diagram we find oligomerization reactions, since the OSc value doesn't change. In the same way, moving upwards and downwards, the number of carbons remains unchanged

while the OSc increases or decreases, suggesting functionalization reactions, whereas in diagonal occur fragmentation reactions.

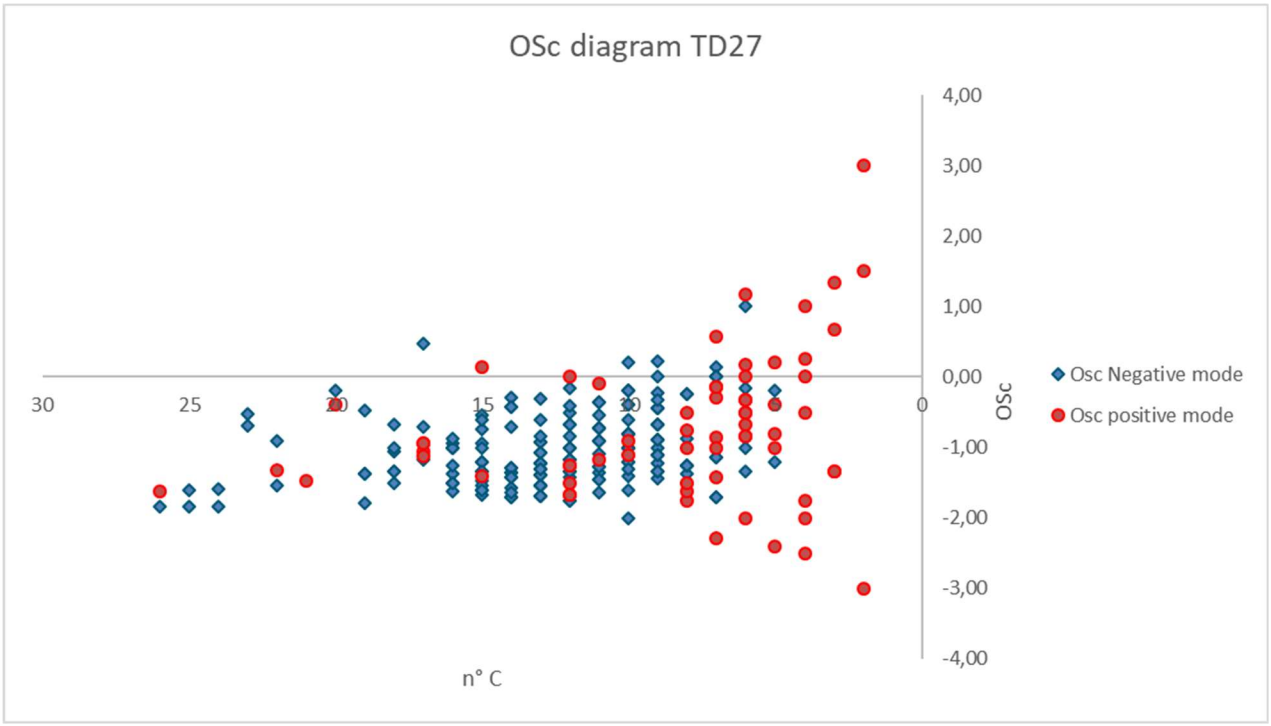

Figure 34 *– OSc diagram of the sample TD27 performed with the frames obtained in negative (blue squares) and positive (red circles) mode.*

From the data elaboration didn't result any significant difference between the samples, since they present a similar composition. In order to evaluate whether there is a difference between the samples in terms of abundance of the species found, were constructed bubble charts of the OSc diagrams including the peak areas. As the major part of the molecules observed are CHO compounds, the attention was focused particularly on the behavior of the latter. The results of this assessment led to the conclusion that the samples belonging to the glacial period are characterized by a more abundant presence of oxidized species whereas for the younger samples was observed a more variable oxidation state value. In the figures below are reported as an illustrative example the OSc bubble charts of CHO compounds in TD27 (103 yrs BP), TD726 (13108 yrs BP) and TD1077 (40294 yrs BP) highlighting the homologous series. It was observed that the series $C_nH_{2n}O_2$ has a different abundance trend in the samples with higher peak intensities of the most oxidized $C_nH_{2n}O_2$ compounds in the youngest samples and a gradual increase of the reduced ones for the oldest

samples. Nevertheless, this is a comparison performed between samples with different number of identified compounds, therefore is only an approximative assessment and need to be completed. In the **Supplementary section** are reported the remaining diagrams of all the samples and homologous series.

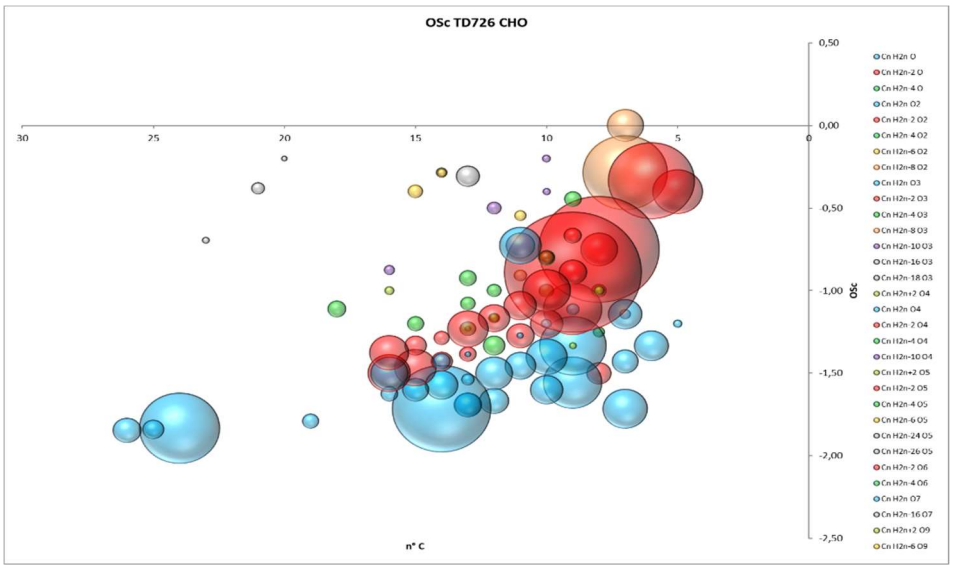

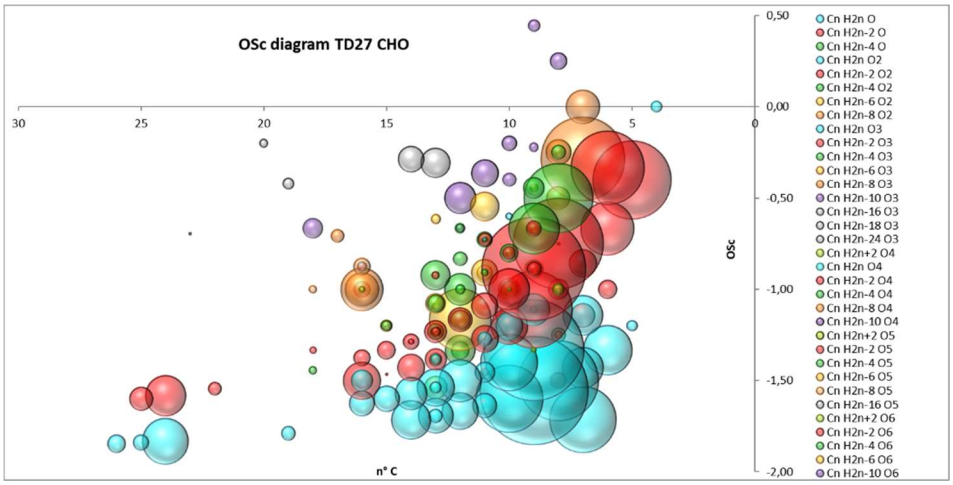

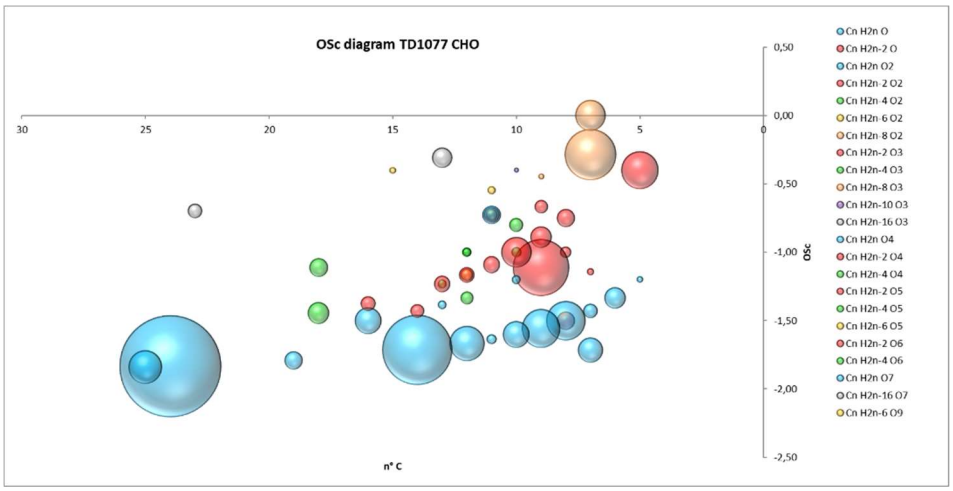

Figure 35 *– OSc bubble charts of CHO homologous series in TD27, TD726 and TD1077. The turquoise bubbles represent $C_2H_{2n}O_2$ family compounds.*

Were not found significant results regarding other family compounds in terms of differences between the samples, probably due to the small number of compounds identified for these families.

5.4 Fatty acids and atmospheric markers in Rendezvous ice core: Preliminary results

The preliminary analyses of fatty acids and atmospheric markers in the snow samples of Rendezvous ice core were performed through a prior preconcentration 1:10 on SPE-SAX cartridges, after a method optimization performed in order to obtain the best recovery. The optimization tests described above led to the choice of an elution solution that consists in a mix of methanol/water 1:1 basified with 5% of ammonium hydroxide. In the graph shown in ***Figure 36*** are reported the concentration factors obtained for each analyte, indicating with CF=10 a recovery performed at 100% of the analyte. As can be seen, the method led to a recovery of about 25% for the first analytes shown in the graph to a higher recovery for the smaller fatty acid, whereas for the bigger fatty acids (oleic acid, palmitic acid, behenic acid, tricosanoic, heptacosanoic and melissic acid) were not preconcentrated. Furthermore, was observed a recovery higher than 100% (β-nocaryophillonic and β-caryophillonic). This preconcentration method was not fully optimized and is still being improved.

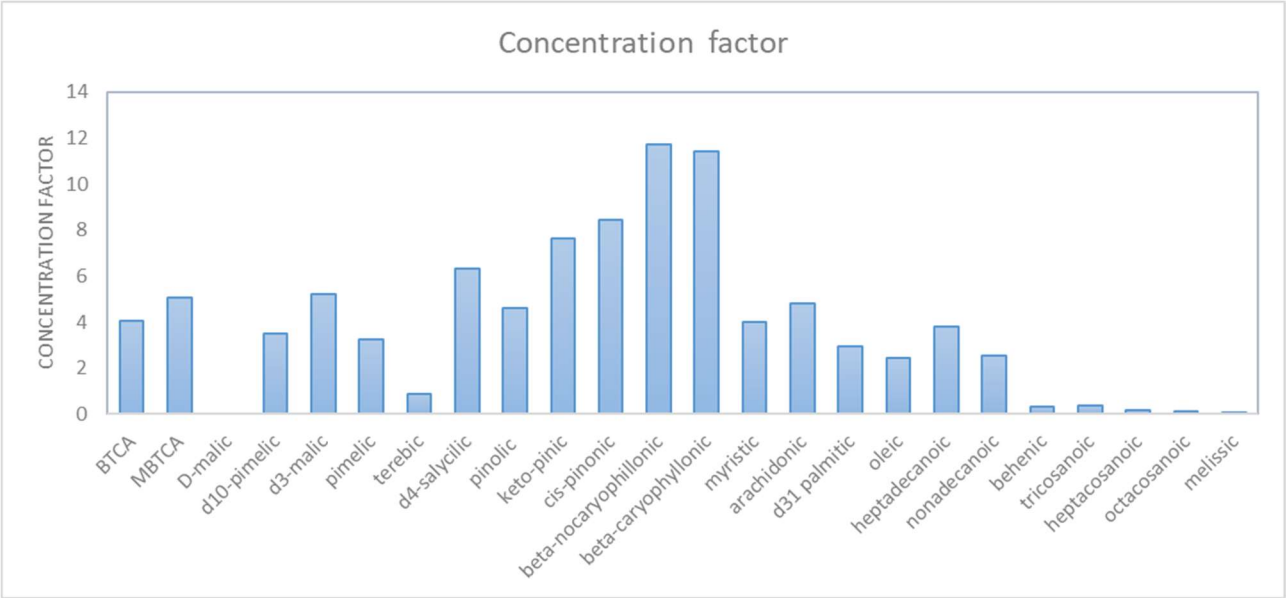

Figure 36 *– Plot of the concentration factors obtain from the last optimized preconcentration method.*

A preliminary analysis in Rendezvous ice core snow samples dated 2010 and 2011 was performed in order to test the applicability of the analytical method to real samples. From a first analysis were detected the following analytes.

	2010 (µg/L)	**2011 (µg/L)**
Terebic acid	0.21	0.29
Cis pinonic acid	0.44	0.23
Salycilic acid	5.52	3.80

Table 19 *– Rendezvous snow sample concentrations of the fatty acids observed after a preliminary analysis performed through SPE 1:10 preconcentration.*

6. CONCLUSIONS

In this thesis were performed quantitative and qualitative analyses of climate change markers in polar ice and snow samples. The analyses were performed in Talos Dome and Renland ice core samples, whereas was performed a preliminary quantitative analysis of fatty acids and atmospheric markers on two snow samples dated 2010 and 2011 from the Rendezvous ice core.

In the Talos Dome ice core samples have been performed both quantitative and qualitative analyses. The quantitative analyses were focused on the quantification of methoxyphenol compounds and D- and L- amino acids after the validations of the respective analytical methods for both the family compounds providing for each analyte the linearity ranges, the error percentage and the matrix effect. From the validation tests, the analytical method that employs labelled internal standards turned out to provide better results in terms of quantification error and matrix effect.

For these analyses was employed a hyphenated technique HPLC-MS using a triple quadrupole mass instrument (API4000) as a detector due to its high sensitivity. Were not detected significant quantities of D-amino acids linked to the bacterial presence in none of the two ice cores.

The phenolic compounds detected were vanillic acid, vanillin and acetovanillone with concentrations ranging from 0.005µg L^{-1} to 66.2 µg L^{-1}. The average ratio vanillic acid/vanillin in the Taldice samples turned out to be 0.76 that is higher than the ratio found in aerosols (0.13 ± 0.06) and seawater (0.04 ± 0.02), confirming the hypothesis of the airborne oxidation progress during the air transport and the atmospheric deposition, as suggested in the submitted work Zangrando et al., 2017, *Free phenolic compounds in waters of the Ross Sea* in which was investigated the VA/VAH ratio as an index of the oxidation process of vanillin into vanillic acid.

The amino acids detected in Taldice samples were the following: L-Ala, L-Asp, L-Arg, L-Leu/Ile, Gly, L-Hys, L-Phe, L-Thr, L-Glu, L-Val, L-Pro, L-4-Hyp with concentrations ranging from 0.002µg L^{-1} to 8.22 µg L^{-1}. The dominant amino acid present is glycine, in accordance to past studies on other environmental matrices due to the higher stability of this amino acid, followed by arginine, alanine and valine. The Talos Dome analyses were performed with the aim of evaluating the applicability of the validated methods to real ice samples due to the low resolution which makes difficult the interpretation and the comparison with other paleoclimatic records. Nevertheless, was noticed a slightly correlation of both methoxyphenols and amino acid compounds with the temperature trend especially in the later part, since the biologic activity is correlated to the temperature. A similar trend was observed also for the phenolic compounds. PCs are produced from lignin combustion and

higher temperatures, as well as higher CO_2 concentrations, increase the plant productivity, hence the probability to have fire activities.

In Renland ice core were detected 7 amino acids: L-Ala, L-Pro, L-Val, L-Arg, L-Ser, Gly and L-Orn with concentrations ranging from 0.001µg L^{-1} to 5.46µg L^{-1}. Glycine and alanine were found to be the most abundant amino acids present, followed by L-Ser, L-Orn, L-Arg, L-Pro and L-Val. In order to evaluate any possible correlation with other paleoclimatic records, was performed a comparison between alanine concentrations and records from regional ice cores and marine sediments. The sites that provided interesting information are the *GRISP2* ice core ammonium data and $CaCO_3$ paleoproductivity of two marine sediments collected in the Fram Strait region. It was found a similar trend between L-Ala and NH_4^+, linked to the temperature variations and biogenic emissions, as well as to bacterial decomposition.

Another comparison was made with marine sediment records, since the Renland ice cap is located in a coastal area and the East Greenland ice shelf is likely to be influenced by the marine circulations deriving from the Fram Strait. For this purpose, was performed a comparison between several sediment records among which particularly interesting resulted the correlation between the paleoproductivity expressed as $CaCO_3$ data, one of the main component of the whole biogenic fraction in sediments linked to the presence of phytoplankton and zooplankton, and alanine. Furthermore, it was noticed that alanine follows a trend that is similar *to* P_BIP_{25}, a monounsaturated hydrocarbon produced by sea-ice diatoms and considered a sea-ice biomarker, found in the sediments in the Fram Strait region.

In order to discover new climate change markers, an untargeted qualitative analysis on Talos Dome ice samples was performed. The instruments employed consisted in a UHPLC coupled to an Orbitrap LTQ XL®. The qualitative analyses were carried out preliminarly using an H-ESI source during which were selected the most interesting samples to be analyzed subsequently in *nano*HPLC-*nano*ESI technique, more sensitive and challenging. The data elaboration and the identification of the new molecules was the following step during this part of the work. The analyses were performed in positive and negative mode with the aim of detecting the greatest possible number of molecules. In negative mode were detected a lower number of family compounds with a large prevalence of CHO, followed by CHON, CHOS and CHONS, whereas in positive mode where detected less molecules belonging to much more family compounds with a slight predominance of CHON, CHOS,

CHO and CHOP followed by CHONP, CHN, CHONS and CHNS. The presence of CHOP and CHON compounds suggests most probably the presence of phospholipids and amino acids and/or derived-compounds. The total number of the molecules identified were 214 in negative mode and 157 in positive mode. In order to assess the oxidation state, an indication on the unsaturation and chemical transformations, were constructed OSc, DBE and *Van Krevelen diagrams*. Moreover, with the aim of assessing the abundance of the detected molecules in each sample, were constructed the bubble chart of OSc diagrams based on the peak areas. At first sight, it resulted that the samples belonging to the glacial period, therefore the oldest samples analyzed, are characterized by a more abundant presence of oxidized species, except for the homologous series $C_nH_{2n}O_2$, that very likely represent fatty acid compounds, which seem to have a reverse trend. In fact, the most oxidized $C_nH_{2n}O_2$ compounds show higher peak intensities in the youngest samples and a gradual increase of the reduced ones for the oldest samples belonging to the glacial period, probably because the low temperatures of the glacial period during which the deposition occurred slowed down the oxidation processes.

In the Rendezvous snow samples were performed analyses of the following atmospheric markers and fatty acids: BTCA, MBTCA, pimelic acid, terebic acid, salycilic acid, meso-erythritol, keto-pinic acid, methyl-tetrols, levoglucosan, cis-pinonic acid, pinolic acid, β-caryophillonic, β-nocaryophillonic, β-caryophillinic, lauric acid, myristic acid, arachidonic acid, palmitic acid, oleic acid, heptadecanoic acid, nonadecanoic acid, behenic acid, tricosanoic acid, heptacosanoic acid, octacosanoic and melissic acid. The analyses were performed through preconcentration 1:10 in solid phase extraction (SPE) strong anionic (SAX) cartridges able to extract carboxylic and weak acids in aqueous and non-aqueous solutions. Several tests were performed using premade standard solutions with the aim of optimizing the recovery factors. The optimization method was not fully optimized and is still being improved. Nevertheless, a preliminary analysis on two snow samples dated 2010 and 2011 were performed employing the best analytical method obtained until then. The instrumentation used consisted in a liquid chromatography-ion trap mass spectrometry (Orbitrap LTQ Velos) system. In these preliminary analyses on the Rendezvous snow samples were detected terebic acid (0.21 μg L^{-1} for 2010 and 0.29 μg L^{-1} for 2011), cis-pinonic acid (0.44μg L^{-1} for 2010 and 0.23μg L^{-1} for 2011) and salycilic acid (5.52μg L^{-1} for 2010 and 3.80μg L^{-1} for 2011).

7. SUPPLEMENTARY SECTION

Sample name	Ice age (cal yr)	L-Ala	Gly	L-Pro	L-Arg	L-Val	L-Orn	L-Ser
Ren- 10	**2012,5**	0,445	0,122	0,055	0,086	0,074	0,094	0,471
Ren- 13	**2010,4**	0,326	0,087	0,057	0,108	0,055	0,172	0,344
Ren- 16	**2009,4**	0,389	0,040	0,039	0,167	0,076	0,223	1,123
Ren- 22	**2005,3**	0,820	0,552	0,221	0,253	0,163	0,449	1,379
Ren- 25	**2003,2**	0,291	0,422	0,004	0,003	0,041	0,139	0,416
Ren- 28	**2001,4**	0,123	0,087	0,013	0,070	0,044	0,089	0,110
Ren- 31	**1999,5**	0,613	0,346	0,063	0,124	0,083	0,108	0,156
Ren- 34	**1997,5**	0,331	0,223	0,074	0,144	0,050	0,196	0,190
Ren- 37	**1995,2**	0,545	0,401	0,112	0,152	0,142	0,335	0,754
Ren- 40	**1993,2**	0,297	0,807	0,043	0,133	0,095	0,186	0,176
Ren- 43	**1990,4**	0,174	0,211	0,029	0,101	0,027	0,098	0,120
Ren- 46	**1988,0**	0,736	0,640	0,087	0,428	0,162	0,360	0,966
Ren- 49	**1986,0**	0,298	0,228	0,026	0,046	0,053	0,089	0,505
Ren- 52	**1983,9**	0,256	0,349	0,054	0,077	0,062	0,205	0,447
Ren- 55	**1981,8**	0,272	0,100	0,049	0,003	0,056	0,089	0,236
Ren- 61	**1976,5**	0,709	0,357	0,083	0,138	0,146	0,258	0,702
Ren- 63	**1975,1**	1,242	0,202	0,004	0,003	0,117	0,089	0,491
Ren- 63	**1975,1**	0,392	0,040	0,066	0,114	0,081	0,161	0,739
Ren- 66	**1972,6**	0,156	0,040	0,029	0,003	0,044	0,089	0,199
Ren- 69	**1970,1**	0,267	0,087	0,033	0,010	0,031	0,089	0,077
Ren- 72	**1967,8**	0,976	0,963	0,229	0,106	0,338	0,782	0,477
Ren- 75	**1964,4**	0,223	0,040	0,053	0,038	0,053	0,109	0,502
Ren- 78	**1961,3**	0,579	0,429	0,073	0,087	0,147	0,332	0,523
Ren- 81	**1959,0**	0,959	0,614	0,147	0,356	0,188	0,583	1,956
Ren- 84	**1956,6**	0,797	0,284	0,095	0,169	0,115	0,432	0,444
Ren- 87	**1953,5**	0,309	0,428	0,058	0,003	0,067	0,302	0,488
Ren- 90	**1950,2**	0,228	0,040	0,004	0,059	0,027	0,089	0,132
Ren- 93	**1946,9**	0,434	0,115	0,053	0,119	0,059	0,153	0,495
Ren- 96	**1944,0**	0,674	0,388	0,638	0,123	0,086	0,089	0,243
Ren- 99	**1941,0**	0,292	0,274	0,022	0,032	0,042	0,142	0,361
Ren- 102	**1937,9**	0,304	0,353	0,050	0,100	0,060	0,210	0,198
Ren- 105	**1934,0**	0,485	0,620	0,114	0,100	0,094	0,254	0,512
Ren- 108	**1931,1**	0,779	0,587	0,139	0,163	0,162	0,587	1,124
Ren- 111	**1927,7**	0,384	0,393	0,087	0,088	0,107	0,296	0,371
Ren- 114	**1924,0**	0,135	0,159	0,037	0,040	0,024	0,089	0,053
Ren- 117	**1920,5**	0,291	0,284	0,061	0,068	0,063	0,110	0,172
Ren- 120	**1917,1**	0,218	0,102	0,035	0,064	0,032	0,089	0,057
Ren- 123	**1913,9**	0,140	0,265	0,037	0,052	0,022	0,089	0,055
Ren- 126	**1910,3**	0,115	0,199	0,053	0,069	0,016	0,089	0,040
Ren- 129	**1906,8**	0,215	0,419	0,028	0,058	0,032	0,124	0,068

Ren- 132	**1902,9**	0,189	0,341	0,012	0,076	0,040	0,089	0,305
Ren- 135	**1898,3**	0,157	0,107	0,026	0,065	0,002	0,089	0,160
Ren- 138	**1894,9**	0,652	0,302	0,107	0,156	0,108	0,368	0,257
Ren- 141	**1897,1**	0,419	0,232	0,070	0,092	0,078	0,176	0,378
Ren- 144	**1893,6**	0,254	0,490	0,056	0,051	0,074	0,098	0,114
Ren- 147	**1888,9**	0,255	0,204	0,047	0,068	0,052	0,120	0,108
Ren- 150	**1884,1**	0,303	0,331	0,014	0,003	0,002	0,091	0,119
Ren- 153	**1879,6**	0,239	0,219	0,030	0,042	0,028	0,089	0,113
Ren- 156	**1875,6**	0,092	0,040	0,039	0,040	0,027	0,120	0,135
Ren- 159	**1872,0**	0,140	0,224	0,084	0,069	0,030	0,114	0,067
Ren- 161	**1868,8**	0,302	0,252	0,060	0,057	0,050	0,126	0,480
Ren- 164	**1864,3**	0,449	0,499	0,098	0,348	0,121	0,349	0,693
Ren- 167	**1852,3**	0,532	0,462	0,081	0,165	0,108	0,374	0,385
Ren- 173	**1843,0**	0,558	0,357	0,086	0,201	0,105	0,312	1,109
Ren- 176	**1838,5**	0,330	0,407	0,045	0,146	0,056	0,293	0,247
Ren- 179	**1833,1**	0,558	0,383	0,053	0,153	0,099	0,271	0,455
Ren- 182	**1828,1**	0,811	0,447	0,082	0,150	0,132	0,099	0,374
Ren- 185	**1823,6**	0,196	0,040	0,041	0,003	0,044	0,141	0,098
Ren- 188	**1819,3**	0,188	0,040	0,034	0,016	0,002	0,089	0,049
Ren- 191	**1815,1**	0,206	0,206	0,012	0,020	0,016	0,089	0,042
Ren- 194	**1811,1**	0,154	0,143	0,040	0,019	0,016	0,089	0,023
Ren- 197	**1806,4**	0,353	0,323	0,075	0,126	0,036	0,103	0,035
Ren- 200	**1803,3**	0,121	0,124	0,024	0,059	0,002	0,089	0,039
Ren- 203	**1799,1**	0,225	0,582	0,051	0,051	0,049	0,089	0,038
Ren- 206	**1794,2**	0,186	0,194	0,031	0,076	0,026	0,093	0,057
Ren- 208	**1791,7**	0,007	0,040	0,004	0,014	0,010	0,089	0,022
Ren- 210	**1788,2**	0,368	0,341	0,067	0,136	0,059	0,118	0,158
Ren- 212	**1785,3**	0,242	0,040	0,017	0,120	0,017	0,089	0,042
Ren- 216	**1778,6**	0,007	0,183	0,043	0,052	0,021	0,089	0,078
Ren- 218	**1774,8**	0,007	0,040	0,015	0,027	0,028	0,089	0,084
Ren- 220	**1771,7**	0,007	0,040	0,060	0,064	0,002	0,089	0,031
Ren- 222	**1768,0**	0,124	0,040	0,023	0,044	0,013	0,089	0,035
Ren- 224	**1764,1**	0,062	0,164	0,028	0,003	0,002	0,089	0,098
Ren- 226	**1761,0**	0,178	0,287	0,031	0,031	0,018	0,089	0,036
Ren- 228	**1757,8**	0,169	0,305	0,022	0,009	0,002	0,089	0,086
Ren- 231	**1752,3**	0,212	0,241	0,046	0,087	0,056	0,089	0,113
Ren- 233	**1748,8**	0,007	0,182	0,033	0,042	0,035	0,089	0,086
Ren- 235	**1745,4**	0,249	0,243	0,056	0,079	0,032	0,113	0,076
Ren- 237	**1741,5**	0,282	0,160	0,049	0,127	0,035	0,091	0,066
Ren- 239	**1738,0**	0,125	0,223	0,041	0,050	0,002	0,089	0,032
Ren- 241	**1734,4**	0,097	0,176	0,028	0,112	0,016	0,089	0,078
Ren- 241	**1734,4**	0,118	0,293	0,052	0,100	0,002	0,089	0,054
Ren- 243	**1731,6**	0,243	0,040	0,043	0,003	0,002	0,132	0,231
Ren- 245	**1727,7**	0,591	0,596	0,135	0,144	0,143	0,591	0,525
Ren- 245	**1727,7**	0,164	0,365	0,021	0,064	0,002	0,089	0,113
Ren- 249	**1720,8**	0,110	0,040	0,036	0,087	0,002	0,089	0,046
Ren- 251	**1717,1**	0,360	0,106	0,064	0,048	0,060	0,090	0,126

Ren- 253	**1713,4**	0,295	0,040	0,061	0,064	0,046	0,089	0,066
Ren- 255	**1709,8**	0,226	0,184	0,023	0,027	0,047	0,089	0,230
Ren- 257	**1705,8**	0,184	0,412	0,050	0,076	0,002	0,092	0,068
Ren- 259	**1701,5**	0,193	0,216	0,044	0,042	0,035	0,089	0,273
Ren- 261	**1697,8**	0,251	0,277	0,042	0,111	0,033	0,098	0,074
Ren- 263	**1693,8**	0,562	0,242	0,084	0,330	0,087	0,125	0,271
Ren- 265	**1689,6**	0,380	0,134	0,004	0,078	0,053	0,089	0,168
Ren- 267	**1685,7**	0,465	0,327	0,049	0,127	0,065	0,106	0,162
Ren- 269	**1682,4**	0,363	0,322	0,112	0,366	0,158	0,098	0,112
Ren- 271	**1678,2**	0,493	0,054	0,140	0,825	0,186	0,136	0,195
Ren- 273	**1674,2**	0,765	0,465	0,196	0,616	0,268	0,228	0,463
Ren- 274	**1650,6**	0,393	0,342	0,047	0,092	0,062	0,089	0,047
Ren- 282	**1632,8**	0,613	0,348	0,083	0,062	0,074	0,151	0,200
Ren- 301	**1614,3**	0,293	0,040	0,083	0,234	0,107	0,089	0,101
Ren- 303	**1610,6**	0,814	0,373	0,206	0,794	0,323	0,209	0,166
Ren- 305	**1605,7**	0,588	0,040	0,118	0,841	0,194	0,113	0,164
Ren- 308	**1599,8**	0,339	0,176	0,077	0,309	0,093	0,118	0,098
Ren- 310	**1595,4**	0,706	0,310	0,181	0,954	0,295	0,089	0,111
Ren- 312	**1590,9**	0,424	0,431	0,108	0,312	0,119	0,089	0,159
Ren- 314	**1586,6**	0,549	0,212	0,110	0,599	0,151	0,091	0,079
Ren- 316	**1582,6**	0,588	0,488	0,115	0,640	0,198	0,099	0,153
Ren- 318	**1577,9**	0,433	0,040	0,054	0,125	0,053	0,120	0,375
Ren- 320	**1573,2**	0,280	0,512	0,072	0,110	0,052	0,151	0,202
Ren- 322	**1569,3**	0,213	0,133	0,051	0,003	0,040	0,098	0,179
Ren- 324	**1564,6**	0,530	0,375	0,140	0,193	0,128	0,210	0,166
Ren- 326	**1559,4**	0,352	0,477	0,081	0,113	0,071	0,143	0,150
Ren- 328	**1554,7**	0,314	0,411	0,050	0,039	0,048	0,097	0,066
Ren- 330	**1550,5**	0,121	0,408	0,037	0,018	0,002	0,089	0,039
Ren- 332	**1546,0**	0,214	0,040	0,040	0,069	0,046	0,089	0,090
Ren- 333	**1543,9**	0,068	0,118	0,035	0,077	0,002	0,089	0,040
Ren- 335	**1539,3**	0,973	0,752	0,140	0,333	0,238	0,393	0,434
Ren- 336	**1537,5**	0,007	0,040	0,087	0,037	0,058	0,089	0,136
Ren- 337	**1535,0**	1,818	1,061	0,277	0,265	0,331	0,489	0,317
Ren- 338	**1532,5**	0,235	0,205	0,064	0,059	0,036	0,089	0,187
Ren- 339	**1530,4**	0,701	0,563	0,138	0,191	0,144	0,292	0,205
Ren- 340	**1528,1**	0,557	0,401	0,133	0,142	0,120	0,194	0,573
Ren- 341	**1525,7**	0,478	0,395	0,085	0,088	0,097	0,168	0,094
Ren- 342	**1523,2**	0,602	0,478	0,167	0,120	0,131	0,240	0,273
Ren- 343	**1520,9**	0,175	0,476	0,048	0,033	0,030	0,089	0,139
Ren- 344	**1518,0**	0,351	0,642	0,122	0,083	0,078	0,140	0,144
Ren- 345	**1515,8**	0,404	0,219	0,065	0,111	0,066	0,201	0,096
Ren- 346	**1513,7**	0,552	0,529	0,131	0,109	0,169	0,285	0,283
Ren- 347	**1511,4**	0,306	0,189	0,085	0,068	0,055	0,095	0,130
Ren- 348	**1509,0**	0,832	0,396	0,147	0,175	0,135	0,353	0,358
Ren- 349	**1506,7**	0,564	0,391	0,095	0,091	0,083	0,110	0,243
Ren- 350	**1504,0**	0,504	0,302	0,112	0,079	0,117	0,334	0,747
Ren- 351	**1501,7**	0,724	0,319	0,114	0,361	0,137	0,199	0,205

Ren- 352	**1499,0**	0,278	0,040	0,056	0,003	0,036	0,089	0,087
Ren- 353	**1496,6**	0,886	0,753	0,175	0,188	0,179	0,291	0,414
Ren- 354	**1494,2**	0,400	0,274	0,067	0,109	0,034	0,105	0,048
Ren- 355	**1492,2**	0,293	0,040	0,071	0,108	0,063	0,089	0,152
Ren- 356	**1489,7**	0,214	0,040	0,063	0,059	0,028	0,089	0,041
Ren- 357	**1487,4**	1,138	0,753	0,169	0,155	0,197	0,511	0,447
Ren- 358	**1484,5**	0,209	0,192	0,024	0,061	0,031	0,089	0,081
Ren- 359	**1482,3**	1,313	0,745	0,231	0,328	0,380	0,723	0,504
Ren- 361	**1478,2**	0,461	0,040	0,082	0,077	0,065	0,097	0,131
Ren- 361	**1478,2**	0,668	0,654	0,172	0,124	0,151	0,384	0,271
Ren- 362	**1476,1**	1,523	1,032	0,361	0,463	0,458	1,190	0,678
Ren- 363	**1473,1**	0,737	0,617	0,148	0,146	0,162	0,461	0,284
Ren- 364	**1470,3**	0,790	0,314	0,086	0,097	0,055	0,140	0,072
Ren- 365	**1467,4**	0,838	0,558	0,175	0,152	0,214	0,480	0,476
Ren- 366	**1464,8**	0,321	0,284	0,079	0,017	0,034	0,089	0,034
Ren- 367	**1462,3**	0,810	0,624	0,194	0,205	0,243	0,456	0,497
Ren- 368	**1460,0**	0,841	0,799	0,193	0,142	0,215	0,394	0,263
Ren- 369	**1457,6**	0,266	0,293	0,073	0,041	0,044	0,110	0,086
Ren- 370	**1455,5**	0,324	0,365	0,092	0,071	0,076	0,196	0,140
Ren- 371	**1452,8**	0,305	0,360	0,082	0,032	0,060	0,120	0,147
Ren- 372	**1450,1**	0,747	0,617	0,120	0,315	0,147	0,251	0,339
Ren- 373	**1447,2**	0,218	0,295	0,061	0,049	0,054	0,095	0,091
Ren- 374	**1444,6**	0,368	0,673	0,072	0,136	0,079	0,253	0,287
Ren- 375	**1442,2**	0,142	0,153	0,039	0,062	0,021	0,089	0,056
Ren- 376	**1439,1**	0,398	0,380	0,054	0,041	0,059	0,089	0,286
Ren- 377	**1436,2**	0,559	0,338	0,134	0,051	0,130	0,271	0,307
Ren- 378	**1433,3**	0,633	0,424	0,128	0,073	0,120	0,210	0,154
Ren- 379	**1430,5**	0,832	0,506	0,132	0,129	0,165	0,401	0,263
Ren- 380	**1427,7**	0,708	0,621	0,234	0,196	0,239	0,716	0,525
Ren- 381	**1424,6**	0,299	0,353	0,067	0,036	0,056	0,089	0,170
Ren- 383	**1418,7**	0,224	0,223	0,091	0,025	0,056	0,114	0,198
Ren- 384	**1415,9**	0,337	0,222	0,035	0,114	0,064	0,089	0,179
Ren- 385	**1413,1**	0,097	0,142	0,027	0,003	0,013	0,089	0,073
Ren- 386	**1410,2**	0,316	0,450	0,091	0,042	0,064	0,126	0,126
Ren- 387	**1407,1**	0,282	0,277	0,055	0,059	0,042	0,124	0,107
Ren- 388	**1404,5**	1,579	0,972	0,330	0,294	0,398	0,953	1,703
Ren- 389	**1401,8**	0,251	0,040	0,042	0,052	0,049	0,117	0,079
Ren- 391	**1395,5**	0,316	0,405	0,067	0,069	0,039	0,106	0,098
Ren- 392	**1392,7**	0,541	0,479	0,091	0,116	0,082	0,098	0,164
Ren- 393	**1389,2**	0,220	0,040	0,074	0,038	0,007	0,089	0,126
Ren- 394	**1385,8**	0,242	0,110	0,042	0,003	0,045	0,089	0,111
Ren- 395	**1382,6**	0,653	0,574	0,050	0,003	0,060	0,134	0,230
Ren- 396	**1379,9**	0,645	0,484	0,136	0,053	0,138	0,249	0,115
Ren- 397	**1376,7**	0,561	0,562	0,120	0,092	0,146	0,239	0,377
Ren- 398	**1373,5**	0,225	0,237	0,053	0,044	0,054	0,089	0,126
Ren- 399	**1370,7**	0,136	0,154	0,028	0,041	0,009	0,089	0,122
Ren- 427	**1277,3**	0,746	0,408	0,110	0,101	0,150	0,477	0,305

Ren- 428	**1273,4**	0,483	0,170	0,078	0,063	0,089	0,316	0,208
Ren- 429	**1269,9**	0,234	0,315	0,043	0,127	0,068	0,186	0,640
Ren- 430	**1266,3**	0,895	0,849	0,105	0,200	0,175	0,606	1,069
Ren- 431	**1262,7**	0,384	0,234	0,004	0,101	0,061	0,216	0,737
Ren- 433	**1258,7**	0,327	0,354	0,086	0,075	0,108	0,262	0,582
Ren- 434	**1254,9**	0,415	0,815	0,039	0,082	0,061	0,184	0,373
Ren- 435	**1247,1**	0,237	0,293	0,029	0,003	0,046	0,089	0,107
Ren- 436	**1243,4**	0,641	0,628	0,170	0,108	0,115	0,278	0,336
Ren- 437	**1239,3**	0,379	0,288	0,054	0,043	0,095	0,262	0,297
Ren- 438	**1235,2**	0,162	0,090	0,017	0,051	0,035	0,109	0,557
Ren- 439	**1230,7**	0,360	0,426	0,067	0,139	0,085	0,279	0,337
Ren- 440	**1227,0**	4,470	1,930	0,856	0,174	1,132	1,489	1,575
Ren- 441	**1223,3**	0,424	0,573	0,074	0,123	0,073	0,150	0,111
Ren- 442	**1219,1**	0,257	0,069	0,073	0,035	0,059	0,114	0,271
Ren- 443	**1214,9**	0,610	0,480	0,077	0,151	0,120	0,300	0,857
Ren- 444	**1211,1**	0,007	0,040	0,004	0,003	0,002	0,089	0,002
Ren- 445	**1206,6**	0,425	0,722	0,019	0,072	0,101	0,166	0,172
Ren- 446	**1202,5**	0,190	0,104	0,034	0,033	0,020	0,089	0,219
Ren- 447	**1198,2**	0,351	0,188	0,080	0,103	0,069	0,269	0,474
Ren- 448	**1194,0**	0,356	0,217	0,053	0,081	0,059	0,191	0,153
Ren- 449	**1190,6**	0,305	0,206	0,073	0,039	0,048	0,134	0,088
Ren- 450	**1186,7**	0,349	0,222	0,088	0,086	0,064	0,142	0,243
Ren- 451	**1183,2**	0,572	0,665	0,119	0,099	0,148	0,291	0,161
Ren- 452	**1179,4**	0,869	0,645	0,178	0,142	0,209	0,399	0,878
Ren- 453	**1174,9**	0,291	0,166	0,047	0,067	0,062	0,162	0,230
Ren- 454	**1170,7**	0,569	0,356	0,131	0,183	0,125	0,279	0,286
Ren- 455	**1166,1**	0,552	0,301	0,146	0,077	0,122	0,220	0,227
Ren- 456	**1161,8**	0,183	0,156	0,048	0,049	0,014	0,089	0,050
Ren- 457	**1157,4**	0,852	0,694	0,156	0,096	0,163	0,322	0,203
Ren- 458	**1153,5**	0,370	0,268	0,073	0,084	0,068	0,180	0,143
Ren- 459	**1149,8**	1,327	0,707	0,296	0,299	0,359	0,743	1,131
Ren- 460	**1145,9**	0,225	0,176	0,016	0,003	0,026	0,089	0,115
Ren- 461	**1142,2**	0,440	0,409	0,092	0,073	0,098	0,282	0,138
Ren- 462	**1137,8**	1,228	0,828	0,211	0,267	0,236	0,354	1,385
Ren- 463	**1133,4**	0,275	0,040	0,082	0,048	0,083	0,089	0,244
Ren- 464	**1129,2**	0,132	0,268	0,028	0,029	0,038	0,129	0,265
Ren- 465	**1124,7**	2,445	1,353	0,515	2,521	0,814	0,653	1,054
Ren- 466	**1120,6**	0,695	0,308	0,148	0,205	0,182	0,789	0,723
Ren- 467	**1116,1**	0,400	0,339	0,071	0,212	0,097	0,609	0,333
Ren- 468	**1111,7**	0,498	0,833	0,087	0,121	0,105	0,262	0,276
Ren- 469	**1107,7**	0,522	0,615	0,073	0,179	0,127	0,490	0,399
Ren- 470	**1103,2**	0,511	0,374	0,057	0,228	0,123	0,316	0,627
Ren- 471	**1099,0**	0,267	0,187	0,061	0,065	0,062	0,247	0,480
Ren- 472	**1093,9**	1,180	0,960	0,203	0,386	0,300	0,724	1,976
Ren- 473	**1089,4**	0,435	0,495	0,058	0,140	0,053	0,188	0,149
Ren- 474	**1085,4**	0,723	0,040	0,052	0,148	0,127	0,268	0,636
Ren- 475	**1081,6**	0,340	0,147	0,063	0,145	0,096	0,291	0,504

Ren- 476	**1077,6**	0,364	0,330	0,071	0,136	0,078	0,324	0,187
Ren- 477	**1072,9**	0,533	0,465	0,232	0,003	0,054	0,258	0,526
Ren- 478	**1068,0**	0,398	0,788	0,083	0,146	0,102	0,296	0,228
Ren- 479	**1063,6**	1,723	1,098	0,226	1,207	0,475	0,489	0,555
Ren- 480	**1058,5**	0,446	0,304	0,088	0,165	0,076	0,282	0,222
Ren- 481	**1054,4**	0,553	1,439	0,092	0,245	0,155	0,346	0,284
Ren- 482	**1049,9**	0,886	0,542	0,195	0,162	0,202	0,337	1,543
Ren- 483	**1045,2**	0,403	0,449	0,067	0,112	0,078	0,292	0,241
Ren- 484	**1040,2**	0,226	0,325	0,035	0,032	0,018	0,089	0,087
Ren- 487	**1026,5**	0,706	0,483	0,105	0,143	0,127	0,232	0,371
Ren- 488	**1021,8**	0,643	0,120	0,110	0,167	0,136	0,371	0,529
Ren- 488	**1021,8**	0,630	0,040	0,059	0,107	0,062	0,167	0,390
Ren- 489	**1017,4**	0,557	0,306	0,123	0,138	0,152	0,459	0,245
Ren- 490	**1013,2**	0,371	0,305	0,063	0,083	0,083	0,293	0,255
Ren- 491	**1009,0**	0,313	0,200	0,061	0,122	0,084	0,126	0,507
Ren- 492	**1004,8**	0,915	0,877	0,171	0,220	0,271	1,027	0,622
Ren- 492	**1004,8**	0,762	0,571	0,134	0,266	0,177	0,606	0,480
Ren- 493	**999,5**	0,408	0,476	0,078	0,133	0,082	0,214	0,290
Ren- 494	**995,5**	0,805	0,712	0,151	0,126	0,229	0,477	0,777
Ren- 495	**990,6**	0,293	0,358	0,038	0,069	0,052	0,089	0,093
Ren- 496	**985,8**	0,982	1,110	0,172	0,143	0,211	0,652	0,451
Ren- 497	**981,1**	1,472	0,825	0,185	0,339	0,236	0,561	0,487
Ren- 498	**976,2**	0,475	0,444	0,106	0,031	0,126	0,349	0,414
Ren- 498	**976,2**	2,591	2,367	0,365	0,287	0,573	1,429	1,866
Ren- 499	**972,0**	0,577	0,354	0,100	0,204	0,179	0,516	0,665
Ren- 500	**967,7**	0,763	1,021	0,060	0,173	0,140	0,400	0,499
Ren- 501	**963,4**	0,376	0,472	0,021	0,054	0,067	0,109	0,095
Ren- 502	**958,9**	0,336	0,040	0,024	0,091	0,060	0,148	0,131
Ren- 503	**954,5**	0,503	0,233	0,154	0,122	0,149	0,327	0,248
Ren- 504	**950,1**	0,672	0,753	0,157	0,128	0,199	0,750	0,540
Ren- 505	**945,6**	0,521	0,309	0,077	0,069	0,074	0,358	0,227
Ren- 506	**940,9**	1,005	1,060	0,205	0,221	0,230	0,835	0,394
Ren- 507	**936,2**	1,093	1,005	0,126	0,167	0,192	0,745	0,666
Ren- 508	**931,5**	0,424	0,431	0,122	0,168	0,111	0,295	0,356
Ren- 509	**926,5**	0,974	0,623	0,179	0,173	0,223	0,754	0,390
Ren- 510	**921,2**	0,627	0,335	0,098	0,120	0,126	0,281	0,213
Ren- 511	**916,7**	0,162	0,040	0,028	0,120	0,033	0,145	0,085
Ren- 512	**912,1**	1,272	1,173	0,123	0,210	0,238	0,553	0,662
Ren- 513	**907,0**	0,182	0,171	0,026	0,005	0,050	0,122	0,235
Ren- 514	**902,0**	0,653	0,566	0,167	0,452	0,246	0,502	0,511
Ren- 515	**897,3**	1,975	1,291	0,446	0,260	0,481	1,915	1,068
Ren- 516	**892,9**	1,321	0,625	0,276	0,362	0,374	1,493	0,717
Ren- 517	**888,2**	0,233	0,078	0,028	0,052	0,051	0,114	0,123
Ren- 518	**883,1**	0,432	0,550	0,070	0,120	0,081	0,322	0,322
Ren- 519	**878,3**	1,794	1,327	0,329	0,325	0,404	1,389	1,152
Ren- 520	**873,5**	4,218	3,869	0,927	0,243	1,448	0,089	4,683
Ren- 521	**868,4**	1,868	1,295	0,352	0,085	0,455	0,641	0,911

Ren- 522	**863,4**	1,648	1,074	0,345	0,230	0,439	0,961	0,932
Ren- 523	**857,9**	1,180	1,233	0,217	0,236	0,288	0,627	1,132
Ren- 524	**852,8**	0,415	0,395	0,074	0,003	0,083	0,169	0,125
Ren- 524	**852,8**	0,375	0,383	0,054	0,090	0,056	0,126	0,081
Ren- 525	**847,1**	0,488	0,040	0,072	0,036	0,108	0,198	0,351
Ren- 526	**841,6**	0,462	0,404	0,085	0,033	0,101	0,263	0,252
Ren- 527	**836,9**	0,007	0,040	0,004	0,003	0,002	0,089	0,002
Ren- 528	**831,8**	1,391	1,074	0,250	0,240	0,334	0,719	0,620
Ren- 531	**816,1**	3,971	2,899	0,819	0,903	1,048	1,911	2,463
Ren- 532	**811,1**	1,591	1,263	0,357	0,268	0,452	0,846	0,730
Ren- 533	**806,2**	1,058	0,983	0,248	0,149	0,246	0,529	0,424
Ren- 534	**801,2**	0,227	0,319	0,074	0,003	0,039	0,142	0,188
Ren- 535	**795,7**	1,968	1,075	0,316	0,196	0,422	0,965	0,893
Ren- 536	**790,2**	3,677	2,542	0,839	0,920	1,102	2,053	1,293
Ren- 537	**784,4**	0,477	0,564	0,114	0,003	0,076	0,191	0,262
Ren- 538	**778,4**	0,765	0,722	0,128	0,080	0,167	0,422	0,424
Ren- 539	**772,5**	1,427	0,957	0,270	0,235	0,329	0,788	0,504
Ren- 540	**767,2**	0,352	0,308	0,074	0,003	0,076	0,342	0,289
Ren- 541	**761,0**	0,623	0,640	0,100	0,108	0,123	0,210	0,162
Ren- 542	**754,5**	0,511	0,564	0,142	0,122	0,101	0,176	0,252
Ren- 543	**748,8**	0,851	0,437	0,167	0,045	0,155	0,415	0,386
Ren- 544	**742,7**	1,348	0,706	0,234	0,184	0,255	0,434	0,545
Ren- 545	**737,4**	0,769	0,578	0,132	0,155	0,185	0,302	0,307
Ren- 546	**732,3**	1,734	1,334	0,323	0,331	0,415	0,758	0,732
Ren- 547	**727,4**	0,371	0,253	0,100	0,041	0,054	0,119	0,181
Ren- 548	**722,3**	0,274	0,219	0,091	0,032	0,073	0,158	0,292
Ren- 549	**716,3**	0,007	0,040	0,004	0,003	0,002	0,089	0,002
Ren- 550	**710,8**	2,657	1,619	0,523	0,567	0,594	1,334	1,397
Ren- 551	**705,2**	0,007	0,040	0,004	0,003	0,002	0,089	0,002
Ren- 552	**699,3**	1,456	1,100	0,294	0,364	0,351	0,759	1,105
Ren- 553	**693,4**	1,159	0,839	0,245	0,767	0,276	0,524	0,446
Ren- 554	**687,7**	0,804	0,696	0,186	0,166	0,239	0,448	0,380
Ren- 555	**682,1**	0,625	0,542	0,097	0,076	0,116	0,278	0,318
Ren- 556	**676,2**	0,848	0,814	0,176	0,073	0,214	0,468	0,654
Ren- 557	**670,2**	1,314	0,911	0,235	0,437	0,321	0,516	0,463
Ren- 558	**664,2**	1,129	1,041	0,163	0,250	0,256	0,431	0,349
Ren- 559	**658,6**	5,645	4,098	1,006	0,515	1,795	0,089	2,221
Ren- 560	**653,1**	1,738	1,348	0,311	0,521	0,356	0,634	0,864
Ren- 561	**647,5**	1,519	1,162	0,257	0,243	0,303	0,707	0,655
Ren- 561	**647,5**	1,248	1,056	0,251	0,242	0,302	0,714	1,249
Ren- 562	**641,8**	1,122	0,795	0,229	0,388	0,304	0,714	0,631
Ren- 563	**636,0**	0,947	0,661	0,176	0,304	0,231	0,471	0,476
Ren- 564	**630,4**	1,712	0,844	0,425	0,626	0,517	1,130	0,793
Ren- 565	**624,7**	1,052	0,909	0,301	0,379	0,317	0,805	0,544
Ren- 566	**619,0**	0,546	0,500	0,135	0,123	0,129	0,271	0,197
Ren- 567	**613,6**	1,923	0,861	0,348	0,554	0,475	1,643	1,877
Ren- 568	**608,0**	0,428	0,246	0,128	0,102	0,109	0,201	0,168

Ren- 569	**602,1**	2,813	1,298	0,532	0,734	0,727	1,576	0,889
Ren- 570	**597,2**	1,919	1,138	0,533	1,767	0,744	1,171	1,611
Ren- 571	**591,2**	0,752	0,571	0,194	0,218	0,199	0,398	0,206
Ren- 572	**584,9**	2,985	1,324	0,521	0,666	0,652	1,359	1,188
Ren- 573	**578,4**	0,095	0,040	0,025	0,036	0,020	0,089	0,058
Ren- 574	**573,0**	0,569	0,340	0,141	0,068	0,105	0,149	0,307
Ren- 576	**560,4**	1,091	0,651	0,245	0,313	0,266	0,614	0,701
Ren- 577	**554,4**	0,453	0,491	0,112	0,105	0,110	0,188	0,593
Ren- 578	**548,2**	1,236	0,831	0,214	0,417	0,313	0,722	0,811
Ren- 578	**548,2**	4,606	2,351	1,077	1,667	1,316	3,175	2,043
Ren- 579	**541,3**	1,840	1,192	0,303	0,404	0,379	0,921	0,550
Ren- 580	**534,2**	0,749	0,682	0,166	0,130	0,179	0,338	0,287
Ren- 581	**528,1**	1,151	0,747	0,290	0,319	0,289	0,498	0,860
Ren- 582	**523,1**	2,005	1,012	0,519	0,694	0,677	0,988	0,774
Ren- 583	**517,9**	1,572	1,140	0,261	0,461	0,348	0,730	1,085
Ren- 584	**510,7**	1,258	1,056	0,285	0,578	0,344	0,948	0,858
Ren- 585	**504,4**	0,958	0,706	0,212	0,261	0,247	0,435	0,574
Ren- 586	**498,2**	1,835	0,534	0,241	0,379	0,256	0,604	0,674
Ren- 587	**492,6**	4,913	2,965	1,044	2,348	1,413	2,722	2,773
Ren- 588	**486,0**	3,287	2,194	0,686	1,203	0,902	1,806	1,494
Ren- 589	**479,2**	1,507	0,734	0,159	0,260	0,200	0,598	0,335
Ren- 590	**473,1**	0,943	1,386	0,215	0,324	0,238	0,687	0,473
Ren- 591	**466,9**	2,082	0,990	0,448	0,619	0,726	1,064	0,609
Ren- 592	**460,9**	1,619	1,029	0,340	0,382	0,436	0,587	0,804
Ren- 593	**454,8**	1,004	0,646	0,198	0,199	0,194	0,471	0,283
Ren- 594	**449,1**	0,524	0,437	0,097	0,155	0,148	0,271	0,002
Ren- 595	**443,4**	1,238	0,733	0,203	0,309	0,213	0,479	0,465
Ren- 596	**437,5**	0,888	0,499	0,162	0,202	0,193	0,520	0,294
Ren- 597	**431,8**	1,534	0,929	0,244	0,299	0,222	0,220	0,699
Ren- 598	**425,6**	1,680	0,965	0,340	0,433	0,419	0,945	1,094
Ren- 599	**419,3**	2,557	1,409	0,450	0,835	0,649	1,511	0,570
Ren- 600	**413,0**	3,539	1,717	0,725	1,369	1,081	2,063	1,930
Ren- 661	**-19,6**	0,335	0,559	0,079	0,153	0,093	0,287	0,188
Ren- 662	**-26,1**	0,729	0,711	0,120	0,136	0,192	0,363	0,280
Ren- 664	**-42,0**	0,302	0,502	0,044	0,043	0,050	0,097	0,106
Ren- 665	**-51,2**	0,340	0,346	0,029	0,068	0,097	0,170	0,497
Ren- 666	**-59,0**	0,834	0,712	0,125	0,107	0,158	0,460	0,735
Ren- 667	**-67,6**	0,575	0,659	0,127	0,078	0,152	0,323	0,314
Ren- 668	**-76,6**	0,481	0,308	0,073	0,050	0,081	0,138	0,258
Ren- 669	**-85,0**	0,527	0,406	0,076	0,216	0,109	0,247	0,225
Ren- 670	**-93,7**	0,398	0,356	0,070	0,144	0,057	0,177	0,226
Ren- 671	**-102,2**	0,676	0,573	0,137	0,164	0,158	0,384	0,465
Ren- 672	**-110,3**	0,145	0,222	0,028	0,003	0,027	0,297	0,249
Ren- 673	**-118,2**	0,538	0,422	0,101	0,156	0,134	0,174	0,320
Ren- 675	**-134,8**	0,765	0,508	0,127	0,156	0,127	0,453	0,491
Ren- 676	**-142,9**	0,776	0,646	0,143	0,211	0,182	0,302	0,642
Ren- 677	**-151,4**	0,266	0,362	0,044	0,054	0,002	0,123	0,114

Ren- 678	**-160,3**	0,319	0,315	0,057	0,080	0,055	0,152	0,108
Ren- 679	**-168,8**	0,561	0,524	0,081	0,188	0,107	0,212	0,207
Ren- 680	**-178,0**	0,602	0,608	0,086	0,082	0,105	0,274	0,400
Ren- 681	**-186,6**	0,491	0,599	0,078	0,153	0,094	0,246	0,165
Ren- 682	**-195,0**	0,821	0,633	0,122	0,093	0,168	0,377	0,261
Ren- 683	**-203,8**	0,680	0,570	0,044	0,134	0,132	0,359	0,194
Ren- 684	**-212,4**	0,416	0,429	0,055	0,147	0,094	0,270	0,113
Ren- 685	**-221,3**	0,791	0,602	0,155	0,154	0,170	0,367	0,294
Ren- 686	**-230,0**	0,196	0,168	0,020	0,050	0,002	0,119	0,129
Ren- 687	**-237,4**	0,949	0,845	0,155	0,072	0,218	0,412	0,828
Ren- 688	**-245,7**	0,276	0,455	0,045	0,086	0,058	0,207	0,130
Ren- 689	**-254,7**	0,692	0,818	0,129	0,204	0,178	0,392	0,330
Ren- 690	**-263,8**	0,594	0,340	0,078	0,054	0,161	0,323	0,236
Ren- 691	**-273,2**	0,386	0,394	0,059	0,242	0,102	0,225	0,135
Ren- 692	**-283,0**	1,141	0,941	0,174	0,197	0,248	0,521	0,772
Ren- 694	**-301,2**	0,343	0,294	0,045	0,098	0,057	0,186	0,173
Ren- 695	**-309,2**	0,738	0,870	0,112	0,109	0,172	0,462	0,350
Ren- 697	**-326,3**	0,337	0,405	0,077	0,067	0,016	0,142	0,119
Ren- 698	**-336,2**	0,281	0,831	0,073	0,141	0,077	0,263	0,163
Ren- 699	**-345,8**	0,407	0,463	0,049	0,180	0,067	0,226	0,160
Ren- 700	**-355,2**	0,418	0,537	0,004	0,059	0,043	0,160	0,096
Ren- 701	**-364,8**	0,413	0,428	0,036	0,066	0,071	0,241	0,168
Ren- 702	**-372,9**	0,448	0,363	0,060	0,091	0,088	0,191	0,002
Ren- 703	**-382,2**	0,412	0,310	0,050	0,122	0,063	0,144	0,208
Ren- 704	**-390,7**	0,255	0,326	0,055	0,070	0,010	0,103	0,107
Ren- 705	**-398,8**	0,312	0,596	0,034	0,098	0,067	0,213	0,095
Ren- 706	**-407,7**	0,293	0,269	0,051	0,050	0,036	0,112	0,086
Ren- 707	**-415,8**	0,388	0,401	0,069	0,136	0,074	0,197	0,126
Ren- 708	**-425,3**	0,470	0,353	0,023	0,134	0,067	0,196	0,145
Ren- 709	**-434,1**	0,185	0,273	0,052	0,057	0,044	0,089	0,065
Ren- 710	**-442,2**	0,524	0,584	0,054	0,091	0,074	0,180	0,225
Ren- 711	**-450,5**	0,350	0,510	0,049	0,061	0,060	0,169	0,114
Ren- 712	**-458,4**	0,175	0,235	0,029	0,072	0,017	0,135	0,081
Ren- 713	**-467,9**	0,727	0,892	0,023	0,226	0,129	0,838	0,445
Ren- 714	**-476,7**	0,007	0,040	0,014	0,022	0,019	0,089	0,044
Ren- 715	**-484,7**	0,477	0,536	0,052	0,151	0,086	0,284	0,254
Ren- 716	**-494,0**	0,283	0,234	0,031	0,066	0,057	0,125	0,118
Ren- 717	**-502,9**	0,483	0,887	0,067	0,107	0,084	0,197	0,172
Ren- 718	**-511,3**	0,178	0,291	0,032	0,052	0,057	0,116	0,114
Ren- 719	**-519,1**	0,722	0,706	0,118	0,149	0,155	0,400	0,264
Ren- 720	**-528,2**	0,185	0,248	0,031	0,023	0,049	0,179	0,131
Ren- 721	**-537,2**	0,417	0,847	0,078	0,145	0,077	0,232	0,135
Ren- 721	**-546,3**	0,283	0,267	0,037	0,003	0,051	0,258	0,205
Ren- 722	**-555,8**	0,620	0,614	0,063	0,151	0,189	0,393	0,307
Ren- 723	**-564,7**	0,367	0,540	0,036	0,132	0,048	0,198	0,136
Ren- 724	**-573,8**	0,742	0,622	0,086	0,214	0,165	0,429	0,273
Ren- 726	**-583,7**	0,305	0,415	0,027	0,054	0,047	0,153	0,111

Ren- 727	**-591,6**	0,340	0,310	0,057	0,126	0,047	0,170	0,145
Ren- 728	**-600,2**	0,344	0,252	0,021	0,311	0,062	0,139	0,150
Ren- 729	**-611,5**	0,387	0,399	0,042	0,187	0,053	0,165	0,188
Ren- 730	**-623,4**	0,583	0,386	0,056	0,118	0,140	0,288	0,259
Ren- 731	**-635,0**	0,273	0,616	0,022	0,087	0,002	0,174	0,146
Ren- 732	**-646,5**	0,292	0,437	0,033	0,054	0,068	0,200	0,122
Ren- 733	**-658,0**	0,316	0,364	0,025	0,089	0,052	0,115	0,118
Ren- 734	**-669,4**	0,340	0,440	0,022	0,051	0,019	0,129	0,134
Ren- 734	**-669,4**	0,488	0,417	0,008	0,193	0,094	0,278	0,180
Ren- 735	**-681,5**	0,472	0,301	0,006	0,118	0,063	0,154	0,126
Ren- 736	**-692,5**	0,356	0,574	0,064	0,142	0,066	0,220	0,166
Ren- 737	**-704,4**	0,228	0,346	0,042	0,050	0,052	0,091	0,070
Ren- 739	**-726,5**	0,718	0,589	0,054	0,265	0,171	0,281	0,320
Ren- 740	**-738,8**	0,239	0,040	0,004	0,053	0,039	0,089	0,069
Ren- 741	**-749,3**	0,339	0,337	0,035	0,085	0,049	0,192	0,147
Ren- 742	**-761,2**	0,370	0,334	0,025	0,031	0,084	0,210	0,143
Ren- 744	**-783,0**	0,362	0,465	0,031	0,059	0,048	0,152	0,150
Ren- 746	**-806,0**	0,375	0,360	0,040	0,047	0,054	0,122	0,129
Ren- 747	**-817,0**	0,253	0,363	0,004	0,003	0,041	0,199	0,082
Ren- 750	**-850,8**	0,157	0,348	0,059	0,036	0,017	0,110	0,052
Ren- 802	**-1517,7**	0,389	0,457	0,076	0,083	0,079	0,340	0,403
Ren- 803	**-1532,8**	0,275	0,307	0,032	0,130	0,026	0,130	0,301
Ren- 804	**-1548,5**	0,691	0,654	0,132	0,060	0,159	0,474	1,454
Ren- 805	**-1564,0**	1,363	1,182	0,245	0,164	0,331	0,682	1,477
Ren- 806	**-1579,3**	0,230	0,414	0,042	0,003	0,018	0,177	0,283
Ren- 807	**-1594,3**	0,685	0,578	0,137	0,139	0,125	0,345	0,321
Ren- 808	**-1609,5**	0,413	0,476	0,085	0,100	0,106	0,229	0,223
Ren- 809	**-1625,0**	0,007	0,399	0,083	0,003	0,095	0,436	0,660
Ren- 810	**-1640,3**	0,226	0,198	0,004	0,003	0,032	0,238	0,137
Ren- 811	**-1655,5**	0,784	0,653	0,099	0,003	0,127	0,677	1,031
Ren- 812	**-1671,8**	0,332	0,269	0,068	0,064	0,063	0,193	0,208
Ren- 813	**-1684,6**	0,323	0,351	0,064	0,075	0,053	0,289	0,221
Ren- 814	**-1697,8**	0,278	0,421	0,040	0,059	0,061	0,118	0,169
Ren- 815	**-1711,4**	0,530	0,331	0,090	0,131	0,106	0,345	0,653
Ren- 816	**-1724,3**	0,612	0,494	0,102	0,279	0,125	0,487	0,533
Ren- 817	**-1737,0**	0,091	0,109	0,004	0,003	0,011	0,095	0,051
Ren- 818	**-1750,0**	0,474	0,512	0,081	0,112	0,069	0,224	0,276
Ren- 819	**-1762,2**	0,356	0,408	0,059	0,057	0,088	0,302	0,221
Ren- 820	**-1779,5**	0,257	0,304	0,037	0,078	0,018	0,089	0,063
Ren- 821	**-1798,3**	0,405	0,288	0,054	0,091	0,060	0,229	0,562
Ren- 822	**-1818,5**	1,221	0,845	0,004	0,420	0,200	0,416	0,512
Ren- 823	**-1837,0**	0,125	0,449	0,044	0,003	0,028	0,134	0,077
Ren- 823	**-1837,0**	0,558	0,550	0,065	0,178	0,099	0,331	0,848
Ren- 824	**-1855,7**	0,087	0,131	0,004	0,003	0,014	0,089	0,089
Ren- 825	**-1873,7**	0,186	0,303	0,036	0,003	0,036	0,187	0,143
Ren- 826	**-1891,3**	0,941	0,737	0,165	0,170	0,220	0,805	0,573
Ren- 827	**-1911,3**	0,328	0,360	0,085	0,047	0,071	0,194	0,143

Ren- 828	**-1931,0**	0,277	0,357	0,053	0,092	0,061	0,167	0,245
Ren- 829	**-1949,6**	0,324	0,575	0,018	0,003	0,036	0,190	0,148
Ren- 830	**-1968,3**	0,225	0,209	0,042	0,038	0,043	0,110	0,094
Ren- 831	**-1987,4**	0,246	0,287	0,052	0,028	0,046	0,166	0,125
Ren- 832	**-2005,3**	0,251	0,040	0,019	0,082	0,046	0,094	0,086
Ren- 833	**-2024,0**	0,254	0,174	0,019	0,033	0,049	0,096	0,063
Ren- 834	**-2042,4**	0,354	0,416	0,062	0,077	0,052	0,131	0,167
Ren- 835	**-2040,7**	0,230	0,431	0,025	0,003	0,042	0,212	0,123
Ren- 836	**-2056,9**	0,248	0,327	0,004	0,084	0,046	0,102	0,083
Ren- 837	**-2073,0**	0,599	0,040	0,059	0,003	0,074	0,239	0,404
Ren- 838	**-2089,2**	0,461	0,465	0,050	0,094	0,095	0,287	0,256
Ren- 839	**-2105,3**	2,014	1,396	0,318	0,274	0,522	1,605	1,997
Ren- 849-850	**-2137,6**	1,685	0,189	0,032	0,028	0,034	0,089	0,074
Ren- 841	**-2153,8**	0,228	0,238	0,047	0,055	0,023	0,134	0,067
Ren- 842	**-2169,9**	0,119	1,068	0,197	0,903	0,376	0,409	0,960
Ren- 843	**-2186,1**	1,441	0,376	0,066	0,030	0,074	0,262	0,410
Ren- 844	**-2202,2**	0,439	0,316	0,034	0,110	0,023	0,089	0,394
Ren- 845	**-2218,4**	0,235	0,040	0,042	0,064	0,071	0,142	0,156
Ren- 846	**-2234,5**	0,259	0,360	0,029	0,003	0,012	0,089	0,129
Ren- 847	**-2250,7**	0,182	0,450	0,033	0,112	0,076	0,229	0,192
Ren- 848	**-2266,8**	0,399	1,488	0,355	0,263	0,594	1,637	0,660
Ren- 851	**-2299,1**	0,178	0,255	0,020	0,044	0,032	0,153	0,057
Ren- 852	**-2315,2**	0,802	0,588	0,120	0,133	0,165	0,382	0,285
Ren- 853	**-2331,4**	0,656	0,484	0,113	0,141	0,146	0,408	0,917
Ren- 854	**-2347,5**	0,380	0,307	0,089	0,086	0,107	0,329	0,800
Ren- 855	**-2363,7**	0,828	0,737	0,118	0,168	0,156	0,606	0,660
Ren- 856	**-2379,8**	0,418	0,356	0,051	0,169	0,060	0,182	0,238
Ren- 857	**-2396,0**	0,155	0,040	0,037	0,077	0,016	0,089	0,052
Ren- 858	**-2412,1**	0,352	0,406	0,068	0,047	0,046	0,166	0,143
Ren- 859	**-2428,3**	0,278	0,266	0,036	0,016	0,045	0,105	0,061
Ren- 861	**-2460,6**	0,340	0,482	0,074	0,111	0,062	0,131	0,181
Ren- 862	**-2476,7**	0,343	0,040	0,047	0,069	0,002	0,183	0,303
Ren- 863	**-2492,9**	0,261	0,236	0,025	0,003	0,002	0,129	0,260
Ren- 864	**-2509,0**	0,170	0,258	0,046	0,025	0,023	0,089	0,031
Ren- 865	**-2525,2**	0,341	0,381	0,038	0,050	0,051	0,138	0,101
Ren- 866	**-2541,3**	0,295	0,103	0,034	0,106	0,002	0,180	0,101
Ren- 867	**-2557,4**	0,300	0,398	0,057	0,135	0,049	0,213	0,153
Ren- 868	**-2573,6**	0,139	0,369	0,034	0,041	0,041	0,089	0,066
Ren- 869	**-2589,7**	0,311	0,424	0,004	0,027	0,014	0,089	0,064
Ren- 870	**-2605,9**	0,328	0,382	0,048	0,048	0,052	0,214	0,142
Ren- 871	**-2622,0**	0,298	0,472	0,051	0,100	0,053	0,281	0,433
Ren- 873	**-2654,3**	0,295	0,264	0,041	0,065	0,041	0,089	0,096
Ren- 874	**-2670,5**	0,165	0,040	0,036	0,036	0,020	0,089	0,041
Ren- 875	**-2686,6**	0,238	0,315	0,016	0,003	0,022	0,193	0,118
Ren- 876	**-2702,8**	0,117	0,177	0,010	0,037	0,020	0,097	0,047
Ren- 877	**-2718,9**	0,196	0,314	0,055	0,048	0,049	0,128	0,123
Ren- 878	**-2735,1**	0,327	0,110	0,051	0,029	0,024	0,089	0,130

Ren- 879	**-2751,2**	0,133	0,218	0,015	0,081	0,014	0,089	0,050
Ren- 880	**-2767,4**	0,164	0,450	0,038	0,054	0,042	0,190	0,099
Ren- 882	**-2799,7**	1,451	0,701	0,173	0,091	0,276	1,043	1,628
Ren- 883	**-2815,8**	0,153	0,134	0,066	0,003	0,012	0,142	0,331
Ren- 884	**-2831,9**	0,227	0,040	0,016	0,064	0,049	0,089	0,113
Ren- 885	**-2848,1**	0,220	0,220	0,033	0,067	0,047	0,317	0,356
Ren- 886	**-2864,2**	0,160	0,283	0,071	0,024	0,024	0,123	0,062
Ren- 887	**-2880,4**	0,529	0,465	0,040	0,202	0,049	0,215	0,145
Ren- 888	**-2896,5**	0,208	0,297	0,042	0,034	0,019	0,089	0,062
Ren- 889	**-2912,7**	0,402	0,040	0,091	0,338	0,148	0,089	0,101
Ren- 891	**-2945,0**	0,077	0,100	0,023	0,003	0,028	0,206	0,123
Ren- 892	**-2961,1**	0,649	0,605	0,094	0,267	0,141	0,449	0,557
Ren- 893	**-2977,3**	0,173	0,385	0,052	0,003	0,037	0,189	0,101
Ren- 894	**-2993,4**	1,356	0,327	0,224	0,918	0,222	0,192	0,253
Ren- 895	**-3009,6**	0,169	0,290	0,054	0,003	0,022	0,107	0,119
Ren- 896	**-3025,7**	0,420	0,415	0,053	0,003	0,066	0,569	0,477
Ren- 897	**-3041,9**	0,589	0,678	0,114	0,433	0,172	0,457	0,350
Ren- 898	**-3058,0**	0,152	0,304	0,014	0,003	0,021	0,101	0,071
Ren- 900	**-3090,3**	0,672	0,429	0,120	0,138	0,128	0,475	0,768

Table 20 *– Amino acids detected in Renland samples. The concentrations are expressed in µg* L^{-1}.

Table 21 – *Identified molecules in Talos Dome ice samples with nanoHRMS-nanoHPLC/MS in positive mode.*

m/z	Formula
107,0708	**C4 H10 O3**
129,0514	**C4 H10 O3**
159,0057	**C4 H8 O4**
167,0548	**C5 H11 O6**
157,0825	**C6 H14 O3**
160,9996	**C7 H6 O2**
207,0492	**C7 H10 O7**
127,1114	**C8 H15 O**
129,1265	**C8 H16 O**
163,0523	**C8 H12 O**
169,1200	**C8 H18 O2**
163,1320	**C8 H18 O3**
217,1032	**C8 H18 O5**
249,0957	**C10 H16 O7**
213,1489	**C12 H21 O3**
241,1770	**C12 H26 O3**
217,0488	**C12 H8 O4**
239,1280	**C13 H18 O4**
293,1740	**C17 H24 O4**
295,1892	**C17 H26 O4**
311,1855	**C17 H26 O5**
367,1382	**C18 H22 O8**
453,3412	**C23 H48 O8**
89,0592	**C4 H8 O2**
425,4332	**C28 H56 O2**
117,0634	**C2 H10 O2 N2**
159,9988	**C4 H5 N O3**
135,1006	**C4 H12 O2 N3**
158,0086	**C5 H4 O5 N**
178,9845	**C5 H4 O3 N2**
170,0197	**C5 H3 O4 N3**
220,0197	**C6 H9 N O5**
161,0111	**C6 H6 O N2**
163,0260	**C6 H8 O N2**
177,0065	**C6 H6 O2 N2**
176,0218	**C6 H7 O N3**
183,0980	**C6 H10 O N6**
185,1140	**C6 H12 O N6**
175,0268	**C7 H8 O N2**
177,0416	**C7 H10 O N2**
189,0060	**C7 H6 O2 N2**
191,0219	**C7 H8 O2 N2**
217,0382	**C9 H10 O2 N2**
176,0474	**C8 H11 O N**
205,0373	**C8 H10 O2 N2**
219,0169	**C8 H8 O3 N2**
201,0879	**C8 H12 O4 N2**
176,0454	**C8 H5 O2 N3**
225,0610	**C8 H8 N4 O4**
233,0316	**C9 H10 N2 O3**
249,0266	**C9 H10 N2 O4**
251,0421	**C9 H12 O4 N2**
249,1550	**C9 H20 O4 N4**
261,1083	**C10 H16 O6 N2**
247,1653	**C11 H22 O4 N2**
226,1790	**C11 H21 O N4**
216,0641	**C12 H9 N O3**
276,0845	**C12 H15 O5 N**
294,2046	**C15 H25 O2 N4**
326,1965	**C17 H27 O5 N**
328,2107	**C17 H29 O5 N**
371,1015	**C19 H17 O7 N**
389,1114	**C20 H18 N2 O5**
415,2359	**C22 H36 O3 N2**
414,2500	**C22 H31 O3 N5**
443,2674	**C24 H40 O3 N2**
131,0007	**C H6 S O5**
158,9961	**C2 H6 O6 S**
157,0165	**C3 H8 O5 S**
173,0113	**C3 H8 O6 S**
141,0047	**C3 H8 O2 S2**
202,9675	**C3 H6 O6 S2**
187,0266	**C4 H10 O6 S**
162,9883	**C5 H6 O2 S2**
165,0037	**C5 H8 O2 S2**
175,0441	**C5 H12 O2 S2**
201,0253	**C5 H12 O4 S2**
180,9721	**C6 H6 O2 S**
159,0118	**C6 H6 O3 S**
211,0271	**C6 H10 S O6**
215,0583	**C6 H14 S O6**
245,0317	**C6 H12 O8 S**
279,0374	**C6 H14 O10 S**
221,0121	**C7 H8 O6 S**
186,9891	**C7 H6 O2 S2**
164,9998	**C8 H6 O2 S**
223,0636	**C8 H14 O5 S**
180,9775	**C8 H5 O S2**
217,0539	**C9 H12 O4 S**
191,0167	**C10 H6 O2 S**
240,9981	**C10 H8 O3 S2**
233,9799	**C11 H5 O2 S2**
235,9956	**C11 H8 O2 S2**
247,0053	**C12 H7 O4 S**
355,2148	**C16 H34 S O6**
383,2454	**C18 H38 O6 S**
91,0576	**C4 H10 S**
133,1046	**C7 H16 S**
185,0452	**C9 H12 S2**
195,1213	**C12 H18 S**
203,0386	**C9 H6 N4 S**
205,0544	**C9 H8 N4 S**
162,0292	**C3 H10 O3 P**
155,0467	**C4 H11 O4 P**
254,9806	**C4 H10 O7 P2**
217,0475	**C5 H13 O7 P**
253,0226	**C5 H12 O7 P2**
268,9963	**C5 H12 O7 P2**
161,0365	**C6 H9 O3 P**
420,9697	**C6 H15 O15 P3**
171,0204	**C7 H7 O3 P**
177,0678	**C7 H13 O3 P**
350,9990	**C9 H13 O9 P2**
231,1167	**C11 H19 O3 P**
253,0255	**C11 H9 O5 P**
267,1705	**C12 H28 O4 P**
299,1620	**C12 H27 O6 P**
441,2966	**C21 H45 O7 P**
396,2415	**C22 H37 O4 P**
116,9853	**C4 H2 N2**
86,0959	**C5 H11 N**
158,0124	**C6 H5 N3**
169,1189	**C6 H12 N6**
172,0271	**C7 H7 N3**
186,0420	**C8 H9 N3**
185,0477	**C9 H10 N2**
419,3149	**C26 H42 O4**
95,0851	**C7 H10**
111,1169	**C8 H14**
155,0859	**C12 H10**
140,0011	**C2 H5 O4 N S**
200,0219	**C4 H10 O6 N S**
148,0546	**C4 H9 O N3 S**
162,0043	**C5 H7 O N S2**
201,0707	**C6 H13 N O4 S**
260,0424	**C6 H13 O8 N S**
262,9790	**C7 H6 O5 N2 S2**
214,0894	**C10 H15 O2 N S**
230,0842	**C10 H15 O3 N S**
244,0649	**C10 H13 O4 N S**
158,0263	**C6 H7 O2 N S**
149,0113	**C3 H5 O3 N2 P**
145,0160	**C4 H6 O2 N2 P**
223,0116	**C5 H7 O6 N2 P**
189,0426	**C6 H10 O3 N2 P**
214,9858	**C6 H3 O5 N2 P**
221,0315	**C6 H9 N2 O5 P**
218,0330	**C6 H8 O4 N3 P**
220,0472	**C6 H10 N3 O4 P**
217,0365	**C7 H9 O4 N2 P**
217,0749	**C8 H13 O3 N2 P**
243,0160	**C8 H7 O5 N2 P**
257,0317	**C9 H9 O5 N2 P**

Table 22 – *Identified molecules in Talos Dome ice samples with HRMS-HPLC/MS in negative mode.*

m/z	Formula
119,0349	**C4 H8 O4**
101,0609	**C5 H10 O2**
115,0402	**C5 H8 O3**
115,0766	**C6 H12 O2**
129,0558	**C6 H10 O3**
145,0508	**C6 H10 O4**
159,0663	**C6 H10 O2**
167,0327	**C6 H10 O4**
179,0561	**C6 H12 O6**
202,0454	**C6 H13 O6**
218,0403	**C6 H13 O7**
218,0403	**C6 H9 O7**
121,0296	**C7 H6 O2**
127,0766	**C7 H12 O2**
129,0922	**C7 H14 O2**
137,0246	**C7 H6 O3**
143,0713	**C7 H12 O3**
145,0871	**C7 H14 O3**
159,1028	**C7 H14 O**
225,0615	**C7 H14 O8**
125,0974	**C8 H14 O**
135,0453	**C8 H8 O2**
141,0918	**C8 H14 O2**
143,1079	**C8 H16 O2**
151,0401	**C8 H8 O3**
155,0714	**C8 H12 O3**
157,0871	**C8 H14 O3**
165,0195	**C8 H6 O4**
169,0873	**C8 H12 O**
171,0665	**C8 H12 O4**
173,0820	**C8 H14 O4**
175,0977	**C8 H16 O4**
187,0613	**C8 H12 O5**
191,0925	**C8 H16 O5**
193,1081	**C8 H18 O5**
214,0485	**C8 H9 O4**
149,0609	**C9 H10 O2**
149,0609	**C9 H10 O2**
153,0921	**C9 H14 O2**
157,1236	**C9 H18 O2**
163,0401	**C9 H8 O3**
165,0195	**C9 H6 O4**
165,0559	**C9 H10 O3**
171,1028	**C9 H16 O3**
173,1184	**C9 H18 O3**
179,0352	**C9 H8 O6**
185,0822	**C9 H14 O4**
187,0978	**C9 H16 O4**
189,1134	**C9 H18 O4**
191,1290	**C9 H20 O4**
201,0771	**C9 H14 O5**
203,0926	**C9 H16 O5**
215,0927	**C9 H14 O3**
217,0721	**C9 H14 O6**
221,1033	**C9 H18 O6**
163,0765	**C10 H12 O2**
171,1391	**C10 H20 O2**
177,0559	**C10 H10 O3**
183,1028	**C10 H16 O3**
185,1185	**C10 H18 O3**
187,1341	**C10 H20 O3**
193,0509	**C10 H10 O4**
199,0976	**C10 H16 O4**
201,1134	**C10 H18 O4**
203,1290	**C10 H20 O4**
211,0977	**C10 H14 O2**
217,1083	**C10 H18 O5**
229,0718	**C10 H14 O6**
231,0876	**C10 H16 O6**
237,1346	**C10 H22 O6**
243,0873	**C10 H14 O4**
251,1137	**C10 H20 O7**
177,0923	**C11 H14 O2**
183,1391	**C11 H20 O2**
185,1549	**C11 H22 O2**
193,0874	**C11 H14 O3**
199,1340	**C11 H20 O3**
201,1498	**C11 H22 O3**
207,0666	**C11 H12 O4**
213,1134	**C11 H18 O4**
215,1290	**C11 H20 O4**
217,1449	**C11 H22 O4**
227,0926	**C11 H16 O5**
229,1084	**C11 H18 O5**
241,1081	**C11 H16 O3**
247,1189	**C11 H20 O6**
265,1294	**C11 H22 O7**
272,9807	**C11 H8 O6**
187,0766	**C12 H12 O2**
189,0921	**C12 H14 O2**
195,1393	**C12 H20 O2**
199,1705	**C12 H24 O2**
205,0869	**C12 H14 O3**
211,1344	**C12 H20 O3**
215,1656	**C12 H24 O3**
221,0822	**C12 H14 O4**
227,1294	**C12 H20 O4**
229,1444	**C12 H22 O4**
239,1292	**C12 H18 O2**
243,1242	**C12 H20 O5**
257,1032	**C12 H18 O6**
259,1187	**C12 H20 O6**
275,1137	**C12 H20 O7**
279,1449	**C12 H24 O7**
193,1599	**C13 H22 O**
209,1548	**C13 H22 O2**
213,0559	**C13 H10 O3**
213,1495	**C13 H26 O2**
225,1498	**C13 H22 O3**
227,1656	**C13 H24 O3**
229,1811	**C13 H26 O3**
243,1603	**C13 H24 O4**
245,1758	**C13 H26 O4**
257,1396	**C13 H22 O5**
269,1393	**C13 H20 O3**
271,1188	**C13 H20 O6**
275,1500	**C13 H24 O6**
287,1499	**C13 H22 O4**
225,0559	**C14 H10 O3**
227,2019	**C14 H28 O2**
241,1812	**C14 H26 O3**
241,1812	**C14 H26 O3**
243,1966	**C14 H28 O3**
257,1760	**C14 H26 O4**
259,1914	**C14 H28 O4**
285,1341	**C14 H22 O6**
307,1163	**C14 H22 O6**
233,1550	**C15 H22 O2**
255,1972	**C15 H28 O3**
257,2122	**C15 H30 O3**
269,1756	**C15 H26 O4**
271,1912	**C15 H28 O4**
301,1647	**C15 H26 O6**
347,1345	**C15 H24 O9**
269,2121	**C16 H30 O3**
271,2281	**C16 H32 O3**
277,1445	**C16 H22 O4**
279,1605	**C16 H24 O4**
285,2069	**C16 H30 O4**
287,2228	**C16 H32 O4**
295,1548	**C16 H24 O5**
307,1553	**C16 H22 O3**
415,2189	**C16 H34 O9**
341,1604	**C17 H26 O7**
295,2279	**C18 H33 O3**
329,2332	**C18 H34 O5**
343,2121	**C18 H32 O6**
353,1606	**C18 H26 O7**
369,1916	**C18 H28 O5**
289,0870	**C19 H14 O3**
297,2794	**C19 H38 O2**
331,1548	**C19 H24 O5**
315,1960	**C20 H28 O3**

m/z	Formula
333,0763	**C20 H14 O5**
335,2226	**C20 H32 O4**
349,2018	**C20 H30 O5**
351,2172	**C20 H32 O5**
365,1967	**C20 H30 O6**
329,2117	**C21 H30 O3**
349,1087	**C21 H18 O5**
369,3003	**C22 H42 O4**
455,1474	**C23 H30 O7**
367,3577	**C24 H48 O2**
397,3318	**C24 H46 O4**
381,3732	**C25 H50 O2**
411,3476	**C25 H48 O4**
395,3888	**C26 H52 O2**
431,0686	**C26 H18 O4**
559,1251	**C30 H24 O11**
128,0353	**C5 H7 N O3**
138,0197	**C6 H5 O3 N**
183,0048	**C6 H4 O5 N2**
158,0824	**C7 H13 O3 N**
168,0303	**C7 H7 O4 N**
197,0206	**C7 H6 O5 N2**
182,9968	**C8 H6 N2 O2**
207,0414	**C8 H6 N2O2**
172,0980	**C9 H15 O3 N**
186,1137	**C9 H17 O3 N**
204,1243	**C9 H19 O4 N**
218,1036	**C9 H17 O5 N**
250,1297	**C9 H19 O4 N**
297,0807	**C9 H16 N4 O6**
191,0461	**C10 H8 O N2**
200,1293	**C10 H19 O3 N**
216,1243	**C10 H19 O4 N**
239,0674	**C10 H12 O5 N2**
261,0487	**C10 H12 N2 O5**
266,0894	**C10 H13 N5 O4**
267,0735	**C10 H12 O5 N4**
283,0684	**C10 H12 O6 N4**
302,0663	**C10 H13 N5 O4**
208,0981	**C11 H15 O3 N**
214,1452	**C11 H21 O3 N**
248,0800	**C11 H11 O2 N2**
253,0832	**C11 H14 O5 N2**
228,1607	**C12 H23 O3 N**
242,1764	**C12 H23 N O**
244,1558	**C12 H23 O4 N**
260,1870	**C12 H25 O2 N**
261,1374	**C12 H22 O2 N2**
271,1664	**C12 H22 O2 N2**
277,0178	**C12 H8 O3 S**
224,1658	**C13 H23 N O2**

m/z	Formula
258,1714	**C13 H25 O4 N**
250,1451	**C14 H19 O3 N**
272,1866	**C14 H27 O4 N**
278,1534	**C14 H23 N O2**
285,1818	**C14 H26 O4 N2**
304,1762	**C14 H27 O6 N**
315,0751	**C14 H14 N2 O4**
317,0777	**C14 H12 N2 O4**
270,2068	**C15 H29 O3 N**
286,2022	**C15 H29 O4 N**
304,2131	**C15 H31 O5 N**
308,1617	**C15 H23 O4 N3**
360,2384	**C15 H31 N4 O3**
369,1916	**C15 H32 N4 O4**
384,1420	**C15 H21 N3 O6**
287,0591	**C16 H14 N2 O**
397,2260	**C16 H34 N4 O4**
306,1710	**C18 H23 N O2**
345,1017	**C19 H20 N2 O2**
359,1016	**C19 H18 N2 O4**
383,2066	**C19 H30 O3 N4**
369,0994	**C21 H14 O3 N4**
385,0730	**C21 H18 O4 N**
351,1840	**C22 H26 O3 N**
426,1896	**C22 H31 N O6**
469,1613	**C23 H24 N2 O6**
514,3242	**C23 H43 O5 N5**
451,3282	**C24 H47 O5 N4**
485,3576	**C24 H52 O6 N2**
577,3222	**C25 H42 O6 N10**
569,2614	**C29 H39 O8 N4**
145,0697	**C7 H14 O S**
143,0713	**C7 H12 O3**
161,0648	**C7 H14 O2 S**
143,0539	**C7 H12 O S**
215,0516	**C8 H14 O2 S**
199,0781	**C8 H18 O2 S**
271,0492	**C8 H16 O8 S**
304,9137	**C9 H7 O2 I S**
243,0698	**C10 H14 O2 S**
207,0124	**C10 H8 O3 S**
121,0131	**C10 H12 O5 S**
243,0335	**C10 H12 O5 S**
255,0334	**C11 H12 O5 S**
257,0494	**C11 H14 O5 S**
257,0854	**C11 H16 O2 S**
265,1478	**C12 H26 O4 S**
271,0646	**C12 H16 O5 S**
277,0178	**C12 H8 O3 S**
287,0591	**C12 H16 O6 S**
234,0713	**C13 H15 O2 S**

m/z	Formula
279,1637	**C13 H28 O4 S**
150,0339	**C13 H18 O6 S**
285,0800	**C13 H18 O5 S**
315,0912	**C13 H18 O4 S**
319,1219	**C13 H22 O4 S**
277,1842	**C14 H30 O3 S**
293,1792	**C14 H30 O4 S**
309,1744	**C14 H30 O5 S**
299,0959	**C14 H20 O5 S**
313,1476	**C15 H24 O2 S**
353,2001	**C15 H32 O4 S**
297,1529	**C16 H26 O3 S**
295,1372	**C16 H25 O3 S**
327,1635	**C17 H28 O4 S**
355,1758	**C17 H26 O5 S**
471,0241	**C17 H14 O11 S**
341,1425	**C17 H26 O5 S**
341,1793	**C17 H28 O2 S**
325,1839	**C18 H30 O3 S**
355,1583	**C18 H28 O5 S**
311,1683	**C19 H32 O3 S**
339,1995	**C19 H32 O3 S**
353,1789	**C19 H31 O4 S**
355,1945	**C19 H32 O4 S**
307,1163	**C20 H20 O S**
421,2265	**C20 H39 O7 S**
156,0124	**C6 H7 N O2 S**
217,0298	**C6 H8 N2 O2 S**
184,0076	**C7 H8 O4 N S**
188,0750	**C8 H15 O2 N S**
236,0965	**C8 H17 O2 N S**
212,0754	**C10 H15 O2 N S**
228,0702	**C10 H15 O3 N S**
258,0806	**C10 H15 O2 N S**
285,0686	**C10 H20 O3 N2 S**
288,0546	**C9 H12 N O2 S**
369,0436	**C10 H16 N2 O6 S2**
294,1380	**C11 H23 N O3 S**
255,0334	**C12 H12 O2 N S**
346,0971	**C13 H19 N O5 S**
298,0886	**C15 H19 N O2 S**
315,0912	**C15 H20 O3 N S**
375,0778	**C15 H14 N4 O3 S**
469,1613	**C15 H27 N4 O8 S**
415,2189	**C22 H33 N4 O2 S**

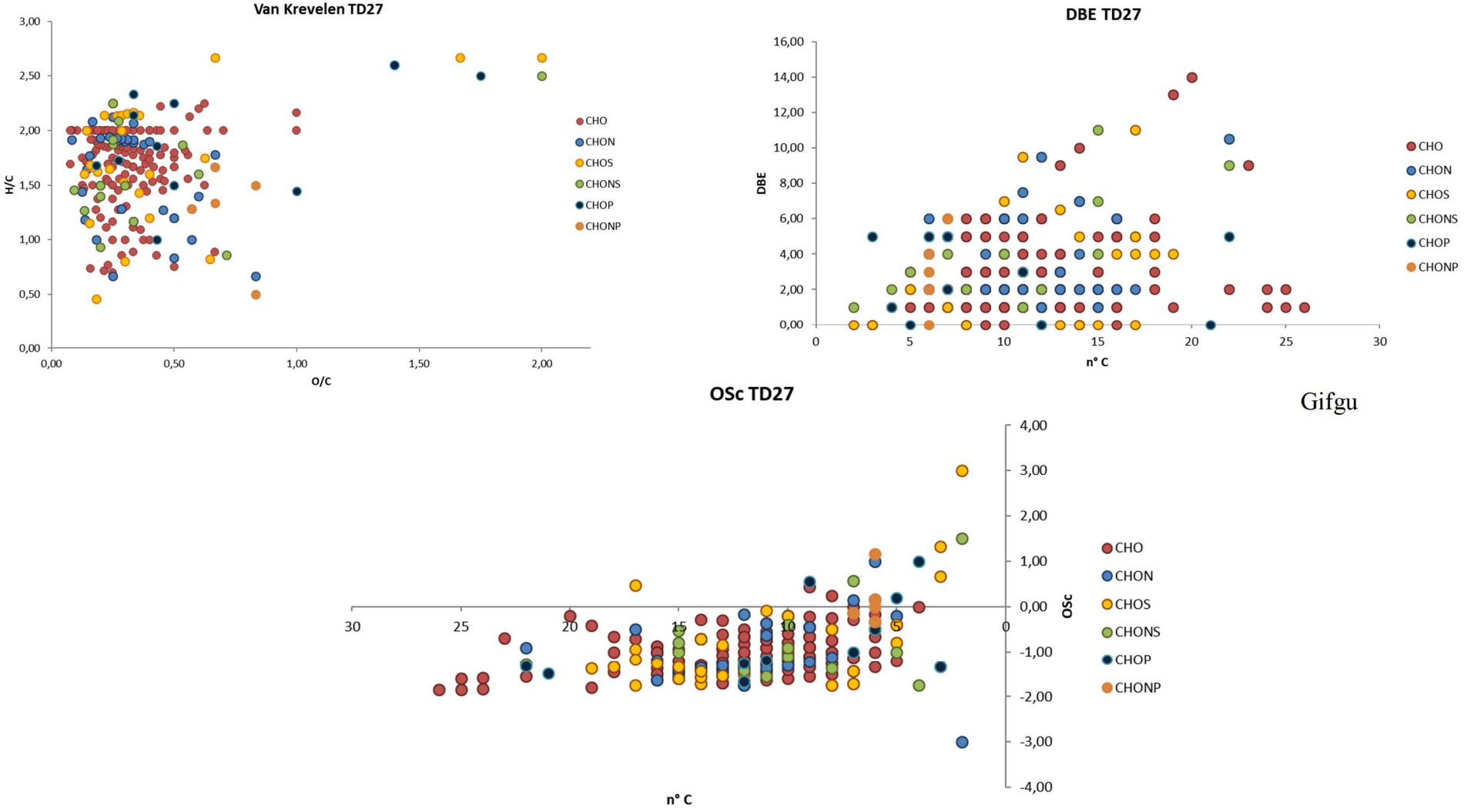

Gifgu

Figure 36 *– Van Krevelen, DBE and OSc diagrams of identified molecules in TD27 Taldice ice sample.*

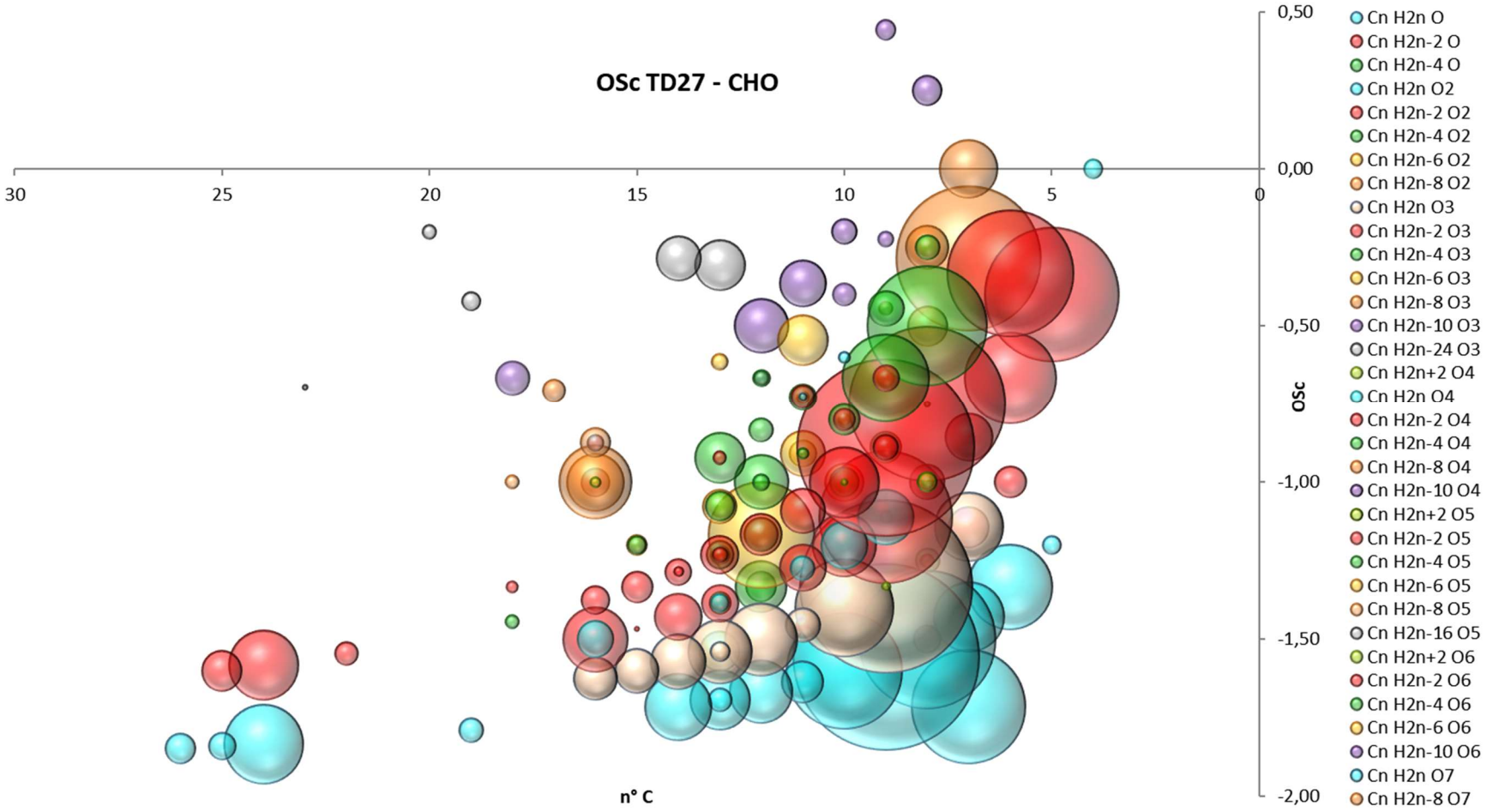

Figure 37 *– OSc diagram of CHO series compounds identified in TD27 Taldice ice core sample.*

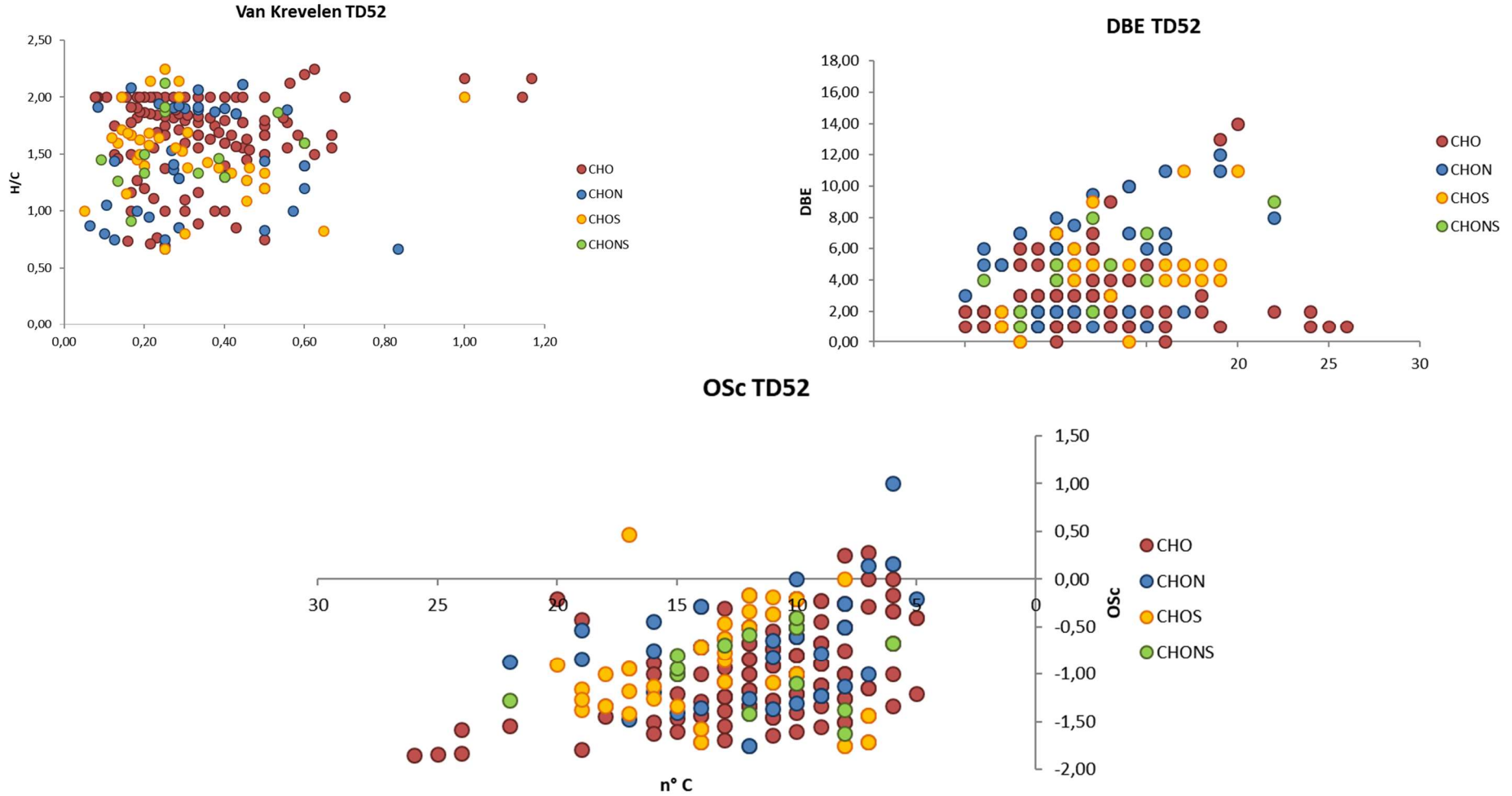

Figure 38 *– Van Krevelen, DBE and OSc diagrams of identified molecules in TD52 Taldice ice sample.*

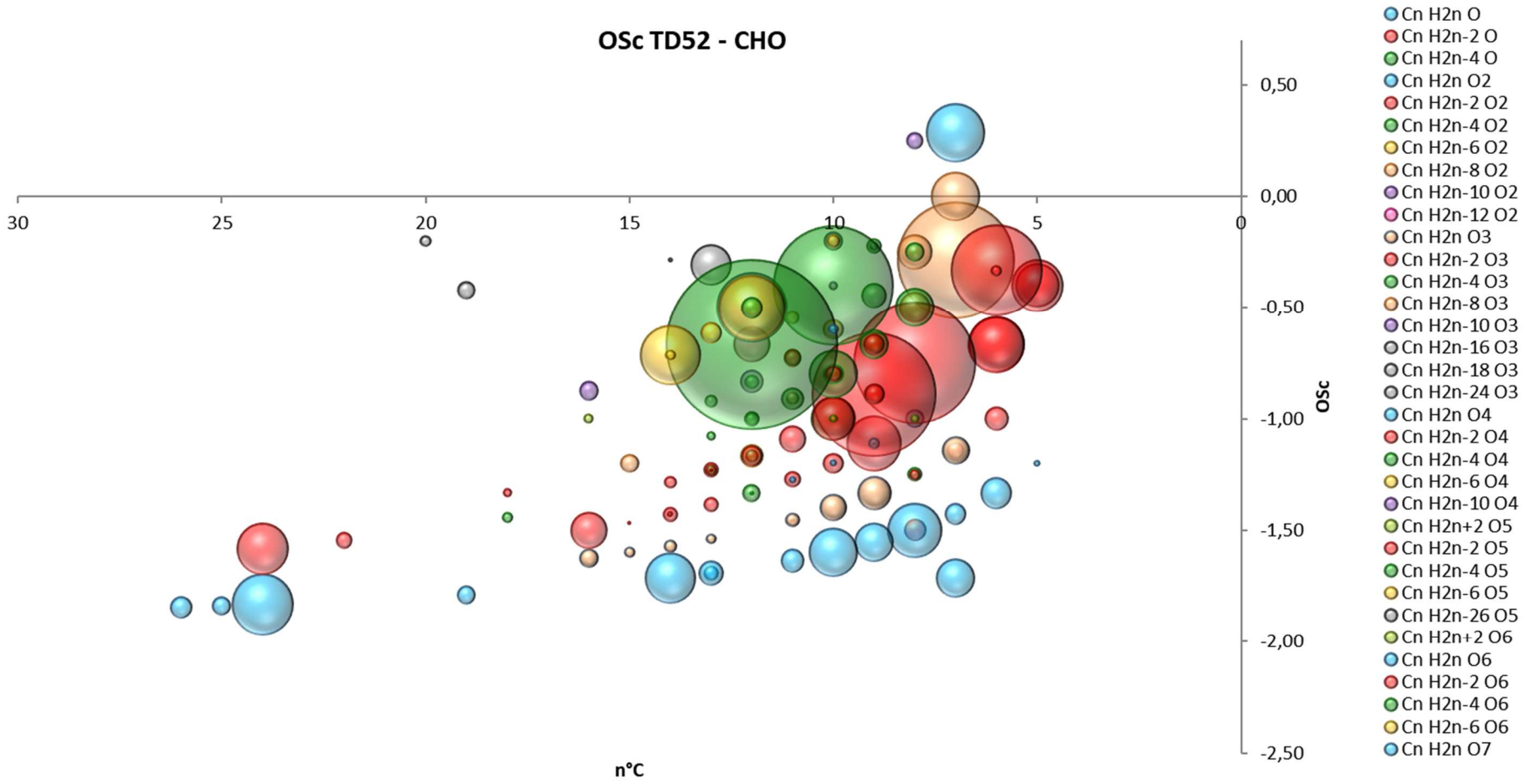

Figure 39 *– OSc diagram of CHO series compounds identified in TD52 Taldice ice core sample.*

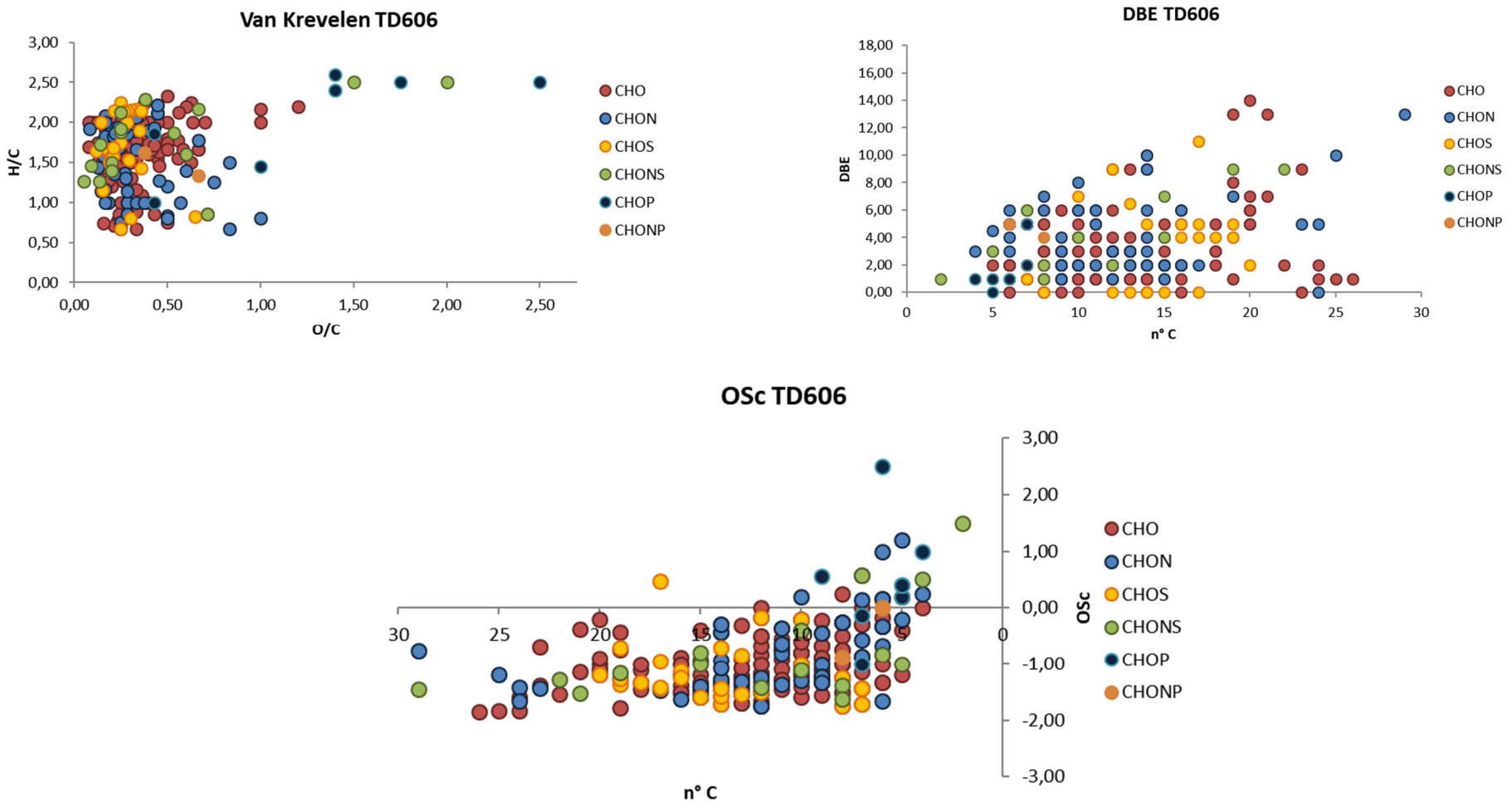

Figure 40 *– Van Krevelen, DBE and OSc diagrams of identified molecules in TD606 Taldice ice sample.*

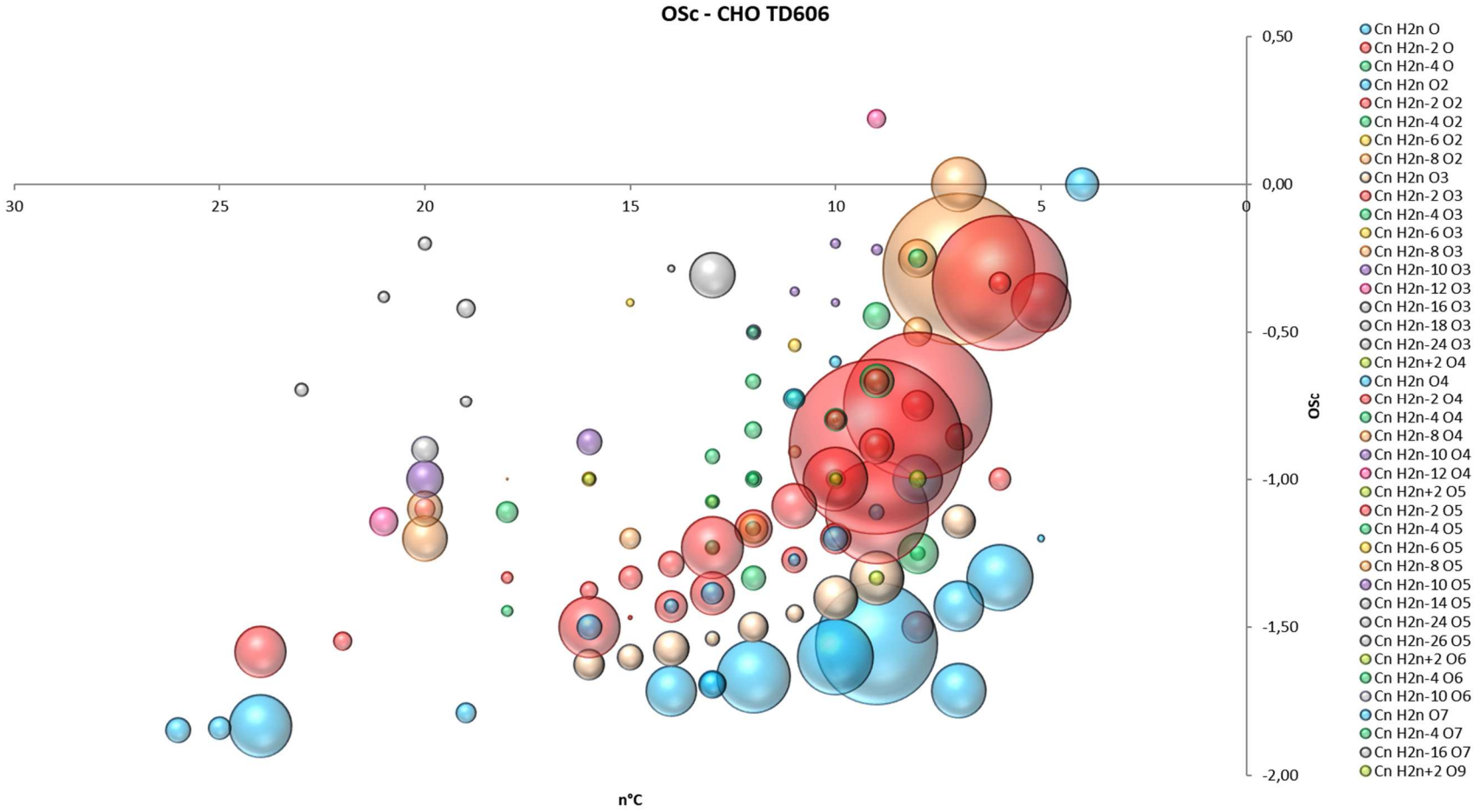

Figure 41 *– OSc diagram of CHO series compounds identified in TD606 Taldice ice core sample.*

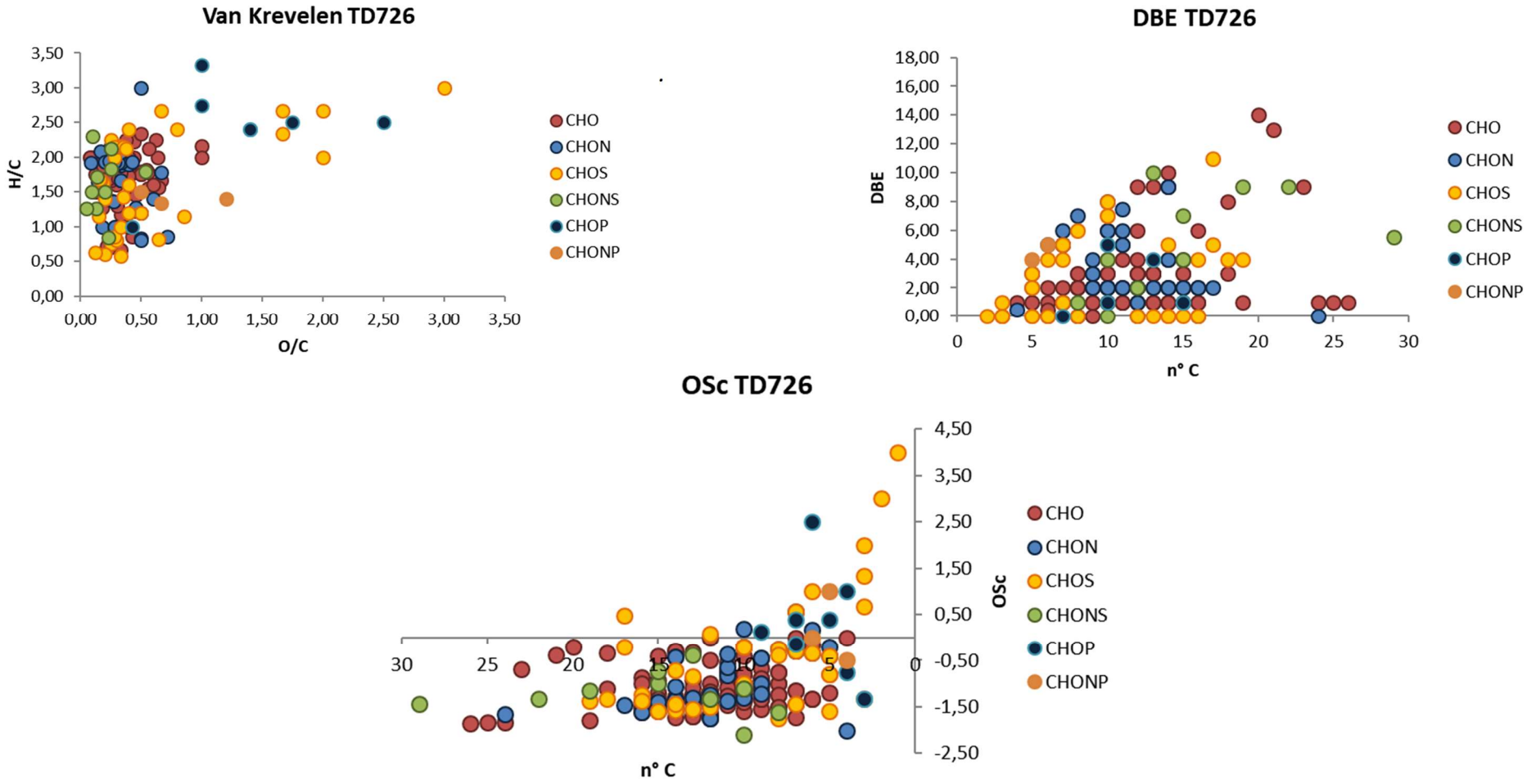

Figure 42 *– Van Krevelen, DBE and OSc diagrams of identified molecules in TD726 Taldice ice sample.*

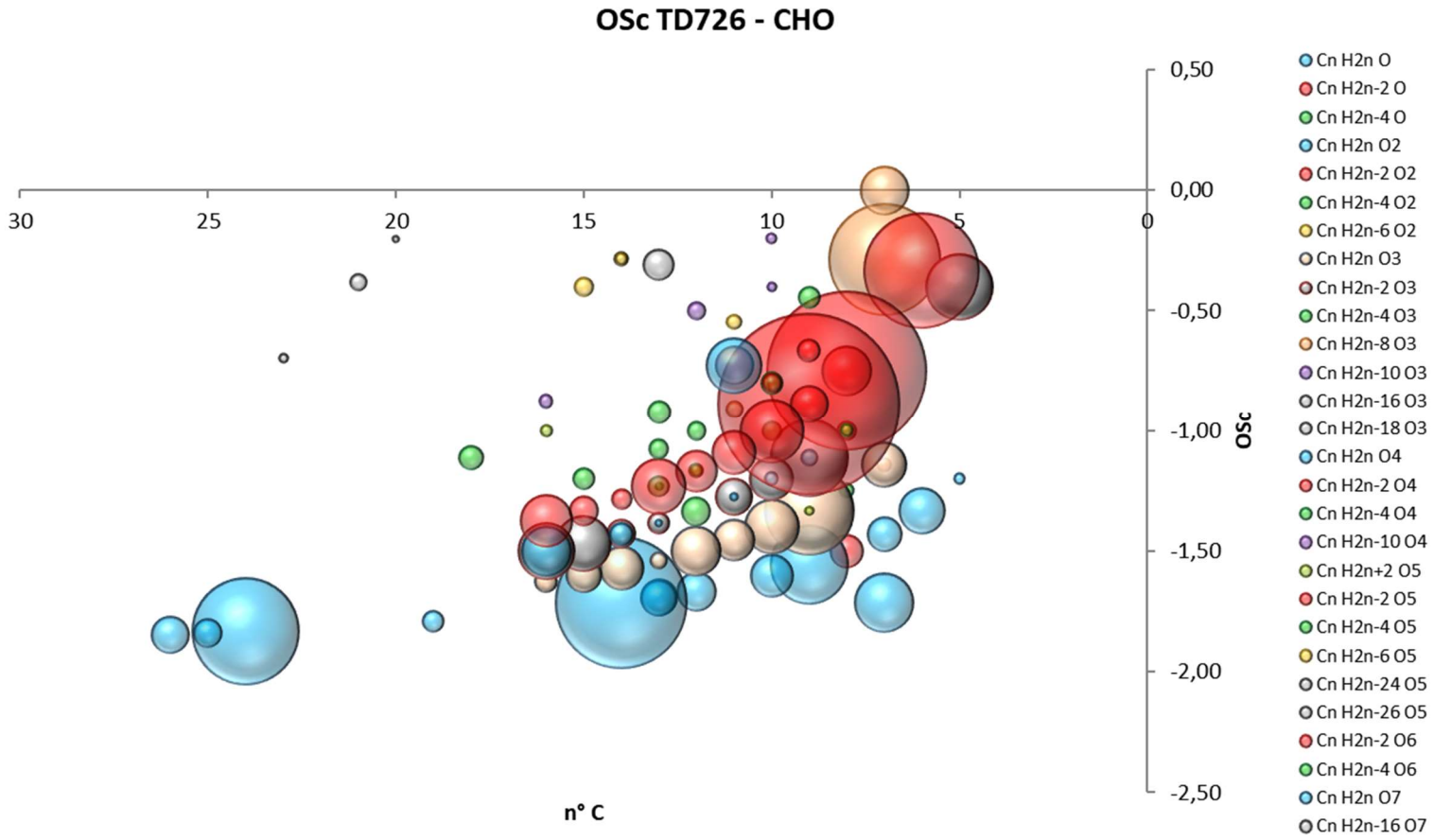

Figure 43 *– OSc diagram of CHO series compounds identified in TD726 Taldice ice core sample.*

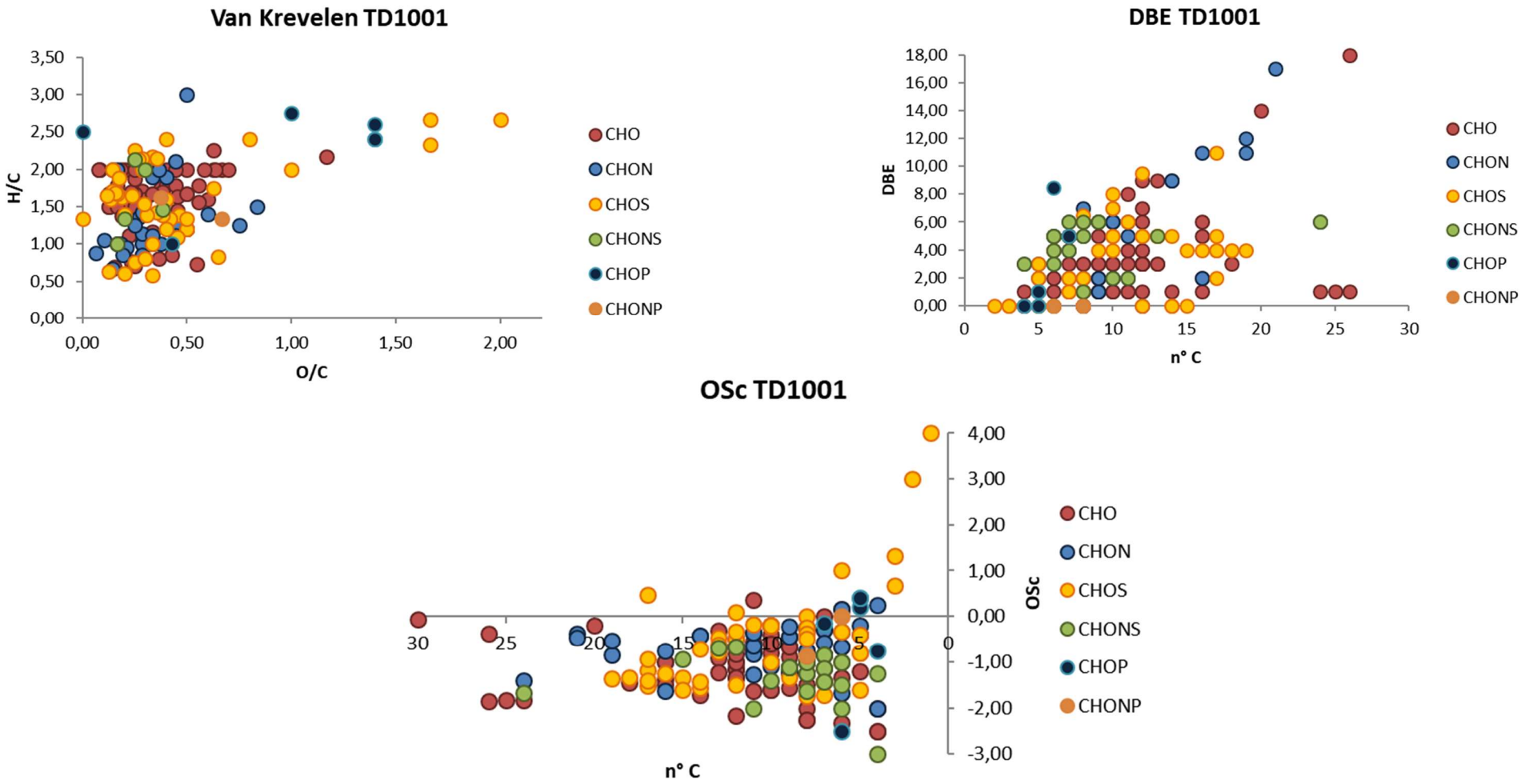

Figure 44 *– Van Krevelen, DBE and OSc diagrams of identified molecules in TD606 Taldice ice sample.*

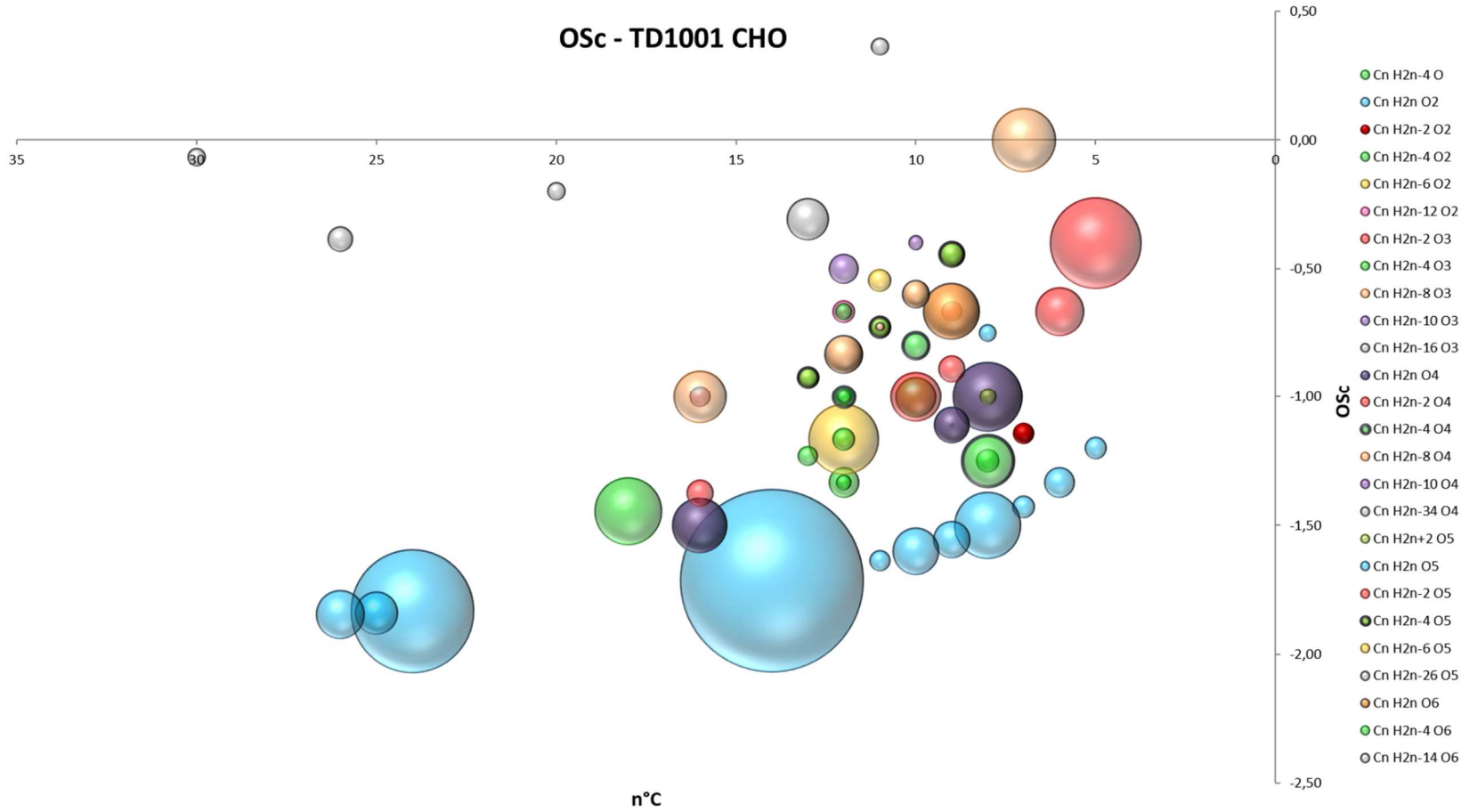

Figure 45 *– OSc diagram of CHO series compounds identified in TD1001 Taldice ice core sample.*

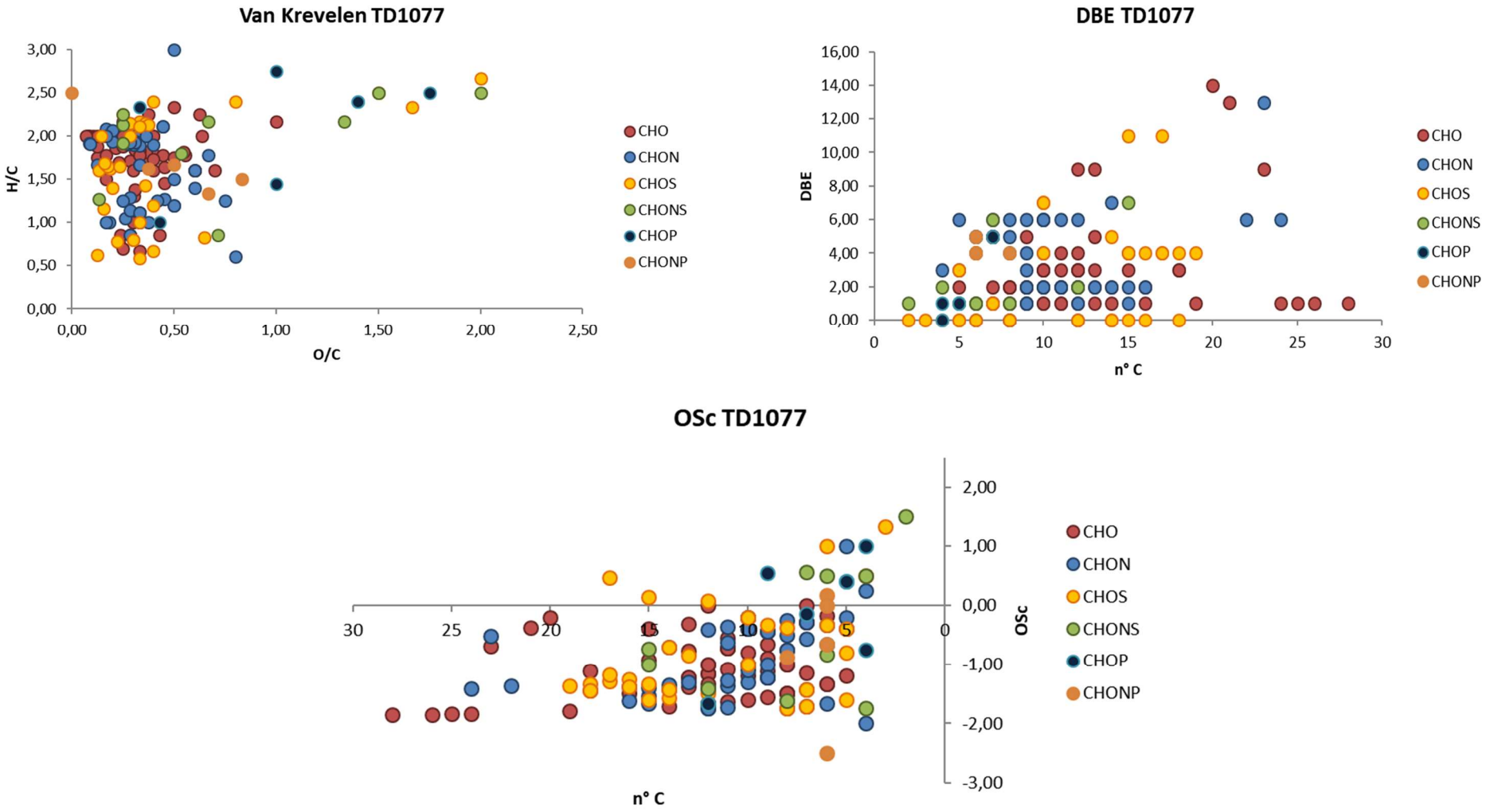

Figure 46 *– Van Krevelen, DBE and OSc diagrams of identified molecules in TD606 Taldice ice sample.*

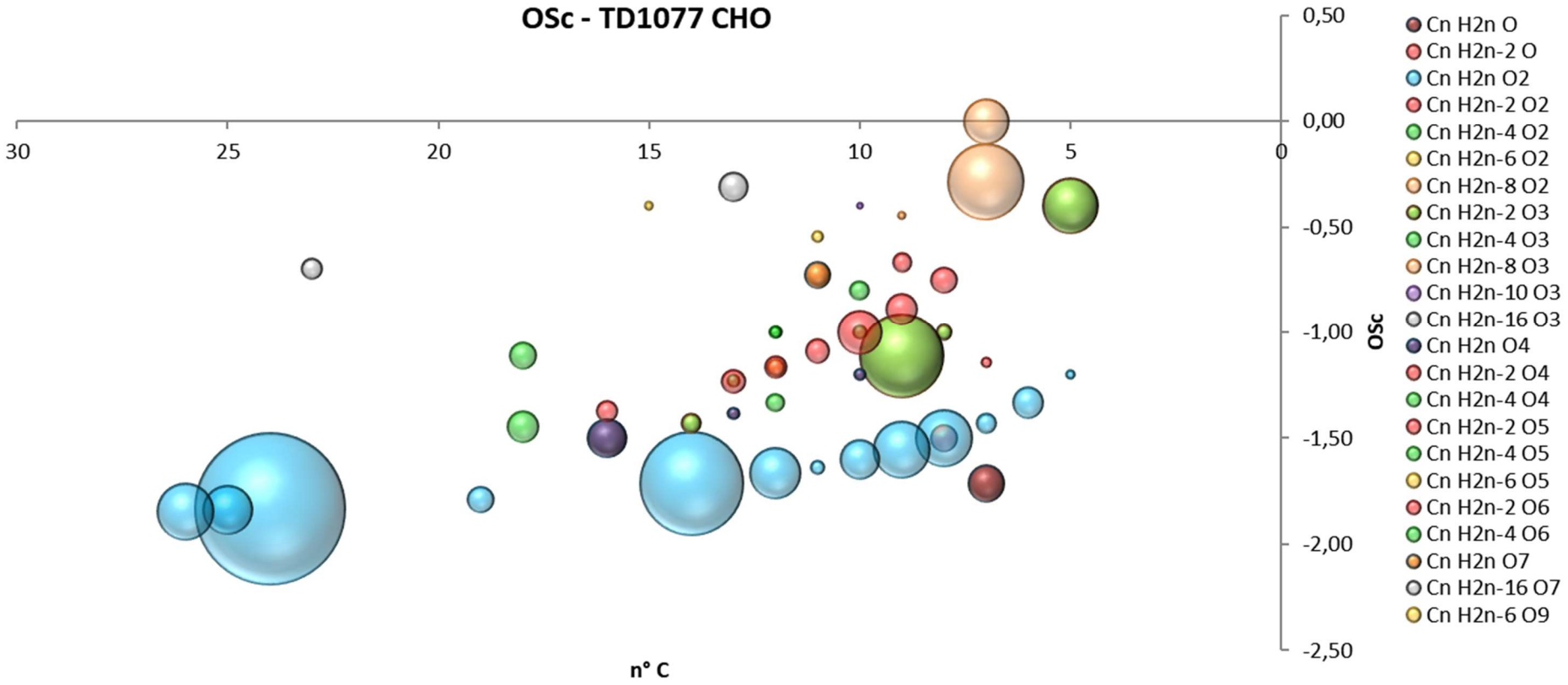

Figure 47 *– OSc diagram of CHO series compounds identified in TD1077 Taldice ice core sample.*

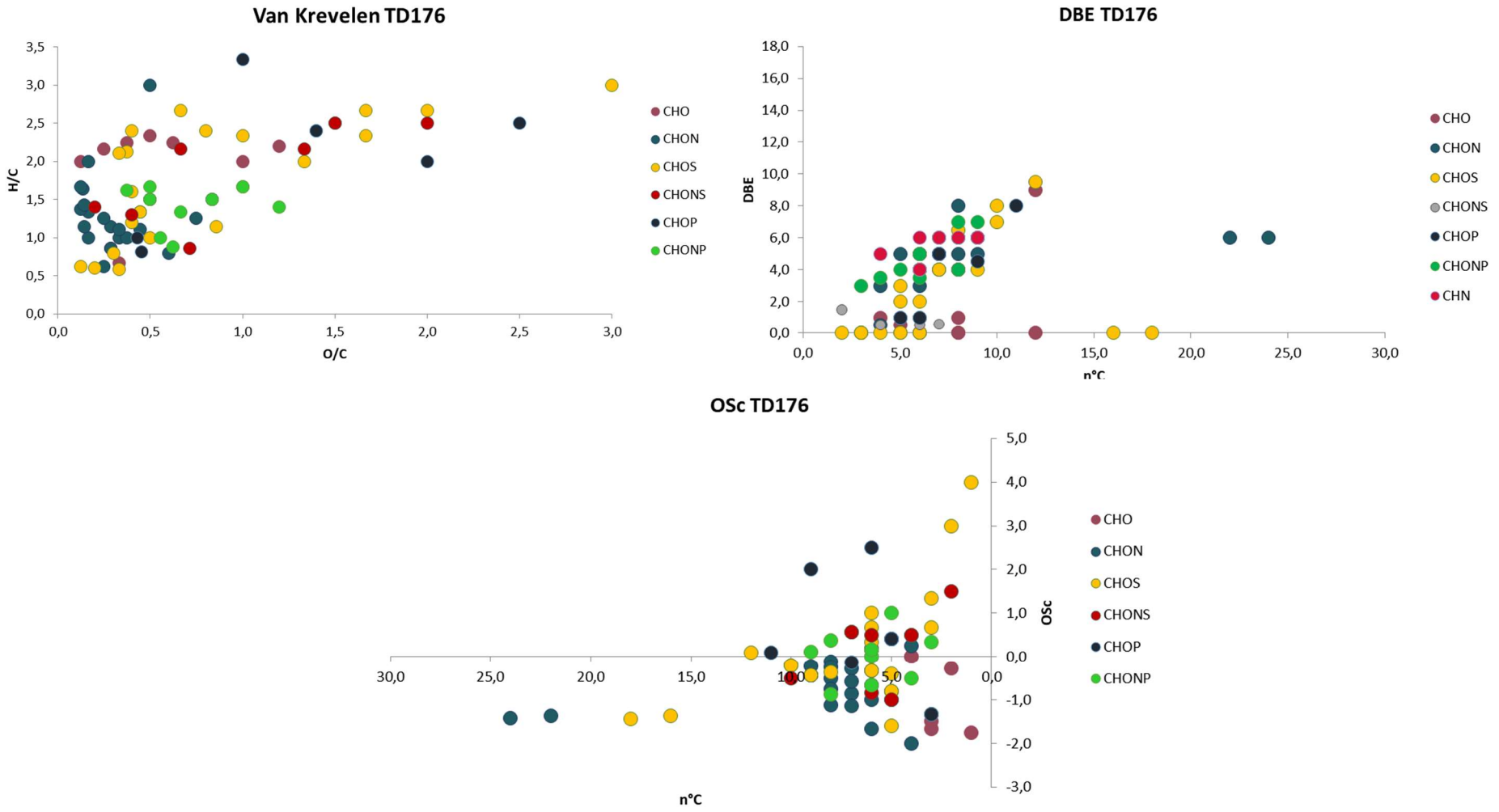

Figure 48 *– Van Krevelen, DBE and OSc diagrams of identified molecules in TD176 Taldice ice sample.*

7. BIBLIOGRAPHY

Abram, Nerilie J., Mark A.J. Curran, Robert Mulvaney, and Tessa Vance. 2008. "The Preservation of Methanesulphonic Acid in Frozen Ice-Core Samples." *Journal of Glaciology* 54(187): 680–84.

Alain Berthod et al. 2000. "Role of the Carbohydrate Moieties in Chiral Recognition on Teicoplanin-Based LC Stationary Phases." 72: 1767 - 1780.

Barbaro, E. et al. 2015. "Free Amino Acids in Antarctic Aerosol: Potential Markers for the Evolution and Fate of Marine Aerosol." *Atmospheric Chemistry and Physics* 15(10): 5457–69.

Barbaro, Elena et al. 2014. "D- and L-Amino Acids in Antarctic Lakes: Assessment of a Very Sensitive HPLC-MS Method." *Analytical and Bioanalytical Chemistry* 406(22): 5259–70.

Barbaro et al., 2017. "Free Amino Acids in the Arctic Snow and Ice Core Samples: Potential Markers for Paleoclimatic Studies." *Science of The Total Environment* 607–608: 454–62.

Bargagli, Roberto. 2005. *Antarctic Ecosystems : Environmental Contamination, Climate Change, and Human Impact*. Springer. Book

Belser, William L. 1959. "BIOASSAY OF ORGANIC MICRONUTRIENTS IN THE SEA*." *Math. Soc. Trans. Amer. Math. Soc. Trans. Amer. Math. Soc. J. L., Math. Zeit. (forthcoming* 45(10): 312–3193.

BenDaniel, D. J., and C. B. Duke. 1966. "Space-Charge Effects on Electron Tunneling." *Physical Review* 152(2): 683–92.

Berman, Tom, and Deborah A. Bronk. 2003. "Dissolved Organic Nitrogen: A Dynamic Participant in Aquatic Ecosystems." *Aquatic Microbial Ecology*. 31(3): 279-305

Bianchi, C et al. 2003. "RES Investigation at Talos Dome." *Annals of Geophysics* 46(December): 1–6.

Bianchi, Cesidio et al. 2001. "Morphology of Bottom Surfaces of Glacier Ice Tongues in the East Antarctic Region." *Ann. Geofis.* 44(1).

Bliesner, David M. 2006. *Validating Chromatographic Methods : A Practical Guide*. Wiley.

Boyd, Robert K., Cecilia. Basic, and Robert A. Bethem. 2011. *Trace Quantitative Analysis by Mass Spectrometry.* Wiley.

Bradley, Raymond S. 1999. *Paleoclimatology : Reconstructing Climates of the Quaternary*. Academic Press.

Bronk, Deborah A., Patricia M. Gilbert, and Bess B. Ward. "Nitrogen Uptake, Dissolved Organic Nitrogen Release, and New Production." *Science* 265: 1843–46.

Buck, R.H., and K. Krummen. 1987. "High-Performance Liquid Chromatographic Determination of Enantiomeric Amino Acids and Amino Alcohols after Derivatization with O-Phthaldialdehyde and Various Chiral Mercaptans : Application to Peptide Hydrolysates." *Journal of Chromatography A* 387: 255–65.

Christopher, Lew Paul, Bin Yao, and Yun Ji. 2014. "Lignin Biodegradation with Laccase-Mediator Systems." *Frontiers in Energy Research* 2: 12.

Cronin, J R, and S Pizzarello. 1997. "Enantiomeric Excesses in Meteoritic Amino Acids." *Science (New York, N.Y.)* 275(5302): 951–55.

Crutzen, Paul J., and Meinrat O. Andreae. 1990. "Biomass Burning in the Tropics: Impact on Atmospheric Chemistry and Biogeochemical Cycles." *Science* 250(4988): 1669–1679.

Daniau, A.-L., S.P. Harrison, and P.J. Bartlein. 2010. “Fire Regimes during the Last Glacial.” *Quaternary Science Reviews* 29(21–22): 2918–30.

Delmonte, Barbara et al. 2010. “Aeolian Dust in the Talos Dome Ice Core (East Antarctica, Pacific/Ross Sea Sector): Victoria Land versus Remote Sources over the Last Two Climate Cycles.” *Journal of Quaternary Science* 25(8): 1327–37.

Faravelli, T et al. 2006. LEAP *FENOMENOLOGIA DELLA COMBUSTIONE DI BIOMASSE*.

Frezzotti, M, and O Flora. 2002. “Ice Dynamics Features and Climatic Surface Parameters in East Antarctica from Terra Nova Bay to Talos Dome and Dome C: ITASE Italian Traverses.” *Terra Antartica* 9(1): 47–54.

Frezzotti, M. et al. 2004. “Geophysical Survey at Talos Dome, East Antarctica: The Search for a New Deep-Drilling Site.” *Annals of Glaciology* 39(1): 423–32.

Frezzotti, M. et al., 2004 “New Estimations of Precipitation and Surface Sublimation in East Antarctica from Snow Accumulation Measurements.” 23: 803-813

Fuhrer, Katrin, Albrecht Neftel, Martin Anklin, and Valter Maggi. 1993. “Continuous Measurements of Hydrogen Peroxide, Formaldehyde, Calcium and Ammonium Concentrations along the New Grip Ice Core from Summit, Central Greenland.” *Atmospheric Environment. Part A. General Topics* 27(12): 1873–80.

Gelencsér, András et al. 2007. “Source Apportionment of PM2.5 Organic Aerosol over Europe: Primary/secondary, Natural/anthropogenic, and Fossil/biogenic Origin.” *Journal of Geophysical Research* 112(D23): D23S04.

Gimenez, François, Mireille Soursac, and Robert Farinotti. 1997. “Enantiomeric Separation of Five Amino Acids by High-Performance Liquid Chromatography on a Chiral Crown Ether Column.” *Chirality* 9(2): 150–52.

“HyperSep™ SAX Cartridges.” https://www.thermofisher.com/order/catalog/product/60108-360

Iinuma, Y. et al. 2007. “Source Characterization of Biomass Burning Particles: The Combustion of Selected European Conifers, African Hardwood, Savanna Grass, and German and Indonesian Peat.” *Journal of Geophysical Research* 112(D8): D08209.

Isaksson, Elisabeth, Teija Kekonen, John Moore, and Robert Mulvaney. 2005. “The Methanesulfonic Acid (MSA) Record in a Svalbard Ice Core.” *Annals of Glaciology* 42: 345–51.

Kebarle, Paul, and Liang Tang. 1993. “From Ions in Solution to Ions in the Gas Phase: The Mechanism of Eiectrospray Mass Spectrometry.” *Anal. Chem.* (65:972A-986A).

Kim, Sunghwan, Robert W Kramer, and Patrick G Hatcher. 2003. “Graphical Method for Analysis of Ultrahigh-Resolution Braodband Mass Spectra of Natural Organic Matter, the Van Krevelen Diagram.” *Anal. Chem.* 75(20): 5336–44.

Kind, Tobias, and Oliver Fiehn. 2007. “Seven Golden Rules for Heuristic Filtering of Molecular Formulas Obtained by Accurate Mass Spectrometry.” 20: 1–20.

King, Richard et al. 2000. “Mechanistic Investigation of Ionization Suppression in Electrospray Ionization.” *Journal of the American Society for Mass Spectrometry* 11(11): 942–50.

Koch, B. P., and T. Dittmar. 2006. “From Mass to Structure: An Aromaticity Index for High-Resolution Mass Data of Natural Organic Matter.” *Rapid Communications in Mass Spectrometry* 20(5): 926–32.

KREVELEN, VAN, and D. W. 1950. “Graphical-Statistical Method for the Study of Structure and Reaction Processes of Coal.” *Fuel* 29: 269–84.

Kristensson, Adam, Thomas Rosenørn, and Merete Bilde. 2010. “Cloud Droplet Activation of Amino Acid Aerosol Particles.” *The Journal of Physical Chemistry A* 114(1): 379–86.

Kroll, Jesse H et al. 2011. “Carbon Oxidation State as a Metric for Describing the Chemistry of Atmospheric Organic Aerosol.” *Nature Chemistry*. 3: 133-139

LAWS, DAVID A., and David A. 1963. “Molecular Formula and Degree of Unsaturation.” *Nature* 200(4912): 1202–1202.

Legrand, Michel, and Paul Mayewski. 1997. “Glaciochemistry of Polar Ice Cores: A Review.” *Reviews of Geophysics* 35(3): 219–43.

Mace, Kimberly A., Paulo Artaxo, and Robert A. Duce. 2003. “Water-Soluble Organic Nitrogen in Amazon Basin Aerosols during the Dry (Biomass Burning) and Wet Seasons.” *Journal of Geophysical Research* 108(D16): 4512.

Magand, Olivier et al. 2004. “Climate Variability along Latitudinal and Longitudinal Transects in East Antarctica.” *Annals of Glaciology* 39(1): 351–58.

Man Nin Chan et al., 2005. “Hygroscopicity of Water-Soluble Organic Compounds in Atmospheric Aerosols: Amino Acids and Biomass Burning Derived Organic Species.” 39(6): 1555-1562

Marfey, Peter. 1984. “Determination ofD-Amino Acids. II. Use of a Bifunctional Reagent, 1,5-Difluoro-2,4-Dinitrobenzene.” *Carlsberg Research Communications* 49(6): 591–96.

Marlon, J R et al. “Climate and Human Influences on Global Biomass Burning over the Past Two Millennia.” Nature Geoscience. 1: 697-702.

Matos, João T.V., Regina M.B.O. Duarte, and Armando C. Duarte. 2016. “Challenges in the Identification and Characterization of Free Amino Acids and Proteinaceous Compounds in Atmospheric Aerosols: A Critical Review.” *TrAC Trends in Analytical Chemistry* 75: 97–107.

Narcisi, Biancamaria, Jean Robert Petit, and J??r??me Chappellaz. 2010. “A 70 Ka Record of Explosive Eruptions from the TALDICE Ice Core (Talos Dome, East Antarctic Plateau).” *Journal of Quaternary Science* 25(6): 844–49.

Net, Sopheak, Elena Gómez Alvarez, Sasho Gligorovski, and Henri Wortham. 2011. “Heterogeneous Reactions of Ozone with Methoxyphenols, in Presence and Absence of Light.” *Atmospheric Environment* 45(18): 3007–14.

O’Dowd, Colin D. et al. 2004. “Biogenically Driven Organic Contribution to Marine Aerosol.” *Nature* 431(7009): 676–680.

O’Dwyer, Jane et al. 2000. “Methanesulfonic Acid in a Svalbard Ice Core as an Indicator of Ocean Climate.” *Geophysical Research Letters* 27(8): 1159–62.

Oros, Daniel R et al. 2006a. “Identification and Emission Factors of Molecular Tracers in Organic Aerosols from Biomass Burning: Part 3. Grasses.” *Applied Geochemistry* 21(6): 919–940.

Perdue, Edward M., Egil T. Gjessing, William. Glaze, and William. Glaze. 1990. *Organic Acids in Aquatic Ecosystems : Report of the Dahlem Workshop on Organic Acids in Aquatic Ecosystems, Berlin 1989, May 7-12*. Wiley.

Petritis, Konstantinos, Claire Elfakir, and Michel Dreux. 2002. “A Comparative Study of Commercial Liquid Chromatographic Detectors for the Analysis of Underivatized Amino Acids.” *Journal of Chromatography A* 961(1): 9–21.

Petritis, Konstantinos, Alain Valleix, Claire Elfakir, and Michel Dreux. 2001. “Simultaneous Analysis of Underivatized Chiral Amino Acids by Liquid Chromatography–ionspray Tandem Mass Spectrometry Using a Teicoplanin Chiral Stationary Phase.” *Journal of Chromatography A* 913(1–2): 331–40.

Poluianov, S., R. Traversi, and I. Usoskin. 2014. “Cosmogenic Production and Climate Contributions to Nitrate Record in the TALDICE Antarctic Ice Core.” *Journal of Atmospheric and Solar-Terrestrial Physics* 121: 50–58.

Reeh, N., S. J. Johnsen, and D. Dahl-Jensen. 1985. “Dating the Dye 3 Deep Ice Core by Flow Model Calculations.” In *Greenland Ice Core: Geophysics, Geochemistry, and the Environment. (1985), Geophys. Monogr. Ser., Vol. 33, Edited by C. C. Langway, Jr., H. Oeschger, and W. Dansgaard, Pp. 57-65, AGU, Washington, D. C.*, , 57–65.

Remelli, Maurizio, Paolo Fornasari, and Fernando Pulidori. 1997. “Study of Retention, Efficiency and Selectivity in Chiral Ligand-Exchange Chromatography with a Dynamically Coated Stationary Phase.” *Journal of Chromatography A* 761(1–2): 79–89.

Roland Warner, W.K Budd. 1998. “Modelling the Long-Term Response of the Antarctic Ice Sheet to Gl...: Ingenta Connect.” *Annals of Glaciology* 27(1): 161–68.

Ruddiman, William F. 2003. “The Anthropogenic Greenhouse Era Began Thousands of Years Ago.” *Climatic Change* 61(3): 261–93.

Ruddiman, William F. 2007. “The Early Anthropogenic Hypothesis: Challenges and Responses.” *Reviews of Geophysics* 45(4).

Scalabrin, E et al. 2012. “Amino Acids in Arctic Aerosols.” *Atmos. Chem. Phys. Atmospheric Chemistry and Physics* 12: 10453–63.

Scarchilli, Claudio, Massimo Frezzotti, and Paolo Michele Ruti. 2011. “Snow Precipitation at Four Ice Core Sites in East Antarctica: Provenance, Seasonality and Blocking Factors.” *Climate Dynamics* 37(9–10): 2107–25.

Schmidt, Andrea, Michael Karas, and Thomas Dülcks. 2003. “Effect of Different Solution Flow Rates on Analyte Ion Signals in Nano-ESI MS, or: When Does ESI Turn into Nano-ESI?” *Journal of the American Society for Mass Spectrometry* 14(5): 492–500.

Severi, M. et al. 2012. “Volcanic Synchronisation of the EPICA-DC and TALDICE Ice Cores for the Last 42 Kyr BP.” *Climate of the Past* 8(2): 509–17.

Simoneit, Bernd R.T. 2002. “Biomass Burning — a Review of Organic Tracers for Smoke from Incomplete Combustion.” *Applied Geochemistry* 17(3): 129–62.

Stenni, B. et al. 2002. “Eight Centuries of Volcanic Signal and Climate Change at Talos Dome (East Antarctica).” *Journal of Geophysical Research: Atmospheres* 107(D9).

Stenni, Barbara et al., 2011. “Expression of the Bipolar See-Saw in Antarctic Climate Records during the Last Deglaciation.” *Nature Geoscience* 4(1): 46–49.

Stenni, Barbara et al. 2000. “Snow Accumulation Rates in Northern Victoria Land, Antarctica, by Firn-Core Analysis.” *Journal of Glaciology* 46(155): 541–52.

Stubbins, Aron et al. 2010. “Illuminated Darkness: Molecular Signatures of Congo River Dissolved Organic Matter and Its Photochemical Alteration as Revealed by Ultrahigh Precision Mass Spectrometry.” *Limnology and Oceanography* 55(4): 1467–77.

Svensson, Anders et al. 2006. “The Greenland Ice Core Chronology 2005, 15–42 Ka. Part 2: Comparison to Other Records.” *Quaternary Science Reviews* 25(23–24): 3258–67.

Szyrmer, Wanda, and Isztar Zawadzki. 1997. “Biogenic and Anthropogenic Sources of Ice-Forming Nuclei: A Review.” *Bulletin of the American Meteorological Society* 78(2): 209–28.

Tabacco, I. E. et al. 1999. “Latest Improvements for the Echo Sounding System of the Italian Radar Glaciological Group and Measurements in Antarctica.” *Annals of Geophysics* 42(2).

Tabacco, Ignazio E. et al. 2002. “Airborne Radar Survey above Vostok Region, East-Central Antarctica: Ice Thickness and Lake Vostok Geometry.” *Journal of Glaciology* 48(160): 62–69.

Tatsumoto, M, … WT Williams - Journal of, and Undefined 1961. “Amino Acids in Samples of Surface Sea Water.” *UNIV, NEW HAVEN, CT 06520-8109*.

Thomas, Elizabeth R., and Thomas J. Bracegirdle. 2014. “Precipitation Pathways for Five New Ice Core Sites in Ellsworth Land, West Antarctica.” *Climate Dynamics* (December 2015): 2067–78.

Thomas, Elizabeth R., Thomas J. Bracegirdle, John Turner, and Eric W. Wolff. 2013. “A 308 Year Record of Climate Variability in West Antarctica.” *Geophysical Research Letters* 40(20): 5492–96.

Urbini, Stefano et al. 2006. “Location of a New Ice Core Site at Talos Dome (East Antarctica).” *Annals of Geophysics* 49(4–5): 1133–38.

Urbini, Stefano et al., 2008. “Historical Behaviour of Dome C and Talos Dome (East Antarctica) as Investigated by Snow Accumulation and Ice Velocity Measurements.” *Global and Planetary Change* 60(3): 576–88.

Veres, D. et al. 2013. “The Antarctic Ice Core Chronology (AICC2012): An Optimized Multi-Parameter and Multi-Site Dating Approach for the Last 120 Thousand Years.” *Climate of the Past* 9(4): 1733–48.

Visser, Simon A. 1903. “Application of Van Krevelen’s Graphical-Statistical Method for the Study of Aquatic Humic Material.” *Environ. Sci. Technol* 17: 412–17.

Wedyan, Mohammed A., and Martin R. Preston. 2008. “The Coupling of Surface Seawater Organic Nitrogen and the Marine Aerosol as Inferred from Enantiomer-Specific Amino Acid Analysis.” *Atmospheric Environment* 42(37): 8698–8705.

Wozniak, A S et al. 2008. “Technical Note: Molecular Characterization of Aerosol-Derived Water Soluble Organic Carbon Using Ultrahigh Resolution Electrospray Ionization Fourier Transform Ion Cyclotron Resonance Mass Spectrometry.” *Atmos. Chem. Phys. Atmospheric Chemistry and Physics* 8: 5099–5111.

“Www.taldice.org.” http://www.taldice.org/ (May 26, 2017).

“Www.taldice.org/project/drilling/index.php.” http://www.taldice.org/project/drilling/index.php (May 29, 2017).

Zangrando, Roberta et al. 2013. “Molecular Markers of Biomass Burning in Arctic Aerosols.” *Environmental Science and Technology* 47(15): 8565–74.

Curran, M.A.J., van Ommen, T.D., Morgan, V.I., Phillips, K.L. and Palmer, A.S. (2003) Ice core evidence for Antarctic sea ice decline since the 1950s, Science 302, 1203–1206.